UNESCO-IHE
INSTITUTE FOR WATER EDUCATION

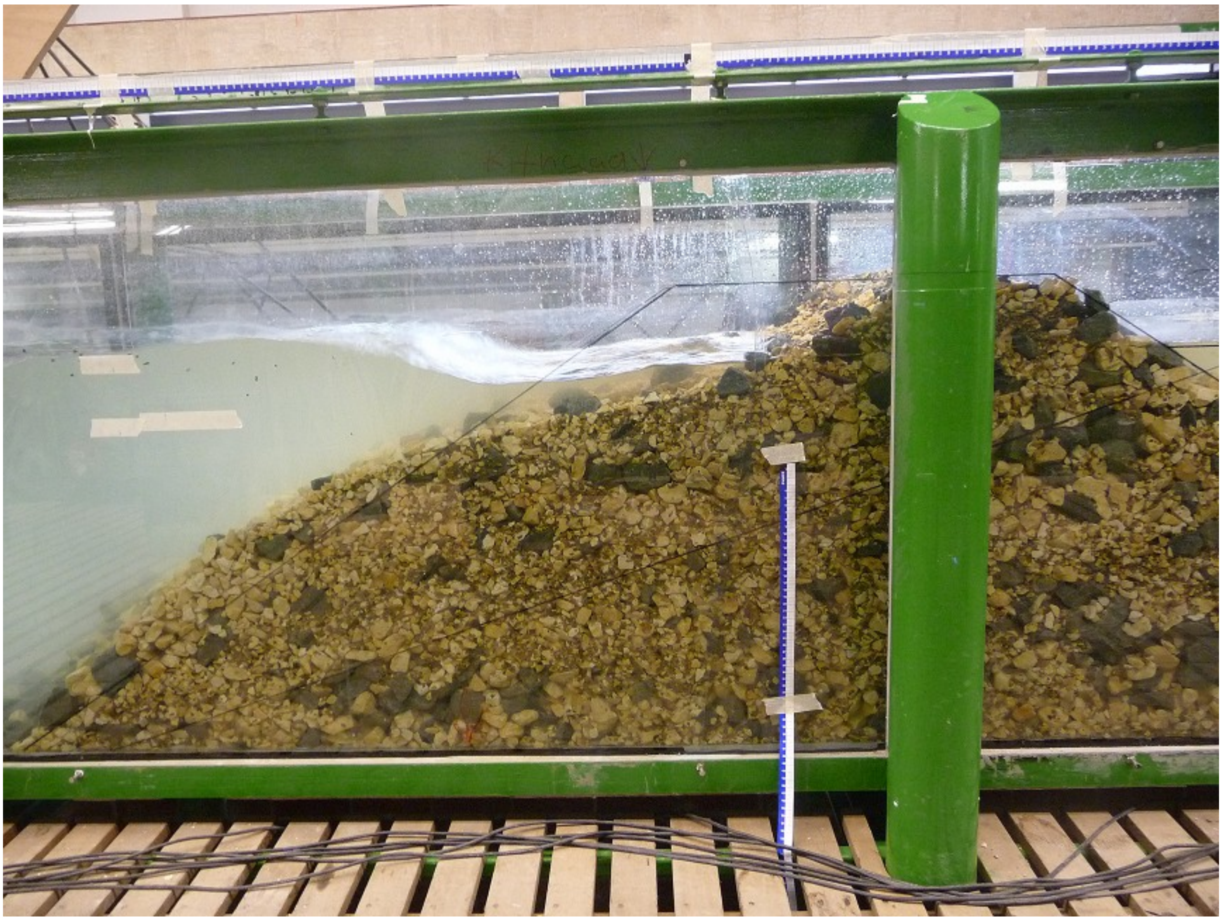

Stability of wide-graded rubble mounds

Davide Merli

MSc Thesis WSE-HECEPD-09.03
April 2009

UNESCO-IHE
Institute for Water Education

Royal
Boskalis Westminster nv

hydronamic bv

TU Delft

UNESCO-IHE
Institute for Water Education

Stability of wide-graded rubble mounds

Master of Science Thesis
by
Davide Merli

Supervisors
Prof. J.A. Roelvink, PhD, MSc (UNESCO-IHE)
Ir. J.P. van den Bos (Hydronamic)

Examination committee
Prof. J.A. Roelvink, PhD, MSc (UNESCO-IHE)
Ir. J.P. van den Bos (Hydronamic)
A. Dastgheib, MSc (UNESCO-IHE)

This research is done for the partial fulfilment of requirements for the Master of Science degree at the UNESCO-IHE Institute for Water Education, Delft, the Netherlands

Delft
April 2009

Abstract

The reshaping of temporary rubble mounds like the core of breakwaters or reclamation bunds is often a concern for contractors (like Royal Boskalis Westminster nv) in the construction stages of marine structures. The formulas found in literature for the prediction of such behavior are few, and they do not provide clear insight on the influence of relevant parameters, in particular the small dimensions and wide stone-size gradation of the material involved, usually consisting of quarry run or resulting from dredging.

The previous research in the field of dynamic stability focused on berm breakwaters and gravel beaches. These two typologies of "structures" define the range to which the rubble mounds considered in this study generally belong. An overview on the design tools provided by the technical literature shows that, whenever the grading was included as a governing parameter, some influence was recognized in the characteristics of the structure (e.g. the permeability) and in the dynamism of the different fractions of stone sizes. However, very wide ranges of the parameter grading were never investigated and a specific analysis in this direction constitutes the main significance of this study.

The Delft University of Technology provided the laboratory facilities to carry out physical model tests on a wide graded rubble mound structure representative of the core of a breakwater. The parameter D_{85}/D_{15}, describing the stone-size gradation of the construction material, was varied between the values 2.71 and 17.7, and two different seaward slopes of the model structure were also tested.

The reshaped cross-shore profiles measured during the tests showed how if the grading increases the stability of the structure is reduced. This is not always in accordance with the findings of previous researchers, showing how the extrapolation of existing empirical formulas to structures with high values of the ratio D_{85}/D_{15} do not give reliable results.

Instead, the formulas given by van de Meer (1992) to estimate the whole reshaped profile of a dynamic slope predict with good agreement the shape of the measured profiles, although the physical model shows a larger horizontal extension of the displacements. This difference is governed by the grading, being more noticeable as this parameter increases. This result leads to the definition of new formulas, some of them being modifications of the ones given by van der Meer, to describe the geometry of a reshaped profile. The formulas, all including the parameter grading, are derived through curve fitting of the measured data. Also a formula for the direct estimation of the crest recession is given. As a final step, a simple numerical model is proposed in which the new formulas are implemented, constituting a quick way to assess the shape of a slope after a wave attack.

As a suggestion for further utilization of the results of physical modeling, a brief comparison is also carried out between the output of the tests and the prediction of the numerical model XBeach (developed mainly at UNESCO-IHE).

In conclusion, this research points out how the formulas provided by the technical literature are not reliable in representing the effects of a very wide stone-size gradation in the stability of a rubble mound structure. Physical model tests proved to

be a suited way to investigate these effects, as the nature of the phenomena who play a role in the stability does not allow a simple analytical representation. The tests carried out within the present study lead to the implementation of a numerical model of practical use for engineers and contractors: further investigations through laboratory tests are recommended to validate and extend the findings of this study. Another proposed direction for further research is the comparison between the results of physical model tests and the output of numerical models.

Keywords:

grading

rubble mound

dynamic stability

core

breakwater

permeability

segregation

Acknowledgements

Since the beginning of this work I always considered myself privileged for the opportunity that I had to develop a thesis which I define a complete “experience”. Looking back at the last six months, doing literature review or writing a report are not the things that come first to my mind: I rather remember the weight of the buckets of stones in the laboratory, the hours in the office with a view on the river Rhine, the feeling of riding my bicycle beneath a dark sky.

For this reason I thank first the persons who gave me such opportunity, namely Prof. Dano Roelvink who suggested my name to the staff of Hydronamic, and the latter for proposing me an interesting research topic. Among them a great thank is due to Jeroen van den Bos, promptly available day by day not in the line of duty but with genuine interest. I also thank Jelle Olthof who followed closely my research both at Hydronamic and in the laboratory.

My work would have lost most of its significance without the practical experience of the laboratory test. In this respect I am grateful to Wim Uijttewaal for making available to me the facilities of the Fluid Mechanics Laboratory at the Delft University of Technology. Nevertheless, the success of my tests would not have been achieved without the big hand of Jaap in the physical work, of Sander and Arie for the technical support, of Wim itself for his advices.

A sincere thank goes also to the people and friends who gave me a (sometimes unexpected) support, showing interest in my research, visiting during the long days in the laboratory or encouraging me in hard times.

A special thank goes to Prof. Alberto Lamberti and Renata Archetti who, without any obligation, contributed to this research in concrete terms despite the physical distance.

List of symbols

a	= coefficient in Forchheimer equation
A	= eroded area
A	= matrix of factor scores
α	= coefficient in Forchheimer equation
α	= seaward slope of a structure
α_1	= equivalent initial slope angle
α_2	= equivalent initial slope angle
α_3	= equivalent initial slope angle
B	= matrix of factor loadings
b	= coefficient in Forchheimer equation
β	= coefficient in Forchheimer equation
β	= angle of wave incidence
c	= coefficient in Forchheimer equation
c	= generic coefficient
d	= water depth
e	= generic exponent
D_{50}	= median diameter
D_{90}	= diameter non-exceeded by 90% (in weight) of material
D_{n50}	= nominal median diameter
D_{85} / D_{15}	= grading
δ	= damping coefficient
Δ	= relative density
F	= matrix of components
f	= component in the PCA
f	= generic exponent
Fr	= Froude number
γ	= parameter of the spectral shape
g	= acceleration of gravity
H_0	= non-dimensional wave load parameter (stability number)

H_0T_0	= non-dimensional wave load parameter
k	= generic coefficient
h_c	= height of the crest of a reshaped profile
h_s	= height of the step of a reshaped profile
H_s	= significant wave height
I	= pressure gradient
K	= modified scale factor
l	= generic length variable
L'	= wave length in the core
l_c	= length of the crest of a reshaped profile
l_s	= length of the step of a reshaped profile
λ	= length scale factor
m	= generic coefficient
m_0	= 0-order moment of wave spectrum
m_2	= 2-order moment of wave spectrum
M	= mass of a stone
M_{50}	= median mass
M_a	= mass of a stone in air
M_w	= mass of a stone in water
N	= number of waver
N_R	= relative number of waves
N_s	= non-dimensional wave load parameter (stability number)
n	= porosity
ν	= cinematic viscosity of water
p	= pressure
p_0	=reference pressure
P_R	= number of rounded stones
R	= correlation coefficient
R_c	= crest freeboard
Re	= Reynolds number
Rec	= berm/crest recession
ρ	= density of dry rock
ρ_w	= density of water

s_m	= wave steepness
t	= generic time variable
T_m	= mean wave period
θ_1	= slope below the step
θ_2	= slope just above the step
θ_3	= slope below the crest
U	= generic velocity
$\overline{U}$	= characteristic velocity
x	= generic horizontal coordinate
$\tilde{Y}$	= matrix of standardized parameters
z	= generic vertical coordinate

List of figures

List of tables

Table of contents

Chapter 1

Introduction

1.1 Rubble mound stability and common practice

The criteria commonly used in the design of maritime structures are based on stability formulas, in order to define the size of the single elements (concrete, natural rock, etc.). In general, static stability is required for the layers directly exposed to wave action, where hardly any displacement or reshaping of the overall structure is allowed.

The stability of the elements constituting a rubble mound increases with their diameter. However big stones are not easy to source, and even if a quarry can provide them the distance from the construction site may arise a transportation (and economical) issue. For this and other reasons the design stage of coastal structures, like in other fields of civil engineering, implies always a compromise between the performance requirements, i.e. the stability, and the economic balance.

In this respect, common practice has taught that it is cheaper to avoid the use of big size elements, even if plenty of natural stone is available: by this way the equipment for construction and maintenance has lower cost (Lamberti and Tomasicchio, 1997). Because of this reason berm breakwaters are commonly built in countries such as Iceland and Norway (PIANC, 2003). On the other hand, the choice of a reduced stone size becomes necessary whenever the availability of rock is limited.

Thus, reality shows that the requirement of static stability can not always be satisfied, or is not always economically feasible. In such cases a valid solution is found in the direction of dynamic stability, where the movement of single elements is allowed until a stable configuration is reached, or the long term trend of the reshaping shows substantial equilibrium. Berm breakwaters are typical examples of such solutions.

Often no applicable design rules can be easily found when rubble mound structures in the transition between static and dynamic behavior have to be built. This issue arises increasingly often in the practice of dredging contractors, like Royal Boskalis Westminster nv. During the construction of a breakwater, for example, the core material will be exposed to storms for a certain time before protective layers are applied. The same can happen to temporary structures like bunds protecting reclamation areas or supporting an adjacent superstructure. Excessive reshaping may constitute a major problem due to the project schedule requirements, or for logistic reasons if, for example, terrestrial vehicles need to go safely on top of the structure and an adequate crest freeboard should be granted.

Nowadays more than in the past, the considerations of above raise an issue as many contracts signed at present include both the design and the construction of maritime structures. It is then economical for a designer-contractor to predict and analyze as early as possible the trends in movement of the dumped material, in order to reduce the possibility of excessive reshaping and the extent of unforeseen damages. This results in a secure planning and execution of the next construction stages.

The instability of such materials can be strongly enhanced by the small average element size. Another relevant feature is the wide stone-size gradation which, although regularly found in practice, is not treated enough in the technical literature. The investigation of the specific effect of wide gradation on the stability of rubble mound structures constitutes the main significance of this study.

Figure 1.1 – Survey on a reclamation bund partly washed away by a storm in Khalifa (UAE) (picture by Royal Boskalis Westminster nv)

1.2 A gap in the available literature?

The issues described above explain how more understanding of the phenomenon of dynamic stability may be needed. Rubble mounds like core of breakwaters can be considered structures "in transition" between static and dynamic behavior: although the features of the constituting material are in favour of instability, excessive reshaping is not allowed with respect to the successive construction stages. In such cases the available literature doesn’t provide direct guidance and often the choice for the designer is not straightforward. Recognizing this gap in the technical literature, the dredging company Royal Boskalis Westminster nv proposed the present study which aims at providing designers and contractors with a better insight in this subject, with particular respect to the influence of a very wide stone-size gradation of the constituting materials.

Studies and laboratory tests have been carried out on the dynamic behavior of rubble mounds (Van der Meer, 1988, followed by others). Empirical formulas to obtain the most relevant dimensions of the reshaped profile are available (van der Meer, 1992), but a range of the parameter grading reaching the values observed in practice for dredged materials or quarry run have never been effectively investigated.

A series of tests on physical model is still a suited way to investigate a topic which involves phenomena difficult to analyze in theory. In this respect, laboratory facilities were provided by the Delft University of Technology for the purposes of the present study. The results of the tests will allow an evaluation of the design methods suggested by the literature, followed by the derivation of a new design tool of practical use which takes into account the stone-size gradation of commonly used construction material.

Following a different direction, attempts to provide a theoretical representation of phenomena like the penetration of waves into porous media and the stability of single stones lead to the development of refined numerical models. This way was undertaken by van Gent (1995) and is still being explored.

Among the perspectives of this study, the possibility of using the results of the laboratory tests in the development of numerical models is certainly attractive. A first step in this direction will be done for the model XBeach, which is currently developed by UNESCO-IHE in consortium with other institutes.

1.3 Outline of the present study

The layout of this thesis is as follows.

The theoretical background of the topic addressed by this study is presented in Chapter 2. It will come out how some phenomena, i.e. the penetration of water through the pores of a structure and the complex interaction between grains with different size, makes it impossible to treat the theory of stability in a complete analytical way, and physical and/or numerical models are a powerful aid always being used to simplify the problem. As this research will be based on the results of laboratory tests, considerations about the possible effects of scaling in the results of physical models will be included.

Chapter 3 describes the tests on physical model carried out as a main part of this thesis. Objective of the tests is to investigate the specific influence of a wide stone-size gradation in the reshaping of a rubble mound. In order to represent the features of temporary structures, a low crested model was built with a relatively small average grain size of the constituting material. Relatively low waves, typical of operational conditions, were used. The tests were performed at the fluid mechanics laboratory of the Delft

University of Technology. All the set-up of the tests and the choices for the input and the investigated parameters will be explained.

In Chapter 4 the data collected as output of the tests are presented. The measured cross-shore profiles of the model structure as a result of the different wave attacks are suited for a direct comparison with the estimation of some features in the reshaping of rubble mound structures (e.g. the recession of the crest/berm) given by the available design tools provided by other researchers, namely Hall and Kao (1991), Tørum et al. (2003) and van der Meer (1988).

Following the outcome of this analysis, in Chapter 5 a parameterization of the measured cross-shore profiles is done in order to perform a more quantitative comparison with the formulas given by Van der Meer for the reshaping of slopes characterized by dynamic stability. Then a curve fitting procedure over the data is carried out to find a suited term taking into account the grading of the material to include in these formulas. Other empirical formulas for the estimation of the recession of the profile above the mean water level are derived through interpolation of the output data of the tests. At this stage, a numerical model for the description of the whole reshaped profile can be implemented.

In Chapter 6 a direction for further research will be given, consisting of an attempt of calibration of the numerical model XBeach using the output data of the laboratory tests.

Conclusions and recommendation for further research are given in Chapter 7.

Chapter 2

Theoretical background

In this chapter an overview will be given on the actual progress of research in the investigation of the stability of rubble mounds. This analysis has the objective to go beyond the traditional assessment of static stability, with focus on the influence of a wide stone-size gradation of the constituting material.

The input for this research comes from a dredging contractor (Royal Boskalis Westminster nv) facing the problem of the stability of rubble mounds typically built as temporary structures during the execution of more complex works. Reference in literature is not found for such specific types of structures: this is the reason why in practice the engineers make use of the design tools valid for berm breakwaters, or similar structures which show reshaping before reaching a stable configuration. This is also the direction of the following overview.

Physical processes like the wave penetration inside the structure or the interaction between stones of different size influence the reshaping, and the choice of carrying out physical model tests was made in order overcome the problem of an accurate analytical representation of such phenomena. However, modeling of reality introduces scale effects which may affect the reliability of the results, and have to be analyzed from a theoretical point of view: the last section of this chapter deals with this issue.

2.1 Beyond the limit of static stability

The design of coastal structures like breakwaters is usually based on the requirement of static stability. This means that the single elements are chosen with such dimensions that the wave action, with the resultant hydraulic pressures, is not able to displace them.

The stability number introduced by Hudson (1959):

$$N_s = \frac{H_s}{\Delta D_{n50}} \qquad (2.1)$$

is a suitable parameter to classify coastal structures with respect to the mobility of the constituting elements. The "load" variable (significant wave height) in the numerator and the "resistance" variables (median nominal diameter and relative stone weight) on the denominator mean that this number grows fast as the stability decreases. The parameter Δ is defined, from here on, as:

$$\Delta = \rho / \rho_w - 1 \qquad (2.2)$$

being ρ the dry density of the stone and ρ_w the density of the water. Generally, in the design of traditional stable breakwaters, the values of N_s are within the range 1-4.

For various reasons, as explained in the introduction, this is not the only design philosophy in use nowadays. Smaller elements can be considered instead of the ones which come from the criteria of static stability: this is an advantage from the economic point of view, because not only the rocks themselves but also the equipment used for construction and maintenance of smaller elements is cheaper and more easily at hand (Lamberti and Tomasicchio, 1997).

Van der Meer and Pilarczyk (1987) and more thoroughly Van der Meer (1988, 1992) paved the way in the research beyond the limit of static stability with the support of an extensive series of laboratory tests carried out at Delft Hydraulics (now Deltares). In these tests the parameter N_s was varying in a range of 1-500, meaning that all the possible behaviors in terms of stability (static, dynamic and transition cases) were investigated.

Together with the definition of the stability number (Eq. 2.1), van der Meer distinguishes two different approaches in evaluating the performance of static and dynamic structures: while for statically stable structures the design parameter *damage* can be defined, which is related to the number of individual stones moved, when dealing with dynamic stability it is more practical to analyze the overall changes of *profile* thus losing track of the single stone displacements.

In his doctoral thesis van der Meer gives, for the latter case, a parameterization of the reshaped profile defining a number of curves passing through relevant points, i.e. a crest and a step respectively above and below the mean water level. Empirical equations are provided to calculate these geometrical parameters: the implementation of such equations in a numerical model resulted in the development of the software BREAKWAT, used nowadays in engineering practice.

With the important research steps described above the border of static stability is crossed. A view on the developments in the knowledge regarding the stability of “structures” with a more dynamic behavior will be given in the following paragraphs, taking into account for each literature case the main theoretical assumptions and findings. Also the formulas and design tools coming out from previous studies will be presented and discussed.

The topic will be addressed distinguishing between berm breakwaters and gravel beaches: this two categories of “structures” represent somehow the two extremes in the range of dynamic stability. In berm breakwaters an initial reshaping takes place, until the profile reaches a statically stable configuration. Gravel beaches are characterized by a continuous movement of the stones due to the wave action, although for a given wave load the overall layout of the cross-shore profile doesn’t change.

2.2 Berm breakwaters

2.2.1 General characteristics

The main feature of berm breakwaters is the presence of an extensive berm on the seaward slope, which reshapes after the first wave attacks until a stable configuration is reached (see Fig 2.1). The main advantage of this solution, clearly reflected in the cost of construction, lies in the fact that the armour stones can be smaller than in a conventional rubble mound structure (PIANC 2003). A disadvantage is the large volume of stones needed, together with the high durability required for the stones (the reshaping may induce breaking and abrasion) and the risk of loss of material due to longshore transport.

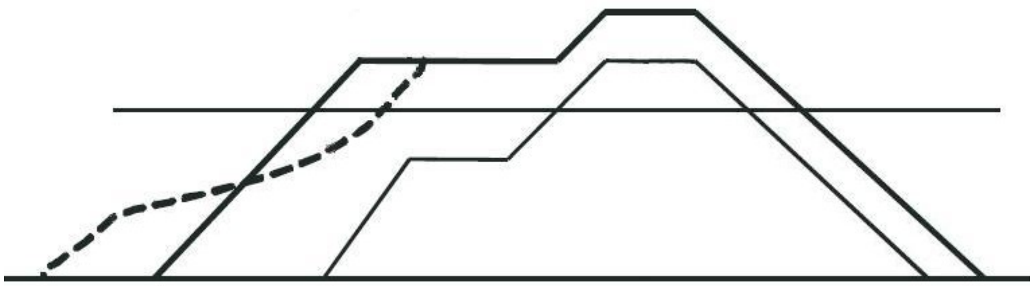

Figure 2.1 – Schematic representation of the behavior of a berm breakwater

The berm breakwater concept is actually old, as 2000 years ago structures like that were already being built. However, only starting from the 1980s this typology was put in practice systematically mainly in countries like Iceland and Norway where plenty of natural stone of good quality is available. Nowadays structures which go under a strict definition of berm breakwaters are not many in the world: about 60 at present, half of which are in Iceland (PIANC, 2003).

Beside the most common typology of berm breakwater, different solutions were developed more recently. In the multilayer (or Icelandic-type) berm breakwaters a diversification is made between areas of the cross section in term of dimension of the stones according to the design wave loads: in this way a higher stability of the sectors hit by the highest waves is combined with an optimization of the quarry yield (see Fig. 2.3).

The Working Group 40 of PIANC (2003) reports that, according to the results of laboratory tests, the recession of the berm (Rec) for these structures “is to some extent larger then for the homogeneous berm breakwater when the D_{n50} for the largest stone class is used to calculate H_0T_0 and Rec/D_{n50}”. H_0T_0 is a load parameter (see Eq. 2.4) involving stone diameter and wave height and period. Reference on multi-layer berm breakwaters is also found in Sigurdarson et al. (2005)

Fig. 2.2 – The Sirevåg berm breakwater (Tørum et al., 2005)

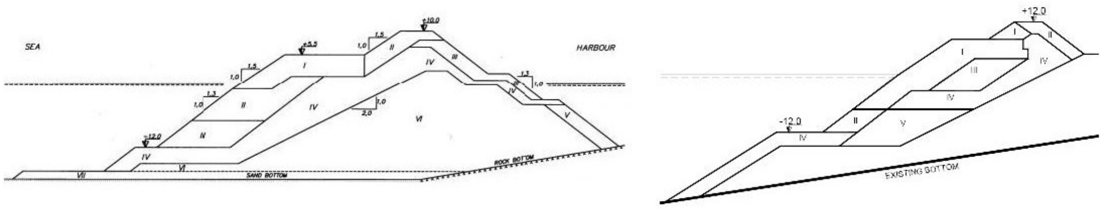

Figure 2.3 – Multilayer berm breakwaters at Sirevåg and Hammerfest (Sigurdarsson et al., 2005)

Among the variety in the typologies existing nowadays, the most relevant for the present study are the traditional berm breakwaters, which can be defined, in agreement with the technical literature, by a stability number N_s greater than 2.7.

2.2.2 Research of Hall and Kao on the grading

An investigation of the reshaping process of the armour layer of berm breakwaters over a rather wide range of stone-size gradations was documented for the first time by Kao and Hall (1990). Their model structure consisted of a core having D_{50} = 1.2 cm covered by an armour layer with D_{50} = 1.9 cm characterized by a berm.

The stone-size gradation (or grading) of the material constituting a rubble mound is defined by the ratio D_{85} / D_{15} (a detailed definition of the parameters involving diameters in given in Par 3.2.1). Four different values of the grading of the armour material were tested by Kao and Hall, ranging between 1.35 and 5.4.

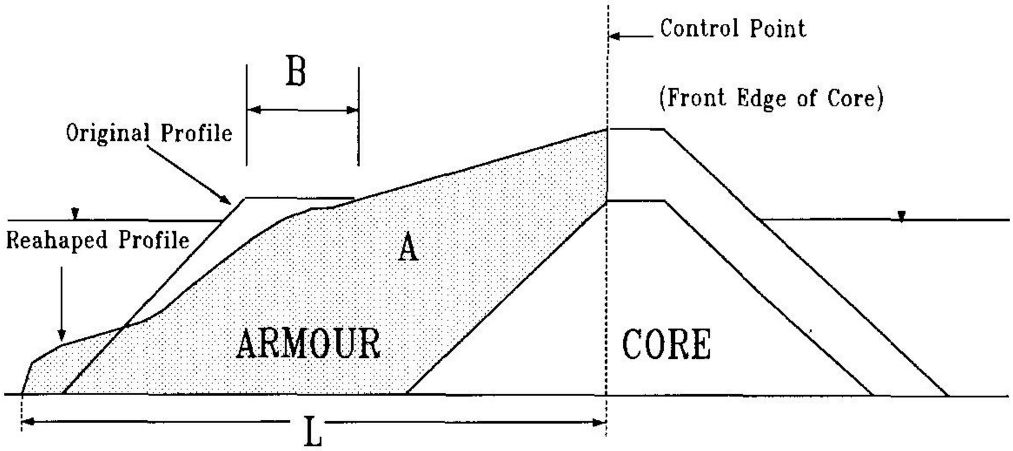

Figure 2.4 – The model structure used in their tests by Kao and Hall (1990)

The three variables investigated in the tests are listed below (see also Fig. 2.4):

$L / D_{50} =$ dimensionless toe width after reshaping;

$A / D_{50}^{2} =$ volume per unit length of armour stone required on the front slope (which means assuming a width *B* of the berm);

$\mathrm{Rec} / D_{50} =$ dimensionless width of berm eroded.

The design formula provided by Kao and Hall (1990) for the estimation of the erosion of the berm, used for comparison also with the data collected for this study, will be discussed in Par 2.4 (Eq. 2.6). Here the qualitative conclusions derived from the authors will be presented.

In the measured values for all the parameters a particular trend was observed with respect to the gradation and discussed further in a subsequent paper (Hall and Kao, 1991). While for the three lower values of the parameter ($D_{85} / D_{15} < 3$) the increase of gradation results in a decrease of stability, for the widest grading an opposite effect is visible (see Fig. 2.5, where the variable plotted in the horizontal axis is N_s).

According to Hall and Kao, this is explained by the presence of a significant proportion of large stones, which has a dominant influence on the stability if a certain threshold in the stone size is exceeded. On the other hand, for low values of grading the uniformity of stone sizes is in favour of the stability.

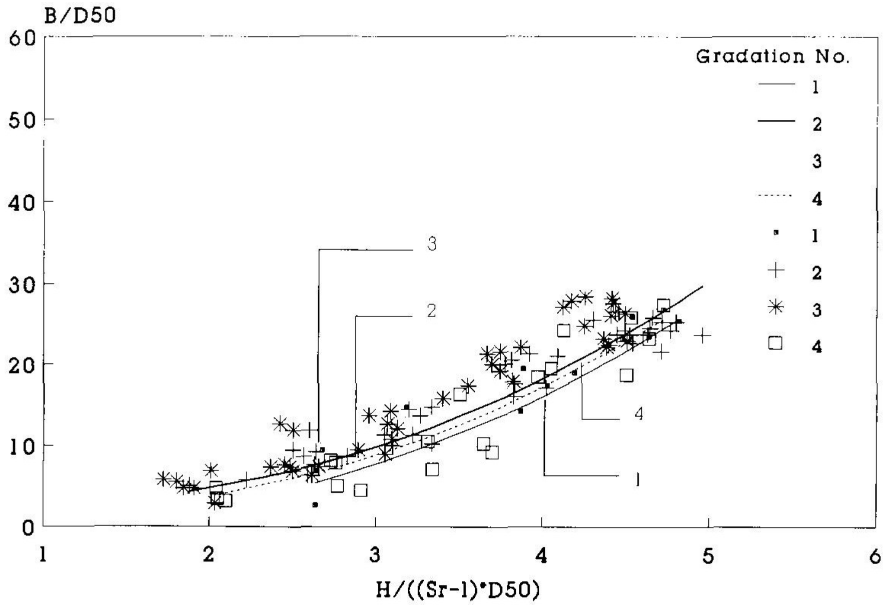

Figure 2.5 – Trend for the berm erosion for the 4 input values of gradation found by Hall and Kao (1991)

In summary, Hall and Kao recognize contrasting effects of the grading on the stability which can find a physical explanation. The stabilizing role of the big stones, if the ratio D_{85}/D_{15} is sufficiently high, is probably due to the enhanced segregation phenomenon which increases locally the grain-size and the resistance to the wave action. If the grading is narrow, instead, the high porosity (and permeability) of the structure provides a more efficient wave energy dissipation, which means again more stability. As a result, within the investigated range of D_{85}/D_{15}, a value of about 3 gives the least stability.

The above consideration about the narrow grading is in accordance with the general meaning of the results by Van der Meer (1988), who considered values of grading up to 2.5 and included a parameter *P* ("notional" permeability) in his formula for static stability. No analytical insight is provided on the phenomenon, and *P* has to be assessed by engineering judgement through comparison with some reference cases. However, the proportionality between the stability of a stone and the permeability of the underlying material is confirmed by the outcome of his tests.

2.2.3 Further research and findings of Tørum et al.

More recent investigations of the effect of grading, although limited to a smaller range of values, by means of physical models were carried out by Mansard et al. (1996), van der Meer et al. (1996), Juhl and Sloth (1998) and Tørum et al. (2003), with the latter providing a new empirical formula to describe berm recession (see Par. 2.4).

Mansard et al. (1996) performed laboratory tests to reproduce the stability of riprap exposed to the wave action of a reservoir. The stone-size gradation, expressed in terms of ratio between the maximum and minimum mass of the stones, varied between 1 and 10, which correspond roughly to D_{85}/D_{15} = 1-2. They derived from the measurements that a positive effect on stability is given by a narrow gradation, although for higher values of such parameter the trend of a lower stability is less clear. A similar trend is found by Van der Meer et al. (1996), who investigated gradations up to 2.5 and found for this value a faster damage development with the wave load (but only for a low wave steepness).

In both the test series, the damage parameter assumed was *S*, defined as the ratio between the eroded cross sectional area and D_{n50}^2. This approach is typical for investigations on armour layers, where the number of displaced elements is usually relatively low: the maximum value of *S* was < 10 in the tests by Mansard et al. and < 20 in the tests by van der Meer et al.

The tests carried out by Juhl and Sloth (1998) at the Danish Hydraulic Institute aimed at analyzing different armour layer solutions for berm breakwaters. Specific tests were intended to study the effect of stone gradation (D_{85} / D_{15} equal to 1.4 or 1.8) and reduced permeability, the latter being obtained adding fine material in the berm. Such a condition may be representative of the outcome of deficient design or construction, or simply the consequence of a temporary construction road on the berm which was not removed.

In Fig. 2.6 the outcome of the investigation on the permeability is shown in terms of recession of the berm (*y*-axis) against significant wave height (*x*-axis).

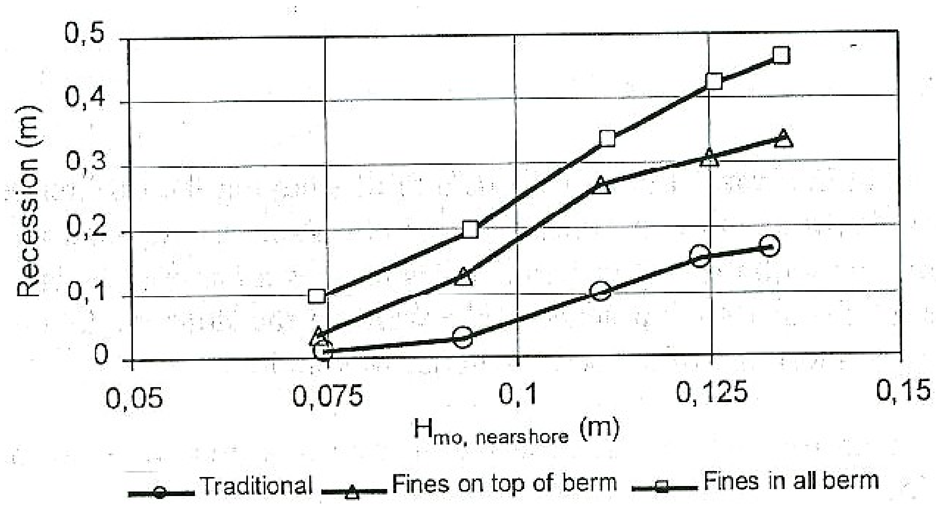

Figure 2.6 – Relation between berm recession and significant wave height found by Juhl and Sloth (1998) for varied permeability

Juhl and Sloth found that the wider gradation and the lower permeability produce similar effects. They deduced that the increase of D_{85}/D_{15} actually consists of a permeability reduction, resulting in a decrease of the energy dissipation in the berm. In such conditions, besides the increase of instability, a significantly larger wave run-up and overtopping was found, with direct influence on the damage of both crest and rear side. Considering the investigated values of grading (1.4 and 1.8), this conclusion is in accordance with the findings of Hall and Kao.

In order to study specifically the recession of the berm of breakwaters, Tørum (1998) collected the data relative to many recent laboratory test series, including the ones from Juhl and Sloth (1998), and carried out additional tests at SINTEF (the Norwegian Foundation for Scientific and Industrial Research). He found a considerable scatter in the test results, probably because “the ways different laboratories carry out tests are not consistent and/or that some relevant parameters are overlooked” (Tørum et al, 2003).

Despite of this, Tørum was able to derive a 2nd degree polynomial fit (Eq. 2.3) which related the recession to the stone diameter, the significant wave height and the mean period, to be used as a design equation at least in a conceptual design phase.

$$\frac{\mathrm{Rec}}{D_{n50}} = 0.00073908\left(H_0T_0\right)^2 + 0.0498855\left(H_0T_0\right) + 0.604 \tag{2.3}$$

The non-dimensional parameter H_0T_0, assumed by van der Meer (1988) as a suitable representation of the intensity of the wave attack for dynamic stability, is defined as:

$$H_0T_0 = \frac{H_s}{\Delta D_{n50}}\sqrt{\frac{g}{D_{n50}}}T_m \tag{2.4}$$

where T_m is the mean wave period.

In Tørum et al. (2003) the formula of above, previously changed into a 3rd degree polynomial fit, was modified with the introduction of terms accounting for stone-size gradation and water depth: in particular, the importance of D_{85}/D_{15} was suggested by the earlier findings by Hall and Kao (1991) and Mansard et al. (1996). The term involving the gradation was obtained as a 2nd degree polynomial fit, based on some of the SINTEF tests by Tørum and some of the DHI tests by Juhl and Sloth (1998).

The resulting formula is given in Par. 2.4 (Eq. 2.8). Only the quadratic term which takes into account the grading is reported here:

$$f\left(\frac{D_{85}}{D_{15}}\right) = -9.91\left(\frac{D_{85}}{D_{15}}\right)^2 + 23.9\frac{D_{85}}{D_{15}} - 10.5 \tag{2.5}$$

In contrast with the findings of Hall and Kao, the above polynomial shows that the estimated berm recession reaches a minimum for a specific value of grading (1.2 from Eq. 2.5), being equal all the other parameters.

2.3 Gravel beaches

2.3.1 Development of numerical models

Gravel beaches represent a typical example of dynamically stable "structure", showing a rather definite cross section under a certain wave attack even though the single stones are still subject to frequent displacements.

The description of the reshaping cannot be done any more only through the evaluation of variables like crest recession or toe displacements. As introduced in Par. 2.1, a parameterization like the one done by van der Meer seems to be more suitable (see Fig. 2.7) as the whole cross shore profile may show a dynamic behavior and look different from the initial slope.

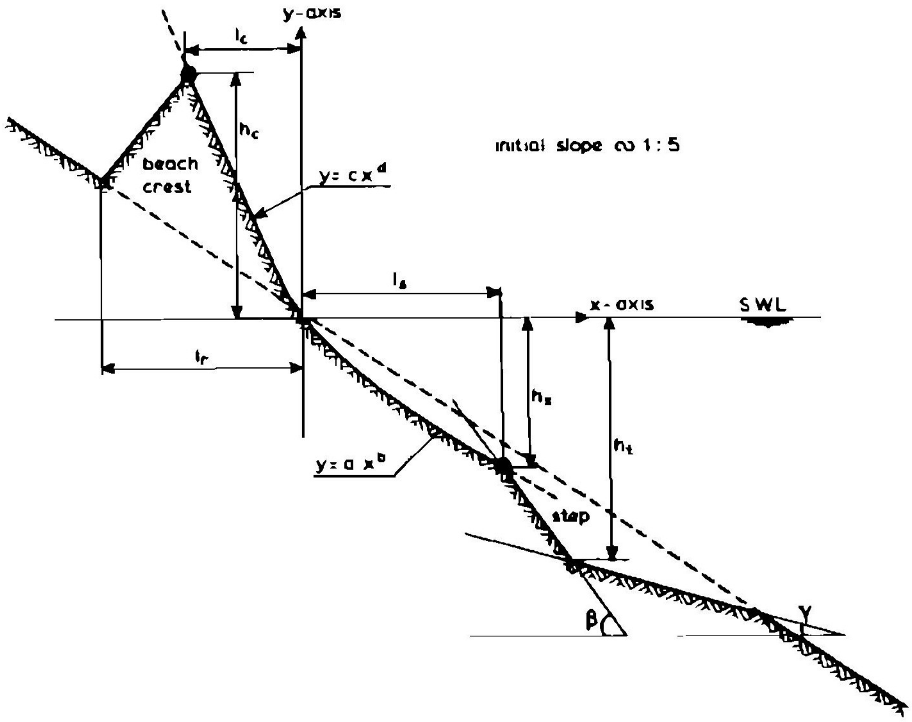

Figure 2.7 – Schematization of the reshaped profile of a dynamically stable structure according to van der Meer (1988)

In his analysis, van der Meer recognizes some common features in the shape of the slopes after exposure to wave attack. In particular a steep slope is observed above the waterline, generating a clear "crest" on the cross-shore profile. Below the still water level, a slope gentler than the initial one develops until the effect of the waves is not felt any more: then, if the initial slope is not steeper then 1:3, one straight surface brings back to the original profile. The point where this last change of slope takes place can be more or less clear, however this area of the reshaped profile should look like a “step”.

When dealing with the response of fine material to wave load the instability of the single stones/grains is not only determined by the reduced size: also the mechanisms of penetration of the waves into the structure plays a role, giving relevance to parameters like the porosity or the permeability of the constituting material. Then for a study on the behavior of gravel beaches the physical models may have disadvantages, like the scale effects which can lead to a wrong representation of the flow through the porous media (see Par. 2.5).

Van der Meer (1988) still based his study on laboratory tests, and scale effects were substantially avoided due to the large dimensions of the Delta flume where he carried out his tests (at WL-Delft Hydraulics, now Deltares). Van Gent (1994, 1995) studied the phenomenon from a different point of view, developing a numerical model (ODIFLOCS) based on the implementation of the shallow water equations for the free-surface hydrodynamics and the Forchheimer equation (Eq. 2.17) governing the flow through porous media. The model is then improved with the implementation of stone displacements, derived through a force balance where the contributions of inertia, drag and lifting mechanism were taken into account. By this way a complete wave load-response model is obtained.

A reliable representation of the water flow both outside and inside the structure was achieved through the combination of analytical considerations and physical model tests, the latter used in the calibration of certain parameters. In particular, a first set of laboratory experiments to measure the resistance of porous media to an oscillatory wave motion was carried out, and the coefficients *a*, *b* and *c* in the extended Forchheimer equation were calibrated. At this stage van Gent remarks that, particularly in small-scale tests, the linear friction term may not be well represented due to scale effects. Then, the results of additional physical model tests were used to validate the numerical representation of the internal end external wave motion.

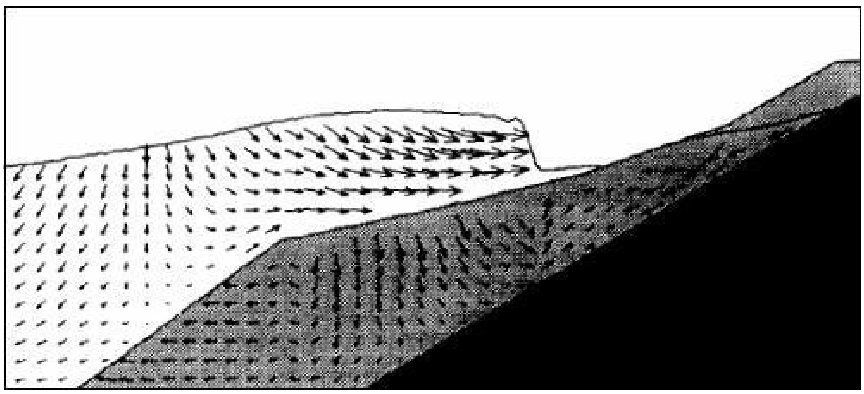

Figure 2.8 – Impression of flow fields on and inside a berm breakwater (van Gent, 1994)

According to van Gent, the new design tool represented by the wave load-response model should be improved through a better specification of the drag and inertia forces and a distinction between the initiation of stone movement and stones moving along the slope. Further developments may include the implementation of other phenomena like segregation, grading effects and three-dimensional effects. Verification over results of physical model tests by van der Meer showed how the predictions of the model are already quite reliable.

The overall approach of van Gent (1995) is clearly summarized by his own words: “through mathematical modeling of this wave motion itself, more detailed information like velocities and accelerations of water moving along the slope can be obtained. Using these properties, assessed through numerical modeling, may lead to more applicable solutions for hydrodynamic processes and stability parameters. In general, a mathematical solution may exclude possible scale effects which occur in small-scale physical modeling. In addition, an accurate mathematical description is an important complementary design tool”.

The study of van Gent is actually not meant for the modeling of only gravel beaches, but it is in the representation of these category of “structures” that lies the significance of his research, as a strong theoretical basis is given in the analysis of a dynamic behavior. His numerical model was also successfully validated for less dynamic structures like berm breakwaters and reef-type structures.

2.3.2 Effect of grading

In his doctoral thesis van der Meer, commenting the plot reported in Fig. 2.9, states that “the grading of the material has no or minor influence on the profile. […] Only for very wide grading a longer profile was found below the still water level”. For this reason, the parameter D_{85}/D_{15} is not included in his formulas for the estimation of the reshaped profile.

A specific investigation of the effect of the grading on the development of gravel beaches was carried out by van Gent (1996) through simulations with his numerical model. Three values of grading are studied: 1, 1.33 and 2. The author specifies how the quantitative nature of the results, e.g. the magnitude of accretion and erosion, should be treated with care as the calibration of important parameters was done through a physical model where $D_{85}/D_{15}=1.5$.

In the previous sections it was shown how laboratory tests confirm the hypothesis that an increase of the grading means a reduction in permeability. Then in the implementation of a numerical model that takes into account the single stones (like the model of van Gent does) for a specific grading both the varying diameters of the stones and the porosity n (directly related to the permeability) can be assigned.

If the stone sizes and the porosity are varied separately, the model shows contrasting results. When only the grain sizes are taken into account (and not the permeability), a wide grading means the presence of bigger stones: the presence of such stones in the top layer results in more stability (compared to narrower gradings). On the other hand, if only the permeability *n* is varied, the stability of the slope follows this parameter and increases for higher *n*. This is explained with the reduction of the velocities along the slope as the porosity increases.

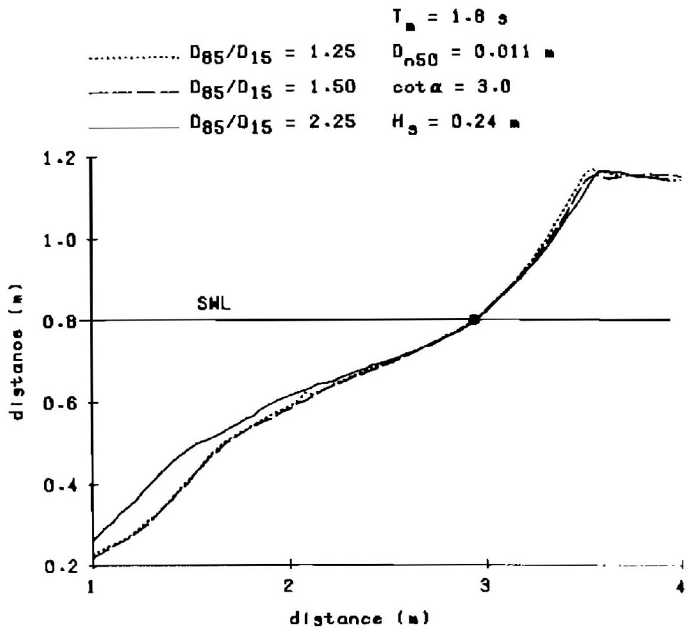

Figure 2.9 – Effect of grading in the laboratory tests of van der Meer (1988)

If both the effects are taken into account, the intermediate grading (1.33) proves to be the least stable: the destabilizing influence of a lower permeability is stronger for the narrow grading (1), while for wide grading (2) the stabilizing effect of the presence of big stones slightly prevails. This result is qualitatively in accordance with the findings of Hall and Kao (1991), although the transition values of grading (3 for the latter) do not coincide.

Different initial slopes were also simulated by van Gent. The results show how the reshaping of mild initial slopes is not significantly affected by the grading. Steeper slopes, instead, need a considerable reshaping to reach an equilibrium profile: in this mechanism the wide graded material shows more stability, because the resulting segregation eventually leaves the bigger stones on the layer exposed to the waves.

2.4 Available design tools

As stated at the beginning of this chapter, the choice of the designer when dealing with dynamically stable structures is not straightforward. The manual for the use of rock in hydraulic engineering, or simply Rock Manual (CIRIA/CUR/CETMEF, 2007), suggests the use of the software BREAKWAT, based on the empirical equations found by van der Meer (1998), which is applicable for a wide range of cases (N_s between 3 and 500) and gives a complete spatial representation of the reshaping phenomenon. More insight in some of these equations will be given in Chapter 5.

An alternative to BREAKWAT is given by the wave load-response model developed by van Gent (1995), mentioned in Par. 2.2.3, which has the advantage of dealing in a more analytical way with phenomena such as the wave propagation inside the structure and the stability of the single stones.

More simple alternatives suggested in the Rock Manual for the estimation of, at least, some significant parameters in the reshaping of berm breakwaters are represented by the formulas of Kao and Hall (1990) and Tørum et al. (2003).

Through a multi-variate regression analysis of their measured data, Kao and Hall (1990) found formulas for the estimation of the toe accretion, the volume involved in the reshaping and the berm recession. This last parameter is particularly interesting from the perspective of a contractor. The general formulation for the recession (Rec) of the berm is as follows:

$$\frac{\text{Rec}}{D_{50}} = \left[-10 + 0.51 \left(\frac{H_s}{\Delta D_{50}} \right)^{2.5} + 7.5 \frac{D_{85}}{D_{15}} - 1.1 \left(\frac{D_{85}}{D_{15}} \right)^2 + 6.1 P_R \right] \cdot \left[1 + \ln N_R^{\ 0.11} \right] \tag{2.6}$$

Use of this formula should be done within the same range of the tests performed by the authors:

$$1.35 < D_{85} / D_{15} < 5.4 \tag{2.7}$$

Another remark can be done about the notation for the diameters: the authors do not refer to the nominal diameter but to the sieve diameter (a precise definition of these quantities is given in par. 3.2.1). P_R is the percentage of rounded stones (a parameter which proved to have effect only on the recession of the berm) and N_R is the relative number of waves, intended as the total number of waves divided by 3000.

The quadratic expression involving the grading in Eq. 2.6 means that, being equal all the other parameters, the relationship between berm recession and grading is represented by a parabolic function. Such function is shown in Fig. 2.10, meaning that according to the authors a grading close to 3 maximizes the berm recession (see also Par. 2.2.2).

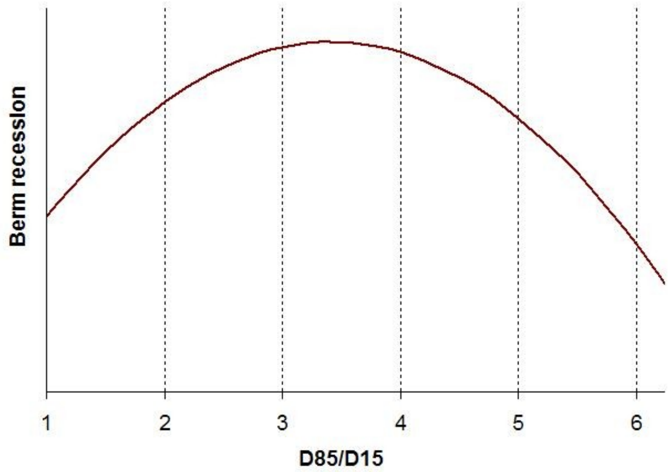

Figure 2.10 – Trend of berm recession as a function of grading according to Kao and Hall

The formula suggested by Tørum et al. (2003), already introduced in Par. 2.2.3, is the following:

$$\frac{\text{Rec}}{D_{n50}} = 0.0000027\left(H_0T_0\right)^3 + 0.000009\left(H_0T_0\right)^2 + 0.11\left(H_0T_0\right) - \\ - f\left(\frac{D_{85}}{D_{15}}\right) - f\left(\frac{d}{D_{n50}}\right) \tag{2.8}$$

with the factors involving the grading and the water depth defined below:

$$f\left(\frac{D_{85}}{D_{15}}\right) = -9.91\left(\frac{D_{85}}{D_{15}}\right)^2 + 23.9\frac{D_{85}}{D_{15}} - 10.5 \tag{2.9}$$

$$f\left(\frac{d}{D_{n50}}\right) = -0.16\left(\frac{d}{D_{n50}}\right) + 4.0 \tag{2.10}$$

The validity of Eq. 2.8 is restricted to the following boundaries:

$$1.3 < D_{85} / D_{15} < 1.8 \tag{2.11}$$

$$12.5 < d / D_{n50} < 25 \tag{2.12}$$

As stated in Par. 2.2.3, the factor involving the grading is quadratic and a parabolic function relates the berm recession to the grading. Fig. 2.11 shows this function, from which it can be derived that the formula by Tørum et al. predicts a minimum berm recession for $D_{85} / D_{15} = 1.2$.

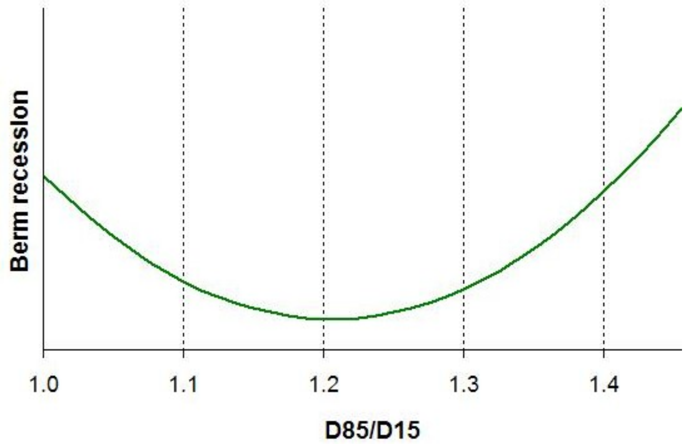

Figure 2.11 - Trend of berm recession as a function of grading according to Tørum et al.

Although meant to simulate the morphological changes of really dynamic bodies (i.e. sand beaches, dunes or storm barriers), the numerical model XBeach, currently developed mainly at UNESCO-IHE (Delft), should be mentioned at this stage as an additional design tool. The possibility of this model to reproduce the reshaping of wide-graded rubble mounds is investigated in Chapter 6, where a brief comparison is carried out between the predictions of the model and the data collected in the present study through physical modeling.

2.5 Scaling of a hydraulic phenomenon

When reality is scaled down for the execution physical model tests, first a qualitative investigation of the governing phenomena and forces has to be done to assure a sufficient reliability of the outcome. The wave attack on a rock slope is dominated by inertia and gravity forces, given the dynamic nature of the wave load and the effect of gravity in the mobility of the single elements. Then a physical model will be able to represent reality as long as the balance between the dynamic action of the wave and the stability of the stones is correctly reproduced.

In this case a model should be built according to the Froude similitude, which means that the following non-dimensional quantity is conserved (Hughes, 1993):

$$Fr = \frac{U}{\sqrt{gl}} \tag{2.13}$$

where g is the acceleration of gravity and U and l are a representative velocity and length respectively.

Imposing the conservation of Fr means also that, if the linear dimensions are scaled with a factor λ:

$$l_m = \frac{l_p}{\lambda} \tag{2.14}$$

then the generic time variable t has to be scaled from the prototype to the model by a factor $\sqrt{\lambda}$:

$$t_m = \frac{t_p}{\sqrt{\lambda}} \tag{2.15}$$

where the subscripts m and p refer to the model and to the prototype respectively.

The response of the stones in a rubble mound structure is also influenced by the permeability of the underlying mass, as shown earlier in the literature review. It becomes then important to distinguish whether the flow between the stones is turbulent or, as the pores become smaller, laminar, giving importance to viscosity forces. This is not usually an issue when dealing with the outer layers of a breakwater, where the dimension of the pores guarantees the development of turbulent flow. On the other hand, if core material is scaled down, the pores where the water flow takes place may become so narrow that the flow regime can not be considered completely turbulent any more. In this case the viscous forces may become relevant and the conservation of the Froude number doesn't imply any more a good representation of reality. Such conditions can be recognized by a noticeable reduction of the Reynolds number in the model below the threshold value which identifies turbulent flow. The Reynolds number is defined as:

$$\mathrm{Re} = \frac{Ul}{\nu} \tag{2.16}$$

where ν is the kinematic viscosity of the water.

An estimation by Jensen and Klinting (1983) set this threshold value to 6000 for the armour layer of breakwater models, but in the inner parts of such models, due to the specific construction material, the limit between turbulent and laminar flow should be lower. In this respect, Jensen and Klinting pointed out the lack of a theoretical method to determine the flow field in a breakwater.

For the model of a breakwater core, in particular, the permeability of the material becomes a governing variable and the velocities U, as well as the hydraulic gradients I, are relevant parameters. The Forchheimer equation shown below is an estimation of I in the one-dimensional case of non-stationary flow (Burcharth and Andersen, 1995).

$$I = aU + b|U|U + c\frac{\partial U}{\partial t} \tag{2.17}$$

With a correct choice of the coefficients a, b, and c, Eq. 2.17 is suited to represent the water energy loss in the transition between laminar and turbulent flow.

Jensen and Klinting (1983) suggest an estimation of a different scale factor K to be applied to the diameter of the core material in the model, which would preserve the ratio of I between model and prototype if the time-varying factor in Eq. 2.17 is neglected. Assuming the same estimation of a and b for model and prototype, they found that K tends to $\lambda^{1/4}$ for low Re and tends to λ if Re goes to infinity. Intermediate values for K can be determined analytically.

In order to derive a scale factor for the size of the particles (D_{n50}) in the core of a breakwater, Burcharth et al. (1999) give a more detailed method which is such that the Froude scaling holds for a characteristic velocity $\bar{U}$, defined as the average pore velocity of 6 points located as shown in Fig. 2.12.

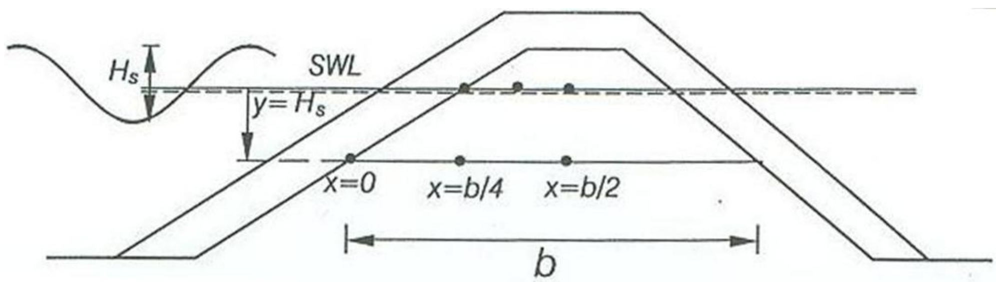

Fig. 2.12 – Representative points in the description of the flow inside the core according to Burcharth et al. (1999)

The method of Burcharth et al. is based on the possibility to estimate the pressure gradient in the points of Fig. 2.12 in a way which is alternative to the Forchheimer equation, if some hypotheses are done about the flow inside the structure. For example it is supposed that the core pressure induced by the waves varies in the horizontal direction following an exponential law:

$$p = p_0 e^{-\delta \frac{2\pi}{L'} x} \tag{2.18}$$

where δ is an appropriate damping coefficient and L' an estimation of the wave length inside the core. The horizontal coordinate *x* has its origin where the dissipation of the hydraulic pressure starts taking place, i.e. at the boundary of the core. Measurements from both physical models and a prototype (the Zeebrugge harbor outer breakwater) confirmed that the reference pressure p_0 can be estimated as:

$$p_0 = \rho_w g \frac{H_s}{2} \tag{2.19}$$

with no dependence on the vertical coordinate. Then the harmonic pressure oscillations in the core (neglecting the internal water set-up) can be calculated as below:

$$p(x,t) = \rho_w g \frac{H_s}{2} e^{-\delta \frac{2\pi}{L'} x} \cos\left(\frac{2\pi}{L'} x + \frac{2\pi}{T_p} t \right) \tag{2.20}$$

and *I* can be derived directly from the gradient of such pressure:

$$I_x = \frac{1}{\rho g} \frac{\mathrm{d}p(x,t)}{\mathrm{d}x} \tag{2.21}$$

The equation below is the Forchheimer equation (2.17) where *a* and *b* are specified according to Burcharth and Andersen (1995), *n* is the porosity and the “unsteady flow” term is neglected:

$$I_x = \alpha \left(\frac{1-n}{n} \right) \frac{\upsilon}{g D_{50}{}^2} \left(\frac{U}{n} \right) + \beta \frac{1-n}{n} \frac{1}{g D_{50}} \left(\frac{U}{n} \right)^2 \tag{2.22}$$

A suggestion for the definition of the coefficients α and β depending on the flow regime is also given by Burcharth and Andersen (1995).

The equalization of Eq. 2.21 and 2.22, provided that characteristic velocity $\bar{U}$ in the model corresponds to the prototype value in a Froude similitude, will provide the value of D_{n50} to be used in the model. The new D_{n50} will be related to the prototype nominal diameter by a different length scale. The value of the Reynolds number defined as:

$$\mathrm{Re} = \frac{\bar{U} D_{n50}}{\nu} \tag{2.23}$$

will provide insight of the actual regime of the water flow in the model, being Re involved in the definition of the coefficients α and β.

In the laboratory tests carried out within this study (see Chapter 3) the stability of the material constituting the model structure is investigated. Because of this reason, a differentiation of the scale factor for the nominal diameter of the stones is not considered as it would directly affect the evaluation of the stability phenomenon. Then, a scale factor as large as possible (about 15) will be assumed for all the geometrical parameters of the model with respect to a generic prototype. Nonetheless, one of the tests will be meant to investigate directly the influence of a reduced pore size in the structure, with all the other parameters kept constant with respect to the previous test. Then the values of pressure measured during the two tests can be used to apply in a quantitative way the method of Burcharth et al. presented above. Such analysis, combined with the actual behavior observed in the model, will allow an evaluation of the influence of scale effects.

2.6 Considerations on the effect of wide grading

At this stage, the findings of previous research about the effect of grading on the stability of rubble mound structures can be summarized.

The authors who considered only relatively low values of the grading (Van der Meer, 1998; Mansard et al., 1996; Van der Meer et al., 1996; Juhl and Sloth, 1998) found a negative effect of an increase of grading in the stability. Juhl and Sloth directly related this phenomenon with the reduced permeability, with smaller stones partly filling the voids between the larger ones: in this way the energy dissipation is reduced and the instability enhanced.

Hall and Kao (1991) investigated a wider range of values for the grading and confirmed this trend for the narrow gradings, pointing out a reverse trend if the grading increases: above a certain threshold value, the presence of big stones in the material results in a increased stability. Hall and Kao proposed an empirical formula for the estimation of the recession of the berm of a breakwater. In their formula, a transition value for the grading giving minimum stability (Par. 2.4) can be deduced.

Tørum et al. (2003) also derive from laboratory tests a formula for the estimation of berm recession. In their formula the quadratic term involving the parameter D_{85}/D_{15} determines a value for which the stability is maximum. No physical insight on this behavior is given by the authors.

All the previous considerations were derived from laboratory tests on berm breakwaters. The investigation on gravel beaches carried out by van Gent (1996) using a numerical model lead to conclusions similar to the ones of Hall and Kao. Van Gent also points out how the mechanism of segregation, simulated by his model, is at the basis of the increasing stability given by wider gradings. Occurrence of a segregation phenomenon is also clearly documented, referring to physical model tests, by Tørum (1998).

It should be noticed that in all the considerations reported above the values of the grading never exceeded 5.4. For structures made of dredged material or quarry run, reality shows how the ratio D_{85}/D_{15} can indeed reach values of 50 or higher. An example is given by Fig. 2.13, showing the limit curves for a number of grain-size distribution curves measured in a real project (Hydronamic, 2006).

Then, with reference to the different behaviors identified in the previous research, for materials like the ones typically found in the core of a coastal structure it is expected that the segregation mechanism plays a fundamental role.

Commenting the results of his laboratory tests, Tørum (1998) reports how a different grain-size distribution is observed between the toe of the structure and the stones at the still waterline. In particular, the size of the stones at the toe is significantly larger. Tørum explains this fact considering that the highest forces are exerted by the wave impacts in the area around the mean water level, and the bigger stones roll to a further location because of the momentum that they gain. This is in accordance with the behavior of a rock slide, where always the elements with biggest size are found at the bottom. Then it can be predicted that, with a very wide range of stone sizes, the mechanisms described above will be emphasized. For example, as studied by Rouault et al. (2005), a similar segregation phenomenon occurs in practice for a breakwater core already during the dumping of the material.

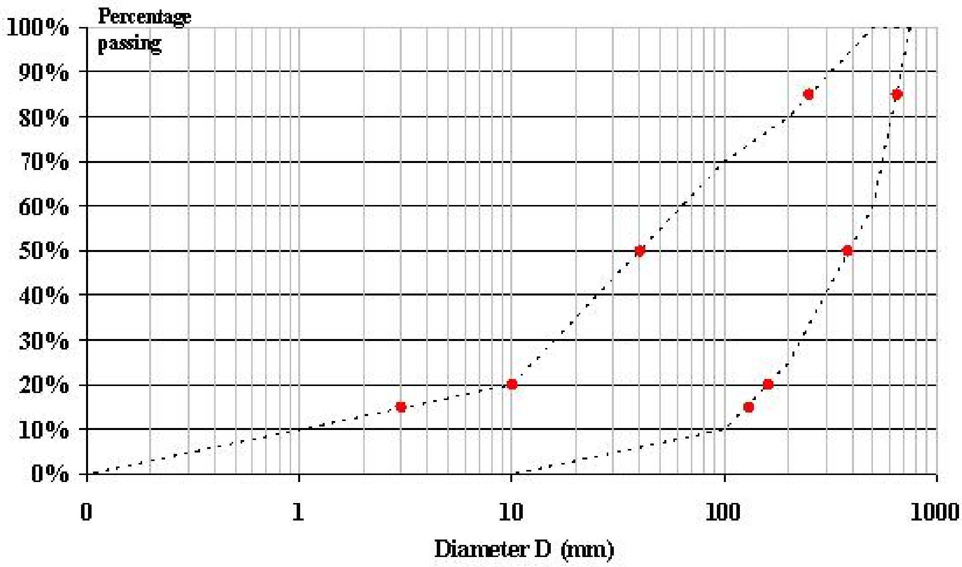

Fig. 2.13 – Example of grain-size distribution of quarry run (lower and upper limit) (Hydronamic, 2006)

The laboratory tests planned for this study will provide an opportunity to verify this prediction. Video recordings of the cross section will be carried out in order to capture the time development of the stone movements. The resulting grain-size distribution at different locations along the slope will be investigated in a qualitative way during the presents test series. Digital pictures will be taken and a possible use may consist of a deduction of the local grain-size distribution through an autocorrelation of the images where pixels of different color intensity identify the single stones. A way to carry out such analysis is presented by Rubin (2004).

Chapter 3

Set-up and execution of physical model tests

As described in the previous chapter, the choice of performing a physical model is suited for the present study, because phenomena like segregation of stones and water flow into a porous medium, which are expected to play a role in the reshaping of wide graded material, are not easily represented in different ways. The Delft University of Technology provided the laboratory facilities and all the support needed to carry out the test series.

In the following sections the tests will be described in detail. Firstly an overview on the main features of the tests will be given, with the identification of the main variables to be varied and investigated. Then all the parameters which play a role will be quantified, with an explanation of the all the choices that have been done according to theoretical and practical considerations.

This leads to a description of the testing procedures, followed by a brief summary of the overall test program. In conclusion, some relevant sources of inaccuracy of the measured data, mainly due practical aspects of the execution of the tests, will be presented.

3.1 Overview of the tests

Physical model tests are usually carried out to reproduce, in a reduced geometrical scale, phenomena which cannot be measured in the real scale and are not easy to describe or interpret analytically. The model has then the purpose to show the behavior of the prototype in a way that such phenomena can be directly observed and more easily studied.

The tests described below were not carried out with the aim of analyzing the behavior of a specific existing structure. By contrast, they are meant to give an answer as general as possible about the influence of specific parameters in the response of a range of rubble mound structures when exposed to a wave attack.

As presented in the above chapters, the parameters which govern the behavior of a coastal structure are manifold. They can be classified in general as follows, as suggested also by Hughes (1993):

- Geometrical parameters: dimensions of the structure, seaward slope, crest height and width, etc.
- Characteristics of the constituting material: dimensions and grading of the stones, shape of the single elements, permeability of the structure, etc.
- Hydraulic conditions and loads: wave height, wave period, mean water level, etc.

It is commonly accepted in literature that the median nominal diameter D_{n50}, synthetically describing the dimensions of the material, is directly related to the stability of a rubble mound structure. On the other hand in the present study the stability phenomenon is investigated with respect to the variability of the grading of the constituting material, given by the ratio D_{85}/D_{15} (see Par. 3.2.1 for a definition of the parameters involving diameters). In particular, the range of this parameter reproduced in these tests is very wide compared to the values chosen by previous researchers (see Chapter 2), and this fact constitutes the main significance of this study.

In the present case, the same D_{n50} was chosen for all the constituting materials, which would result in a comparable overall stability of the tested structures. On the basis of this common "background", the effects of the variation of the parameter grading are expected to be more evident. This way of proceeding is in accordance with the common practice for laboratory tests, which is to investigate the influence of specific parameters keeping others as constant as possible (Hughes, 1993).

Due to the limited time available and to practical reasons, choices had to be made about other parameters to vary. Regarding the geometry of the structure, specific tests will be meant to investigate the influence of the initial seaward slope in the reshaped profile. As for the hydraulic conditions, the load in terms of height and period of the waves will be varied within a range typical of storms with low return period: they are meant to represent the loads on a structure which is exposed to storms during the execution of maritime works. The water level, instead, is kept constant in all the tests.

3.2 Model set-up

3.2.1 Nominal and sieve diameters

At this stage the notation adopted for the diameters has to be clarified. The materials used in the tests consist of both sand and stones: the grain-size distribution of the different classes has been determined by weighting (for stones) or sieving (for sand).

The material passing through a series of sieves can be characterized by the sieve diameters (D). The diameter of the sieve through which the 50% by weight of a sample of sand passed gives the value of D_{50} for that sand. In practice, sieves with standard openings are used and the value of D_{50} is obtained through linear interpolation.

On the other hand, from the mass M of a stone it is possible to derive the nominal diameter D_n according to the following definition:

$$D_n = \sqrt[3]{\frac{M}{\rho}} \qquad (3.1)$$

where ρ is the dry density of the stone. The nominal diameter is thus defined as the dimension of an ideal cube of mass M and is not a dimension directly visible.

According to the Rock Manual (CIRIA/CUR/CETMEF, 2007) the nominal diameter and the sieve diameter can be related as follows:

$$D_n = 0.84D \tag{3.2}$$

meaning that through a sieve with square openings characterized by a diameter D the biggest passing sand grain has a nominal diameter equal to $0.84D$. This specific coefficient is valid for stones of common angular shape.

Then for each class of stones the median nominal diameter D_{n50} can be defined as:

$$D_{n50} = \sqrt[3]{\frac{M_{50}}{\rho}} \tag{3.3}$$

where M_{50} is the weight which is exceeded by the heaviest 50% (by weight) of the constituting elements.

Similarly, for all the sand and stones samples the values of D_{n85} and D_{n15} can be calculated, and the ratio of these values gives the grading of a certain material. In this thesis, the subscript *n* is always specified to indicate the median nominal diameter while it is omitted in the parameter grading.

3.2.2 Structure geometry and composition

The tests will be carried out on a simple structure with trapezoidal shape, made of homogeneous material, on a horizontal bottom. The only varied parameter in the geometry is the seaward slope α, which assumes the values 1:1.5 and 1:3. The cross sections of the model structures with the two different layouts of the seaward slope are shown in Fig. 3.1.

The slope value of 1:1.5, being close to the natural slope angle of loose material, is representative of the common practice for a mass of stones which has not usually strict geometrical requirements in the design. The value 1:3 is investigated to quantify the improvement of stability due to a milder slope, although this implies the need of a bigger amount of material which is not the usual choice for economical reasons. On the other hand, even if literature shows that the different initial slope should not influence the resulting slope for a long part of the profile (van der Meer, 1988), the milder slope should at least determine a smaller stone movement which means, potentially, a smaller volume of structure to be repaired.

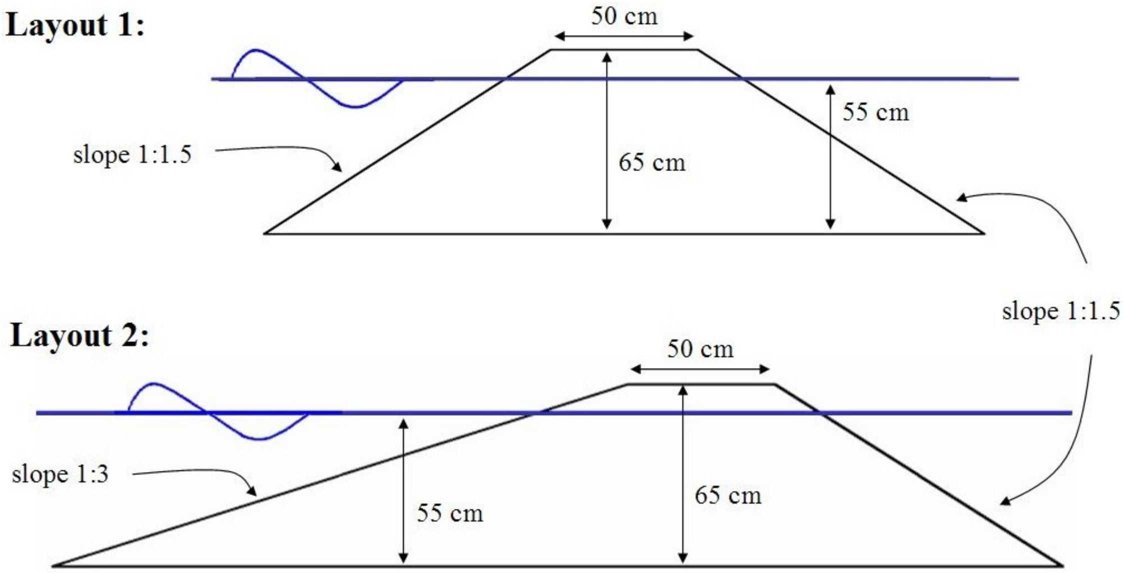

Figure 3.1 – Layouts of the model structure

The height of the crest above the mean water level is always equal to 10 cm. This choice is representative of the common practice for land-based structures which need a certain freeboard above water level to allow the transit of vehicles during construction. Nevertheless, the crest freeboard is a variable which may have influence on phenomena such as overtopping or wave transmission. As these phenomena are not directly of interest in this study, no variability of the crest height is intended during the test series.

In the two layouts shown above, being the width of the flume equal to 80 cm, the volume of the structure is 0.77 m^3 and 1.02 m^2 respectively. Approximate values for stone density and porosity ($\rho = 2650$ kg/m^3, $n = 0.4$) set the amount material needed for each structure to about 1225 kg and 1620 kg respectively.

The dimensions of the tested structure are such that it can be considered as the model of a prototype with a geometrical scaling of about 15. Again, it should be reminded that this model is not meant to reproduce a specific real structure, but the chosen dimensions are representative of a wide range of possible existing cases.

A summary of the grain-size distribution of the 7 classes of material available to build the structure is given in Tab. 3.1. The grain-size distribution of the single fractions is shown in Fig. 3.2 (sand) and 3.3 (stones).

Class	*Typology*	D_{n15} *(mm)*	D_{n50} *(mm)*	D_{n85} *(mm)*	ρ *(kg/m^3)*
1	Sand 0-3 mm	0.16	0.51	1.33	2650
2	Sand 1-3 mm	1.00	1.64	2.32	2650
3	Stones 2-6 mm	2.6	3.4	4.4	2598
4	Stones 8-11 mm	6.0	7.6	8.6	2652
5	Stones 11-16 mm	9.8	11.4	13.5	2648
6	Stones 20-40 mm	19.7	22.1	24.8	2664
7	Bigger stones	27.0	32.5	37.0	2697

Table 3.1 – Characterization of the 7 classes of stones and sand

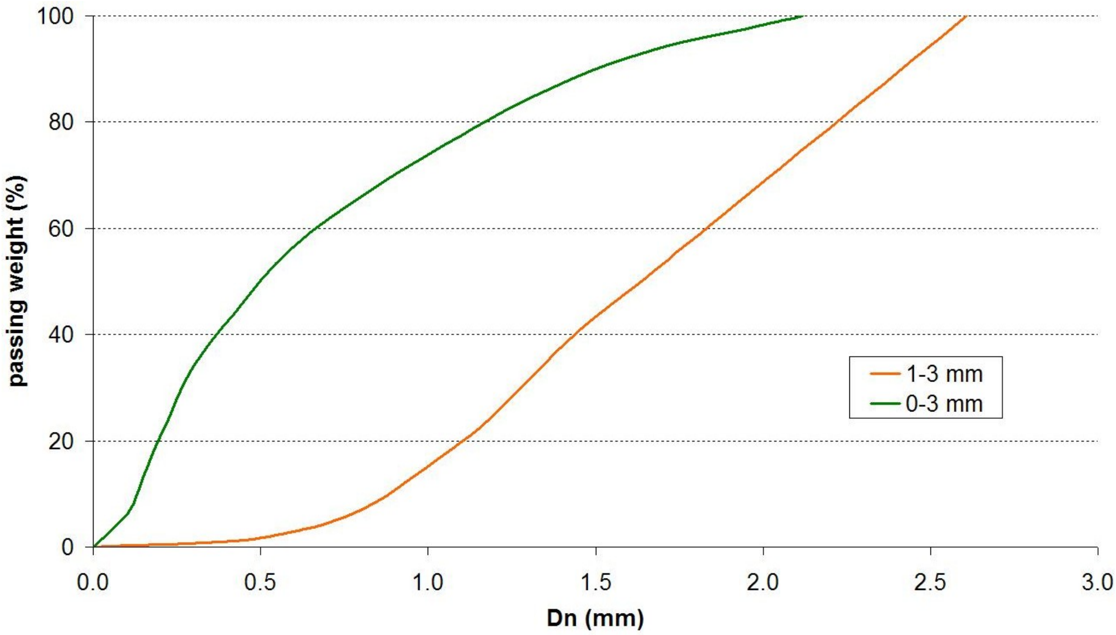

Figure 3.2 – Grain-size distribution of the 2 classes of sand

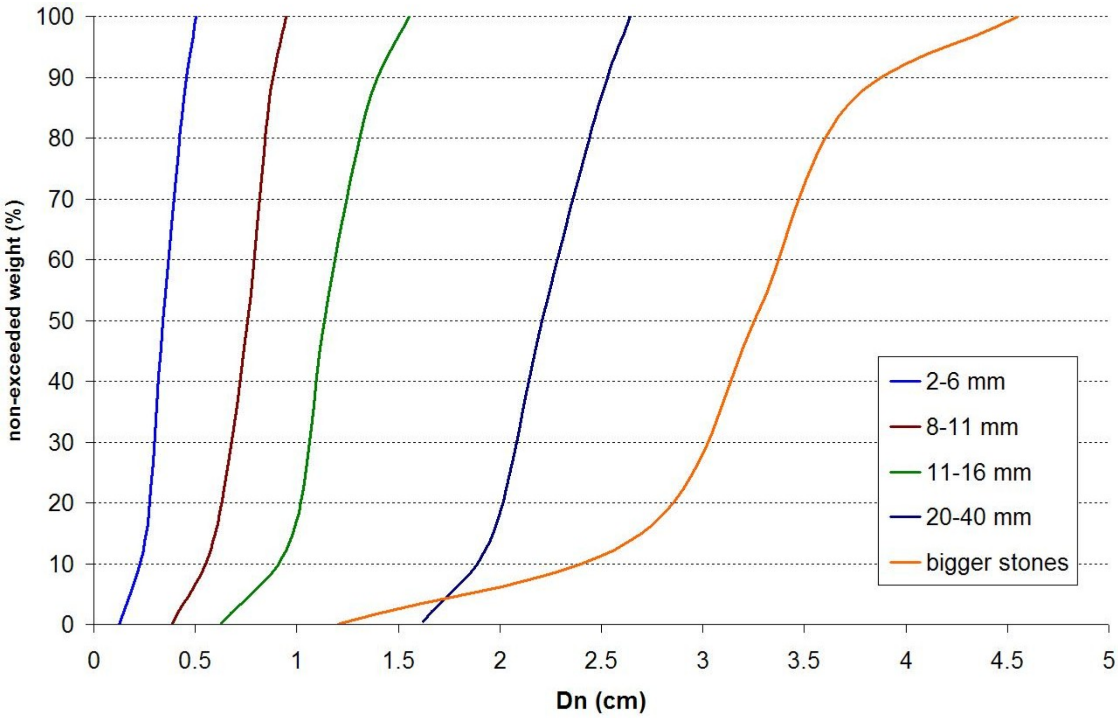

Figure 3.3 – Grain-size distribution of the 5 classes of stones

For the stones the density has been calculated, after weighting a sample both in air (M_a) and in water (M_w), through the following formula:

$$\rho = \frac{M_a - M_w}{M_a} \rho_w \qquad (3.4)$$

where $\rho_w = 1000$ kg/m^3 is the density assumed for clear water (used in the measurement). Pictures of the 7 fractions of materials are shown in Fig. 3.4.

The mixtures to be used in the tests are meant to represent dredged material or quarry run, which are characterized by small size and wide grading. Data form real projects provided by Royal Boskalis Westminster nv show that the grading can reach values up to 50 or higher. However, according to the initial planning of the tests (see Par. 3.1) the available 7 classes of sand and stones have to be combined in order to obtain homogeneous mixtures with the same D_{n50}.

At this stage of the test planning, practical limitations due to the time and material available play a role. As video recordings and pictures will be taken during the tests, the water in the flume has to remain rather clean: for this purpose a preliminary washing of the stones is required. The fastest way to wash stones of such dimensions is using a high pressure water jet with the stones spread on the floor and shaked manually: this operation was conveniently done in a separate space, outside the building of the laboratory (see Fig. 3.5). The time needed for this operation, combined with the fact that some of the stone classes had to be ordered and required days to be available at the laboratory, limited the actual usable amount of each class of stones within a range of 350-700 kg.

Figure 3.4 – The 7 classes of stones and sand

Figure 3.5 – Washing of the stones

Given then the requirement of an equal D_{n50} for all the mixtures, but with the widest range of gradation as possible, the compositions of the materials to be used in the tests cannot be of arbitrary choice. Considering the volumes of stones needed to build the two layouts of the model structure, it was possible to plan a test series involving four different mixtures. Tab. 3.2 explains the composition of each of them, while Tab. 3.3 and Fig. 3.6 illustrate the resulting grain-size distributions.

	Classes (% of the total mixture)						
Material	*1 (sand)*	*2 (sand)*	*3 (stones)*	*4 (stones)*	*5 (stones)*	*6 (stones)*	*7 (stones)*
I - intermediate grading (2.71)				30.3	50.0	19.7	
II - wide grading (7.44)			21.3	18.3	25.3	17.1	18.0
III - very wide grading (17.7)		22.6	11.6	10.0	13.8	14.7	27.3
IV - very wide grading (17.7) with fines	7.0	16.3	8.4	11.5	17.3	19.8	19.7

Table 3.2 – Composition of the four different tested materials

Material	D_{n15} *(cm)*	D_{n50} *(cm)*	D_{n85} *(cm)*	$\frac{D_{85}}{D_{15}}$	ρ *(kg/m^3)*
I - intermediate grading (2.71)	0.75	1.09	2.04	2.71	2652
II - wide grading (7.44)	0.37	1.10	2.74	7.44	2650
III - very wide grading (17.7)	0.18	1.10	3.23	17.7	2659
IV - very wide grading (17.7) with fines	0.17	1.10	2.93	17.7	2657

Table 3.3 – Grain size distribution of the four different tested materials

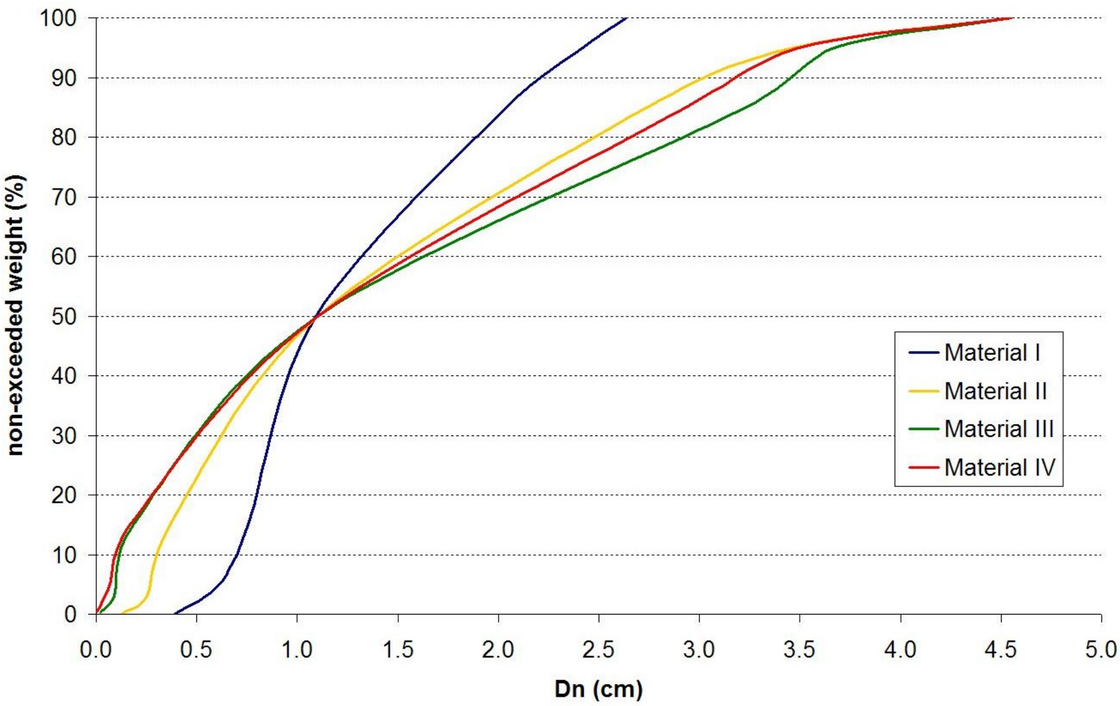

Figure 3.6 - Stone size gradations of the tested materials

In the first test a material with a relatively low value of grading (2.71) will be studied, in order to provide a reliable term of reference with tools to estimate the reshaping provided in literature. Material IV has the same parameterization of the previous one (in terms of D_{n50} and grading) but the presence of more fine particles in the overall grain-size distribution will result in a reduced porosity. A comparison with the results given by material III will show a direct influence of the porosity and, as a consequence, of permeability. The pressure measured inside the structure, by virtue of the considerations of Par. 2.5, may eventually provide more information about the scale effects in the model.

3.2.3 Hydraulic load

The load on the structure consists of irregular waves characterized by a JONSWAP spectrum ($\gamma = 3.3$), produced by a mechanical piston-type wave generator. The generator was able to provide reflection compensation. However this system was not used in all the tests because an excessive horizontal displacement of the paddle of the generator was required to compensate the reflection of the highest wave trains.

Fig. 3.7 shows the stages for the input to the wave generator. Firstly a *.pcf* file is created, which can be accessed by a text editor and contains all the main input variables (including H_s and the peak period T_p). Then the application *Multilin.exe* developed by Delft Hydraulics (now Deltares) elaborates the input, giving as output a *.dat* file containing a time series of water level, i.e. the wave to be generated. Details on the implementation of the *Multilin.exe* application are found in Verhage and van Dongeren (2003). On a different computer, the DOS application *CDCWave.exe* processes that time series and governs directly the movement of the wave generator through an analogical input.

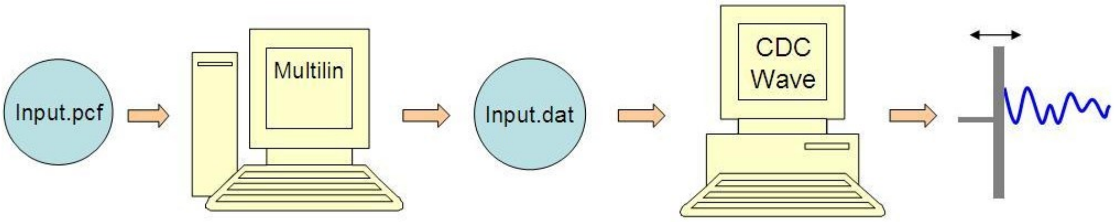

Figure 3.7 – Steps in the wave generation

Due to the processing of the digital signal in the *.dat* file, the input to the wave generator does not actually coincide with the measured output. Moreover, different wave reflection was induced by each of the structures built in the flume, and this did not allow the repeatability of the generated wave, in terms of H_s and T_m, for the same input. As a consequence, the wave input was determined every time according to the observed output of the previous tests: the duration of the test and the period of the waves were chosen with the objective of having 2000 waves in each train.

This procedure did not result in a constant output in terms of wave steepness, considering also that the reflection compensation being switched on or off reduced the predictability of the wave generation. Without reporting the parameters of every single wave train, Tab. 3.4 summarizes in a number of classes (characterized by the same input to the generator) all the waves produced in the test series. The first row in the table represents the first wave tested, when no previous wave trains were available for a calibration of the input: due to the particularly low steepness this wave train represents somehow an outlier, although it is not excluded from the overall data analysis. The following wave classes are listed in order of increasing load for the structure.

In summary, the wave loads on the structure correspond, for a prototype case scaled up to a factor 15, to storms with a range of significant wave height given by $H_s = 1 - 2\ \mathrm{m}$. This values are suited to represent, depending of course on the local wave climate, storms characterized by return period of approximately 1 year, which means storms likely to occur during the construction stages of the structure.

H_s (cm)	T_m (s)	s_m	reflection compensation
7.2	1.50	0.021	yes
7.0 - 7.1	0.96 - 0.97	0.048 - 0.049	yes
8.3 - 8.7	1.07 - 1.09	0.046 - 0.048	yes
9.7 - 10.7	1.17 - 1.21	0.046 - 0.048	yes
10.4 - 12.4	1.27 - 1.33	0.042 - 0.045	yes
10.5 - 12.1	1.43 - 1.47	0.33 - 0.036	no
11.2 - 12.0	1.50	0.032 - 0.034	no
12.4 - 13.4	1.68 - 1.69	0.028 - 0.030	no

Table 3.4 – Summary of the tested wave trains

3.2.4 Instrumentation

Besides the wave generator, other instrumentation installed in the flume consisted of 6 wave gauges and 3 pressure sensors. A description of their set-up is given below.

The wave gauges have the objective of recording the water level at different locations along the flume: three of them are located at 10 m from the structure (16 m from the wave generator), while the remaining three are placed 4 m in front of the structure. Only the measurements of the latter are used, but whether the reflection of the structure may disturb the wave signal, the gauges further away from the structure provide a better measurement.

The digital signal from the wave gauges is in volts and a calibration of the instruments was necessary to obtain the appropriate scale factor (in m/V) to which the measured signal has to be multiplied. The calibration consisted in the measurement of different output signals corresponding to known values of still water level set in the flume. An appropriate MATLAB routine commonly used in the laboratory computes, given the signal of the three gauges, all the necessary parameters to characterize the waves actually travelling in the flume, providing also the distinction between incident and reflected wave.

In particular, the mean spectral wave period presented in Tab. 3.4 and assumed further on in the data analysis is calculated from the 0-order and the 2-order moments of the incident wave signal:

$$T_m = \sqrt{\frac{m_0}{m_2}} \qquad (3.5)$$

The moments m_0 and m_2, as well as the incident significant wave height H_s, are given as output by the MATLAB routine.

A picture of the wave generator and of the three of the wave gauges is given below.

Figure 3.8 – The wave generator and three wave gauges

Pressure sensors were put inside the structure in order to keep track of the propagation of the wave oscillations through the porous medium constituted by the rubble mound. Locations were it is significant to measure the pressure are the toe of the structure (where the oscillations are not yet influenced by groundwater flow), mid-length of the seaward slope, the outer and inner edge of the structure crest.

The pressure sensors were placed at the bottom of the flume: by this way the movement of stones could not interfere with the cables providing air to the sensors, and vice versa the rigid lodging of the instruments did not affect the reshaping phenomenon. Nevertheless, one of the four sensors put in place did not provide a reliable measurement and during each test only three time series of pressure values were actually collected. The positioning of the sensors is described below, and Tab. 3.5 provides the x-coordinate of the location of the sensors if the toe of the structure is chosen as origin. The offset from the bottom of the flume was always equal to 3 cm.

In Test 1, the pressure sensors properly working were located as shown by the red dots in Fig. 3.9.

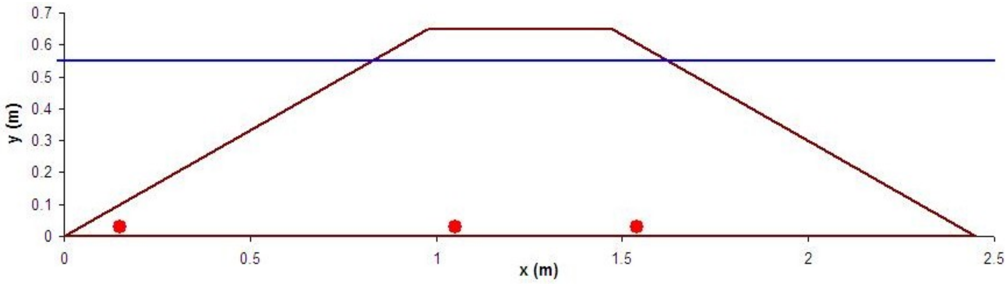

Figure 3.9 – Positions of the pressure sensors during Test 1

As for the following tests a structure with milder slope had to be built, the relative positions of the two structures was chosen in order to provide clear visibility of the reshaping area through the glasses of the flume. The model with slope 1:3 was built without complete removal the material constituting the previous structure: this choice allowed a considerable time saving in the execution of the tests. The resulting layout of the flume is shown in Fig. 3.10, with the same relative positions of the sensors because of a failed attempt to repair the faulty sensor after the removal of the first model structure.

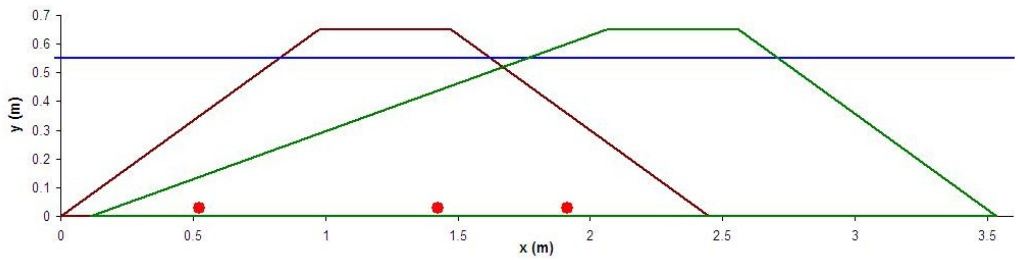

Figure 3.10 – Positions of the pressure sensors during Tests 2-5

Before the execution of Test 6, the position of two of the sensors were switched in order to leave the faulty one on the extreme right. The resulting points where the pressure was measured in the remaining tests are shown in figures 3.11 and 3.12.

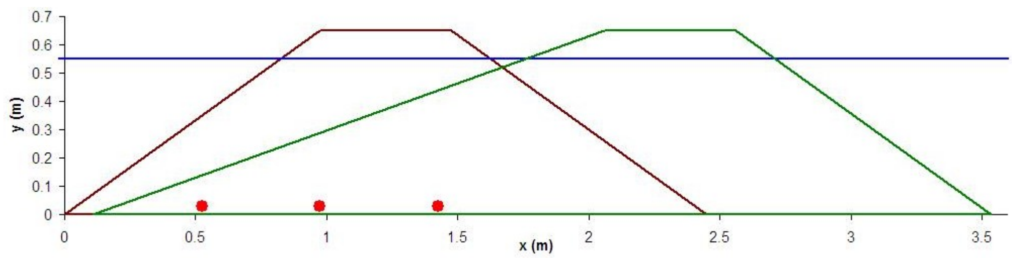

Figure 3.11 – Positions of the pressure sensors during Tests 6-8

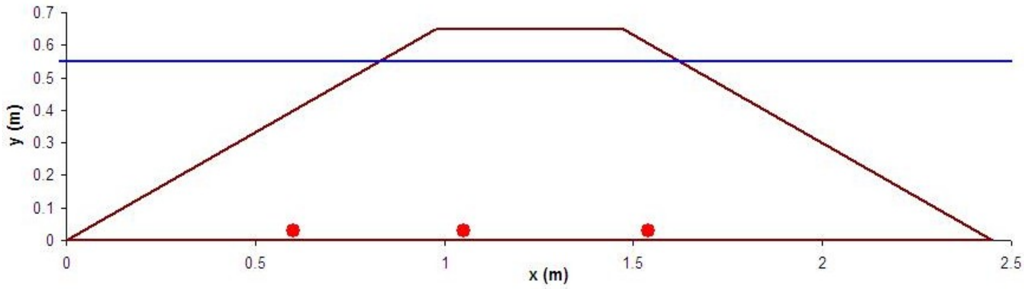

Figure 3.12 – Positions of the pressure sensors during Test 9

Test n.	**1**	**2-5**	**6-9**
x sensor 1 (cm)	15	52.5	52.5
x sensor 2 (cm)	105	142.5	97.5
x sensor 3 (cm)	154	191.5	142.5

Table 3.5 – Summary of the locations of the pressure sensors

Figure 3.13 – The lodging of sensors in the flume (left) and during calibration (right)

Due to the accuracy of the measurement that the pressure sensors can provide, a calibration of these instruments was carried out before and after the test series. As for the wave gauges, the calibration aimed at the definition of the scale factor (in m/V) to be multiplied to the measurements. Figure 3.13 shows the lodging of the sensors placed in the flume (left) and inside the separate basin where the second calibration was carried out (right).

3.3 Testing procedure

The material for the model structures are obtained mixing together, in different proportions, the seven narrow-graded classes of sand and stones. The tests are ordered according to an increasing value of the grading. This sequence has to be chosen for practical reasons: due to the limited amount of material available, the stone constituting a mixture will be used in the preparation of the next mixture together with new material from the original classes.

Then, the building of the model structure needs particular care to avoid segregation which can easily determine a local ratio D_{85}/D_{15} significantly different from the design value. Segregation may happen during the transportation of the material from the concrete mixer to the flume: this was done with 60 kg of mixture at a time using wheelbarrows conveniently lifted by a crane and set down into the flume. Some of the steps in the building the model structure are summarized by Fig. 3.14.

Figure 3.14 – Phases of the construction of the model structure

At the very beginning of the test series, a first wave attack was held for 3 hours (= 7300 waves, about 12 h in a prototype with a scale factor of 15) in order to have a first feeling of the development of the profile reshaping in time. Then the seaward slope of the model was reconstructed and all the following trains were made of approximately 2000 waves, quantity which was considered reasonably sufficient to reach an equilibrium profile (See also Par. 4.1).

Seven of the nine tests (according to the classification of Tab. 3.6 in the next paragraph) consisted of a succession of wave trains characterized by increasing wave height until the initial crest of the structure was completely destroyed: normally this happened after 5 wave trains. Two of the tests, instead, consisted of a single attack of 3000 high waves: by this way the influence of the "load history" could be assessed as these test, except for the typology of wave attack, had the same input condition (geometry, grading of constituting material) of others. The model structure is rebuilt at the end of every test, while the reshaped profile in the middle of the structure is measured mechanically at the end of the attack of each wave train.

The development of the profile of the model structure was recorded on video during the first half of each wave attack, when most of the reshaping takes place. After the second and the last wave attack of each test digital images of the reshaped slopes were taken, in order to capture the local grain size distribution resulting from segregation and transport of stones.

3.4 Summary of the test program

According to the available time for laboratory tests (5 weeks), nine tests were performed.

Test n.	D_{85} / D_{15}	α	Features
1	2.71	1:1.5	
2	7.44	1:1.5	
3	7.44	1:1.5	Repetition with same "input"
4	7.44	1:1.5	Only high wave attack
5	7.44	1:3	
6	17.7	1:1.5	
7	17.7	1:1.5	Only high wave attack
8	17.7	1:3	
9	17.7	1:1.5	Fine sand included

Table 3.6 – Overview of the test series

As every wave train was characterized by unique values of H_s and T_m, in Tab. 3.6 the main characterization of each test is given in terms of:

- Grading of the constituting material (D_{85} / D_{15});
- Slope of the seaward side of the structure (α);
- Other specific features of the test.

A detailed list of all the input parameters of every test is given in Appendix A.

3.5 Uncertainties and limitations of the measured data

The following list briefly summarizes the set of data collected during the whole test series:

- Profiles of the middle cross-section of the structure, measured mechanically after the attack of every wave train (see Appendix B);
- Video recordings of the evolution of the profile during approximately the first half of every wave attack, when most of the reshaping phenomenon takes place;
- Digital pictures of the reshaped slopes taken, after the second and the last wave attack of each test, at significant locations, i.e. where a modified grain-size distribution in the surface stone layer was visible;
- Continuous measurements of the water level both in front and far from the structure;
- Continuous measurements of the pressure at three different location inside the structure;

The pictures may be used to determine in a quantitative way the local grain-size distribution, in the same way suggested by Rubin (2004). The video recording can not provide a precise representation of the reshaped profile as a significant wall effect (see Fig. 3.15) was observed during some tests. This effect consisted in less erosion in some areas adjacent to the walls of the flume, with a direct influence on the cross-section captured by the camera. Nevertheless, the videos can provide full insight in the segregation phenomenon, as they show a time-space evolution of the movements of the different stone classes in the wide-graded mixture.

The data analysis of Chapters 4 and 5 is mainly based on the profiles measured midway in the width of the model structure. The mechanical device used for the measurements is shown in Fig. 3.16.

Figure 3.15 – Wall effect observed during Test 3 (left) and Test 5 (right)

Figure 3.16 – The mechanical device for measuring the cross-shore profile

The horizontal offset between single measured points was equal to 2 cm around the mean water level, where significant reshaping always occurred, and 5 cm elsewhere (see Appendix B). The receded edge of the crest was assumed at the intersection between the interpolated measured points and a horizontal line at the level of the structure crest.

The head of the measuring device consists of a flat square plate (5x5 cm). Although a spherical joint provided the possibility for the plate to be aligned with the local slope, the roughness of the surface, emphasized by the presence of big protruding stones, limited the accuracy of this measurement. Nevertheless, the vertical coordinate of each point is measured with the accuracy of a millimeter. This remark should be taken into account in a further utilization of these data.

Another uncertainty lies in the values of grading assumed for the different materials. Even though the stone-size gradations of the 7 original classes of sand and stones were measured accurately, local variations of this parameter within the same model structures are likely to occur. The unloading of the mixture from the concrete mixer into the wheelbarrow and then into the flume did not help in this sense. An initial segregation was actually observed already during the building up of the model, with the larger stones rolling down to the toe, and attempts to prevent this phenomenon were generally unsuccessful.

Finally, due to the small dimension of the material used in the tests, possible scale effect may have occurred. For this reason a specific test was planned with all the input variables equal to the ones of a previous test, but with a mixture of stones containing finer material. The measurements of pressure inside the model structure may also provide further insight into this aspect (see Par. 4.2).

Chapter 4

Analysis of tests results

The considerations derived in this chapter are mainly based on the reshaped cross-shore profiles of the model structure which were measured mechanically at the end of each single wave attack, consisting in most cases of 2000 irregular waves.

In all the tests the wave load was increased until complete failure of the structure was reached, i.e. the whole crest was washed away. For each test, the input parameters (geometry, material characteristics, hydraulic load) are given in Appendix A. The measured profiles, including both the front and the rear side of the structure whenever the latter was reached by the reshaping, are given in Appendix B.

Firstly, considerations will be made about the duration of the wave attack and the possible influence of scale effects. In this respect the results of Tests 4, 7 and 9, carried out with the objective of studying these specific features, will be analyzed.

Then a quantitative comparison between the prediction of available formulas and the observed features in the reshaping will be done, with focus on a specific parameter of interest for contractors (the recession of the crest) and on the overall layout of the profiles.

4.1 Effect of the duration of the wave attack

An issue which arises in the evaluation of the soundness of the data is whether an equilibrium profile was reached at the moment when the cross-shore measurement was carried out (about 2000 waves). From direct observations during the tests, the waves actually sent to the structure were reasonably sufficient to reach a stable profile: this is qualitatively shown in Fig. 4.1 to 4.3.

Tests 4 and 7 had the specific objective of showing the influence of the load history foregoing a certain wave attack. Fig. 4.4 and 4.5 compare the reshaping measured at the end of Tests 3 and 6 with the profile photographed after 2000 waves during Tests 4 and 7, when the same waves of the last train in Tests 3 and 6 were sent to the structure.

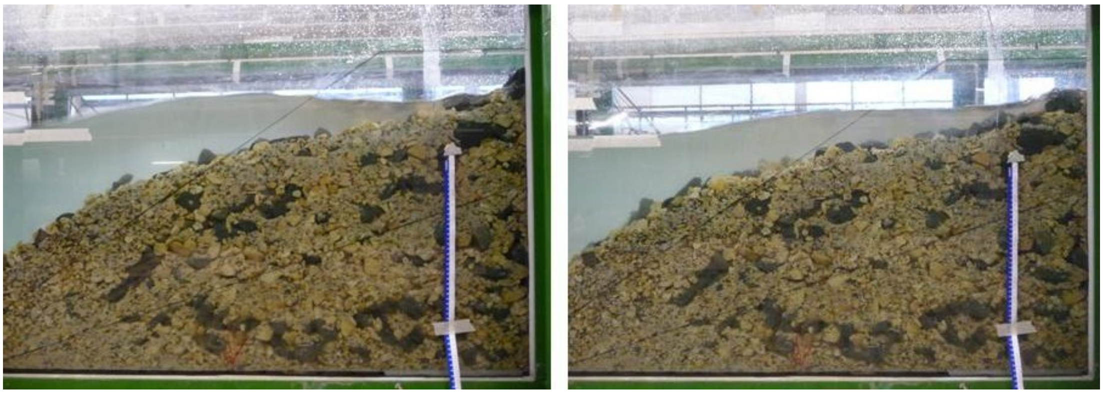

Figure 4.1 – Damage on the same structure during Test 6 after the attack of about 1000 (left) and 1500 waves (right)

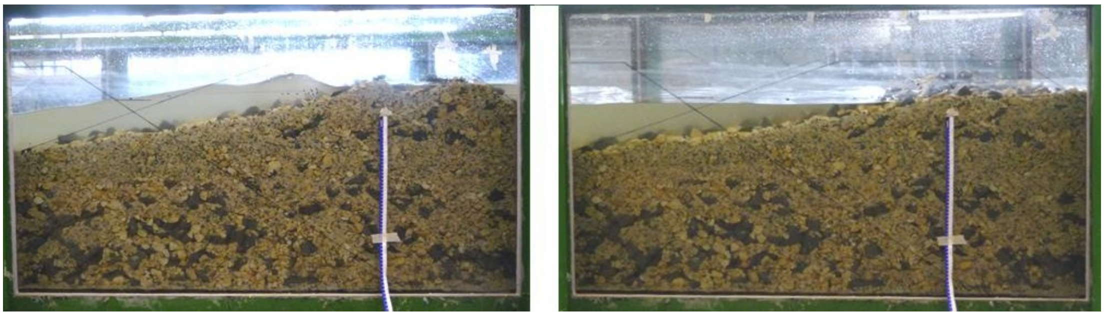

Figure 4.2 - Damage on the same structure during Test 8 after the attack of about 1000 (left) and 2000 waves (right)

Figure 4.3 - Damage on the same structure during test 9 after the attack of about 1500 (left) and 2000 waves (right)

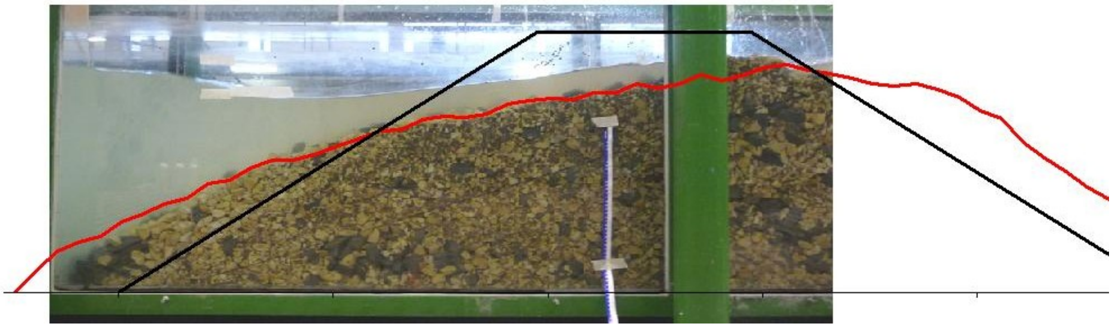

Figure 4.4 – Comparison between the profile measured at the end of Test 3 (red line) and the profile after 2000 waves during Test 4 (picture)

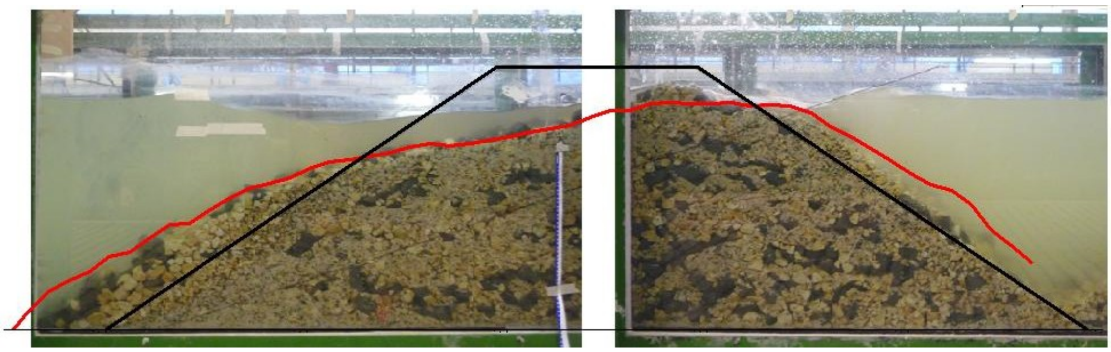

Figure 4.5 – Comparison between the profile measured at the end of Test 6 (red line) and the profile after 2000 waves during Test 7 (picture)

The figures above show a slightly larger reshaping at the end of Tests 3 and 6, in terms of both erosion of the crest and accretion of the toe. This could be due, however, to the wall effect explained in Par 3.5, according to which the reshaping captured during tests 4 and 7 is underestimated. The profiles measured at the end of Tests 4 and 7 (3000 waves) show that, anyway, some reshaping still occurs after 2000 waves.

From the above considerations it can be concluded that after an attack of few thousands waves the equilibrium profile is almost completely reached. This is only partly in agreement with the findings of van der Meer (1998), who found out that small reshaping of the structure can occur even after several thousands of waves. For this reason he included the parameter N (number of waves) in his prediction formulas for the profile development, although with small exponents (0.04 to 0.15).

As in the following sections a direct comparison between the measured profiles and the formulas of van der Meer will be done, the problem of associating an absolute number of waves (which considers the load history) to each reshaped profile should be addressed. Solution to this problem will be given in Par. 5.2.

4.2 Scale effects

Test 9 was carried out to investigate the behavior of a model built with a fraction of fine sand (material IV in Tab. 3.2), giving less permeability to the structure, with all the governing variables being the same of Test 6. The profiles measured in the two tests are compared in Fig. 4.6.

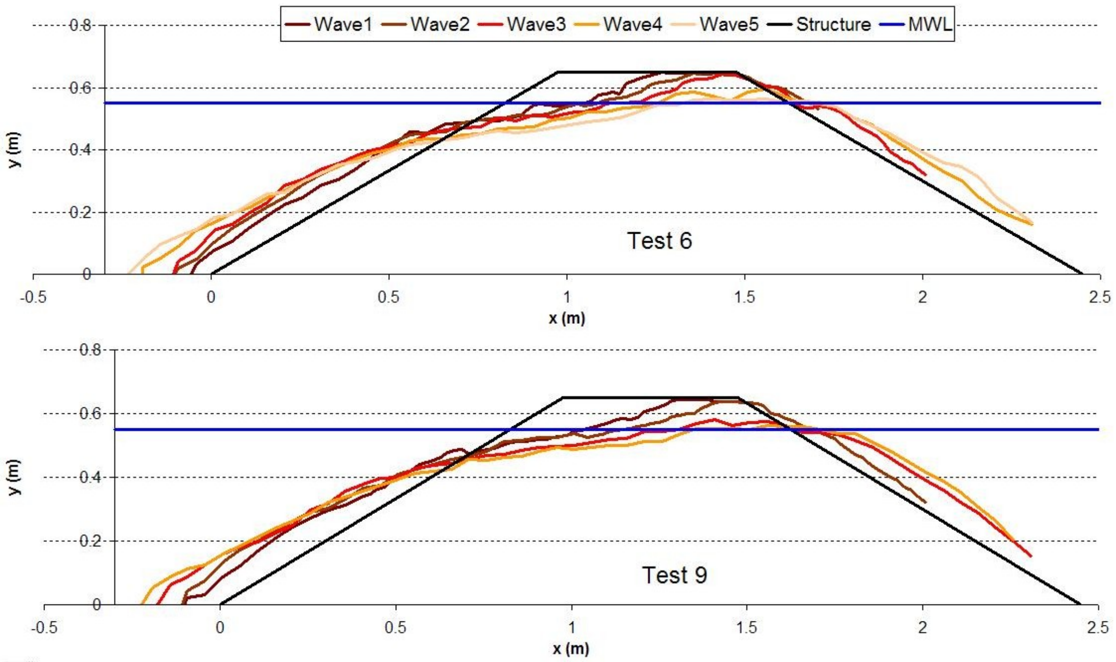

Figure 4.6 – Comparison between the results of tests 6 and 9

The graphs above shows how the evolution of the toe displacements does not differ much between the two cases, although in Test 9 the crest is eroded faster and the fifth wave train was not needed to induce a complete failure of the structure.

The interpolation of the pressure measurements obtained for tests 6 and 9, according to Eq. 2.18, gives values of the damping coefficient δ close to 0.2 and 0.4 respectively. Such low values do not provide a significantly different numerical result for the method of Burcharth et al. (1999), which means that the estimated ideal stone size for the model would be similar in the two cases.

However, more uncertainties in the application of such method lie in the evaluation of the coefficients α and β to be used in the Forchheimer equation. Burcharth and Andersen (1995) suggest ranges of values which do not lead to a clear estimation of a modified D_{n50}. Moreover, although both Burcharth and Andersen (1995) and van Gent (1995) predict a dependency of α and β on the grading of the material, no reliable estimations are given in literature for the very wide gradings considered in this study. The above considerations lead to the conclusion that the method of Burcharth et al. should not be applied quantitatively in this case.

The simplified method by Jensen and Klinting (1983), also introduced in Par. 2.5, may be by some extent more reliable because it does not require the definition of suited coefficients α and β for the model. Assuming α = 1500 and β = 3.6 (values typical of irregular angular grains), the Reynolds number defined by Eq. 2.23 (where the velocity is found according to Burcharth et al., 1999) is equal to about 10000, resulting in a suggested scale factor for the D_{n50} of about 12. This result is obtained for a wave load characterized by H_s = 0.1 m and T_m = 1.18 s on a structure with slope 1:1.5, and does not actually depend on the grading of the material.

Given the different properties of the model structures in terms of grain-size distribution and permeability, the last consideration shows that the geometrical scaling probably modified the flow regime inside the model structure with respect to an ideal prototype. What can not be estimated analytically is to which extent the stability of the material is affected: the magnitude of the differences in the reshaping between tests 6 and 9, together with the low values of the damping coefficient δ observed in both cases, suggest that the effect on stability of the presence of fine sand is small.

By virtue of all the above results, scale effects in the reshaping process of the different model structures are supposed to be small and therefore are neglected in the analysis that follows. However, because of the differences in the results of tests 6 and 9 (see Fig. 4.6), the latter is left out from the quantitative analysis carried out in the next sections.

4.3 Comparison of the reshaped profiles with the predictions of existing design tools

In the analysis that follows, only the results of the tests where the crest was not completely destroyed are considered, as only in these tests quantities like the crest recession or the average slope above mean water level can be actually measured. This restricts the set of data available for the quantitative analysis of the reshaping to 21 profile measured during Tests 1, 2, 3, 5, 6 and 8.

The comparison carried out in the next section will follow 2 main directions. First the formulas for the estimation of the crest recession are considered. Then the predictive capability of the whole profile reshaping of the method given by van der Meer (1988) will be assessed: this will provide the basis for the development of a design tool which may take into account the specific effect of the parameter grading.

4.3.1 Berm recession: Hall and Kao

The influence of the gradation of the armour stone was specifically studied in the laboratory tests carried out by Hall and Kao (1990, 1991). As a consequence, the range of values of D_{85} / D_{15} that they investigated covers most of the practical cases for big size stones. Nevertheless their highest value of 5.4 is not representative of the wide gradations which are found in quarry run.

In their formula for the estimation of the berm recession the authors used the parameter D_{50} instead of D_{n50} (see Eq. 2.6). The same formula modified in terms of nominal diameter is given by the Rock Manual (CIRIA/CUR/CETMEF, 2007):

$$\frac{\text{Rec}}{D_{n50}} = \left[-12.4 + 0.39 \left(\frac{H_s}{\Delta D_{n50}} \right)^{2.5} + 8.95 \frac{D_{85}}{D_{15}} - 1.27 \left(\frac{D_{85}}{D_{15}} \right)^2 + 7.3 P_R \right] \cdot \left[1 + \ln N_R{}^{0.11} \right] \tag{4.1}$$

In Fig. 4.7 the same formula is plotted against the measurements obtained in the present study, with the variable H_0 plotted in the *x*-axis given by:

$$H_0 = N_s = \frac{H_s}{\Delta D_{n50}} \tag{4.2}$$

In the curves representing Eq. 4.1 the parameter P_R (percentage of rounded stones) is assumed equal 0 and the number of waves is set to 2000 for all the measurements except the first one (for which N = 7300).

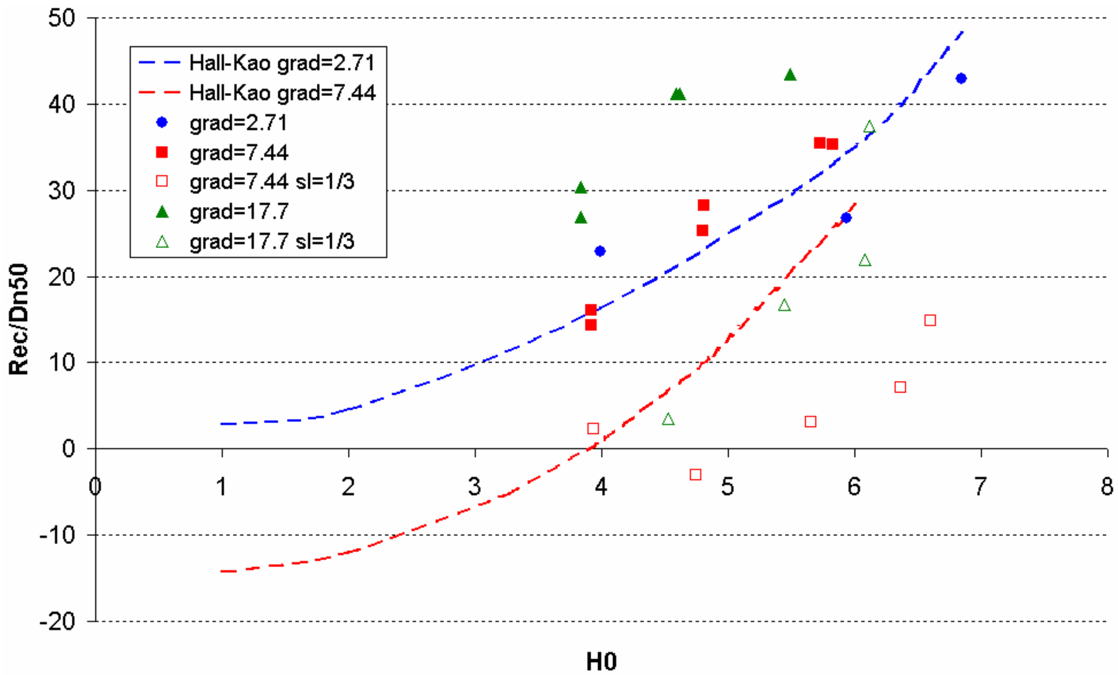

Figure 4.7 – Comparison between the measured data and the prediction by the formula of Hall and Kao

An evident response given by the graph above is that the estimations of formula 4.1 do not match in general with the points measured in the present laboratory tests. Even though a fair agreement could be observed for the narrow grading (D_{85}/D_{15} = 2.71), which is in the range of the values investigated by Hall and Kao, the cloud of points obtained for a grading of 7.44 cannot apparently be interpolated with a single function. The curve predicted for D_{85}/D_{15} = 17.7 is not plotted as it will lie far below the *x*-axis and such negative values of crest recession would not be realistic.

The curves by Hall and Kao in Fig. 4.7 confirm the trend observed by the authors which is an increase of stability for grading higher than about 3 (see Par. 2.2). This conclusion can not be drawn from the points measured in the present tests, which show decreasing stability for increasing grading.

This can be explained observing the resulting grain size distribution along the profile shown by Fig. 4.8, which refers to the third wave train of Test 3. In the left picture it is clear how the fine material (darker) is moved up into the more dynamic zone, around the mean water level, while the right picture shows most of the bigger stones fallen at the toe. With such an emphasized segregation, the mechanism hypothesized by Hall and Kao, i.e. the biggest stones providing more resistance to the wave action, can not occur as such stones are quickly moved away from the area where most of the wave action takes place.

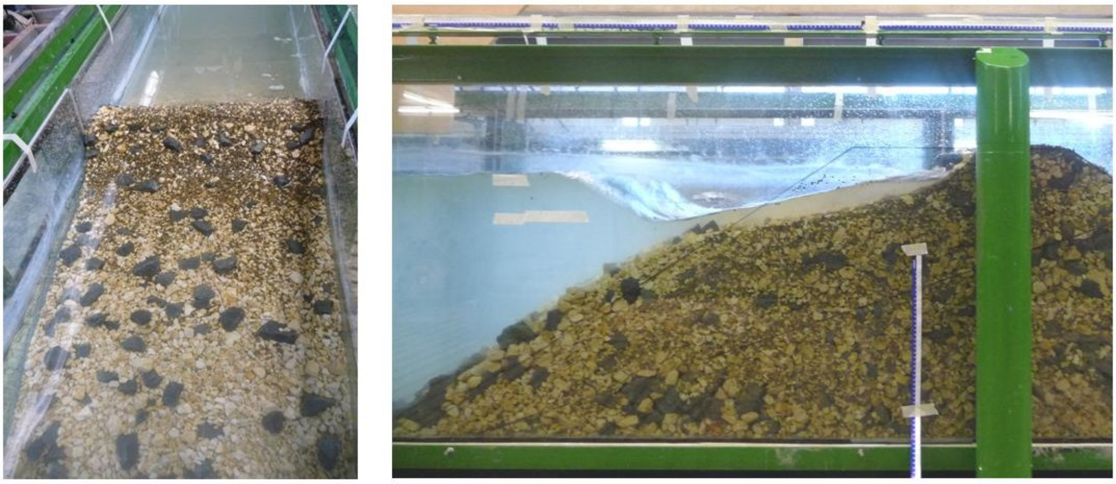

Figure 4.8 – Segregation observed during Test 3

The measurements show also that different initial slopes results in very different trends for the crest recession as a function of the parameter H_0. This is shown in Fig. 4.7 where the distinction between the tests is made, and the points found for a mild initial slope lay significantly below the points obtained for the same grading but a steeper initial slope, meaning that the mild slope results in less recession of the berm.

Given that the initial slope is strongly influencing the recession, it should be considered that the tests of Hall and Kao were performed on a structure with the seaward slope equal to 1:1.25 (see Fig. 4.9), which is supposed to be less stable than the slopes tested in the present study. This is somehow confirmed, for Test 1, by the two points characterized by high values of H_0 in Fig. 4.7, while the other measured recession is above the prediction of Eq. 4.1. However, this particular point was obtained after the attack of steeper waves, and should be considered as a sort of outlier in this case because the parameter H_0 doesn't take into consideration the period of the wave.

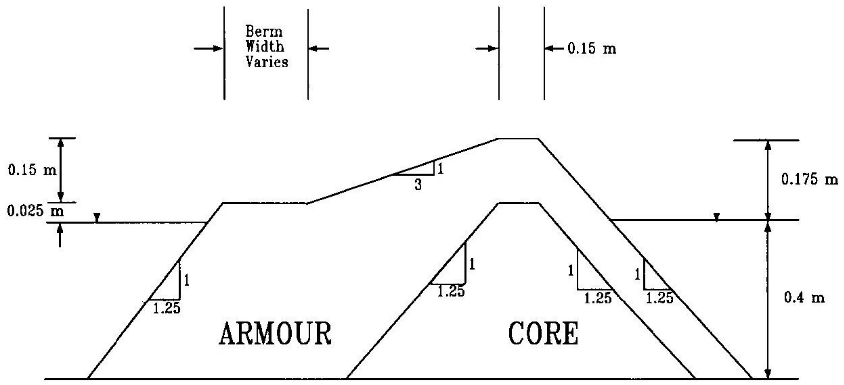

Figure 4.9 – Geometry of the structure tested by Hall and Kao

Common sense suggests that the berm height above the water level has also a direct influence on the resulting berm erosion. In both the test series considered this parameter was kept constant. The value of the freeboard was 2.5 cm for the tests by Hall and Kao (1.3 times the nominal diameter) and 10 cm in the tests of the present study (9 times the nominal diameter). This fact makes the quantitative comparison between the two sets of measured recessions less reliable.

4.3.2 Berm recession: Tørum et al.

Another empirical formula for berm recession as a function of the grading is given by Tørum et al. (2003). The equation is shown below, together with the definition of the factors involving grading and water depth:

$$\frac{\text{Rec}}{D_{n50}} = 0.0000027\left(H_0T_0\right)^3 + 0.000009\left(H_0T_0\right)^2 + 0.11\left(H_0T_0\right) - f\left(\frac{D_{85}}{D_{15}}\right) - f\left(\frac{d}{D_{n50}}\right) \quad (4.2)$$

$$f\left(\frac{D_{85}}{D_{15}}\right) = -9.91\left(\frac{D_{85}}{D_{15}}\right)^2 + 23.9\frac{D_{85}}{D_{15}} - 10.5 \qquad (4.3)$$

$$f\left(\frac{d}{D_{n50}}\right) = -0.16\left(\frac{d}{D_{n50}}\right) + 4.0 \qquad (4.4)$$

The authors specify the validity ranges of the equation (4.5 and 4.6). Then it should be noticed that not only the gradings, but also the water depth adopted in the present tests ($d / D_{n50} = 50$) are out of the range prescribed for the formula.

$$1.3 < D_{85} / D_{15} < 1.8 \qquad (4.5)$$

$$12.5 < d / D_{n50} < 25 \qquad (4.6)$$

As a result, the comparison between the prediction of Eq. 4.2 and the measured crest recessions shows poor agreement (see Fig. 4.10).

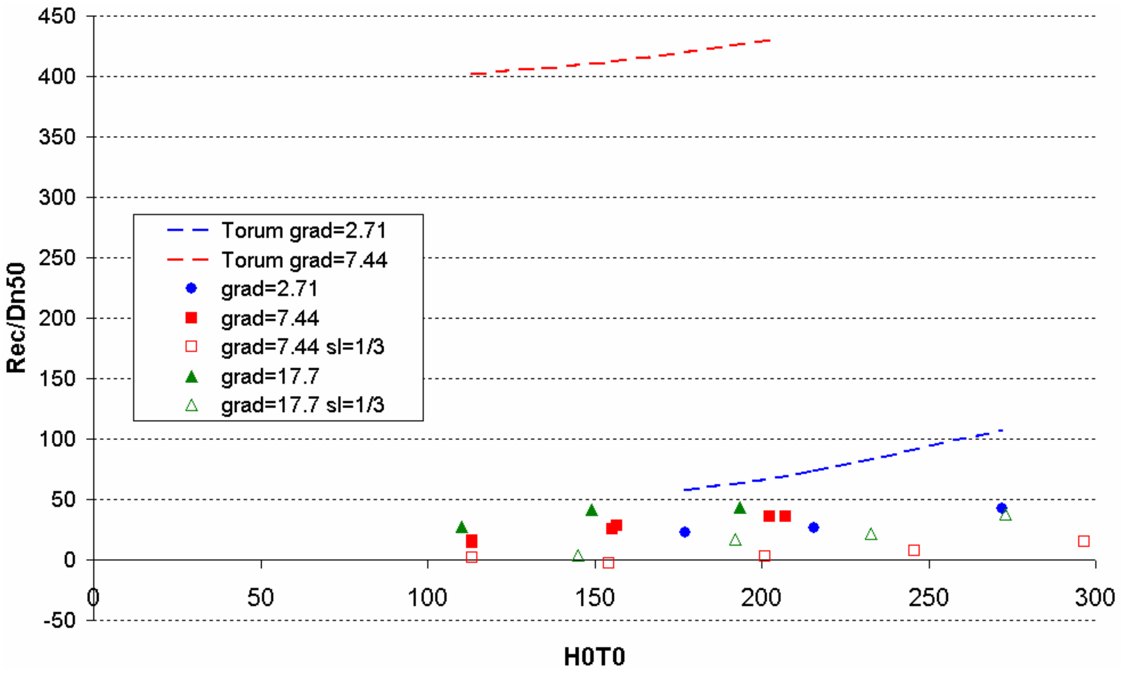

Figure 4.10 - Comparison between the measured data and the prediction by the formula of Tørum et al.

The estimation for D_{85}/D_{15} = 7.4 gives already values of Rec/D_{n50} which are 10 times bigger than the observed ones: this prediction is unrealistic and consists of an excessive extrapolation of the validity of the formula. The curve obtained for D_{85}/D_{15} = 17.7 would show values of the non-dimensional recession higher than 2500 and therefore it is not plotted.

In this case is even more clear how the extrapolation of the formula outside its validity ranges does not provide comparable results. Despite of the different order of magnitude in the values, the trend of decreasing stability for increasing stone size gradation is confirmed by the measured data.

A conclusion regarding the recession of the crest can be drawn at this stage, considering the trend in segregation shown by Fig. 4.8. Although both Hall and Kao and Tørum et al. investigated only rather low values of grading, the interpretation given by the formula of Tørum et al. seems more correct for wider gradings, as a strong segregation phenomenon would move up along the structure the finer stones, thus reducing the stability of the crest.

4.3.3 Profile: Van der Meer

While the formulas by Hall and Kao (1991) and Tørum et al. (2003) predicted only specific features of the reshaped profile, the formulas found by van der Meer (1988, 1992) for dynamic stability constitute a model able to predict in its overall shape the modified profile of a slope.

The description of the profile given by the formulas of the van der Meer requires as input a rather complete description of the profile to be reshaped, giving to the method a much more general nature. The software BREAKWAT, in which the complete set of formulas of van der Meer is implemented, requires the following input variables:

- The detailed geometry of the initial seaward side, including the water depth;
- The significant wave height and spectral mean period, H_s and T_m;
- The median mass of the constituting material, M_{50};
- The density of the dry material and of the water, ρ and ρ_w;
- The grading of the material, D_{85} / D_{15};
- The number of incoming waves, N;
- The angle of wave incidence, β.

The software was run reproducing the input conditions of the 21 wave attacks chosen for this quantitative analysis. The following graphs show the comparison between the prediction of BREAKWAT and the measured profiles. A number of waves equal to 2000 is given as input for all the profiles (except the first one, for which it was $N = 7300$) and β is always set to 0. First the comparison for the tests where the initial slope was 1:1.5 is presented. The origin of the *x*-axis in the graphs corresponds to the inner edge of the crest of the structure.

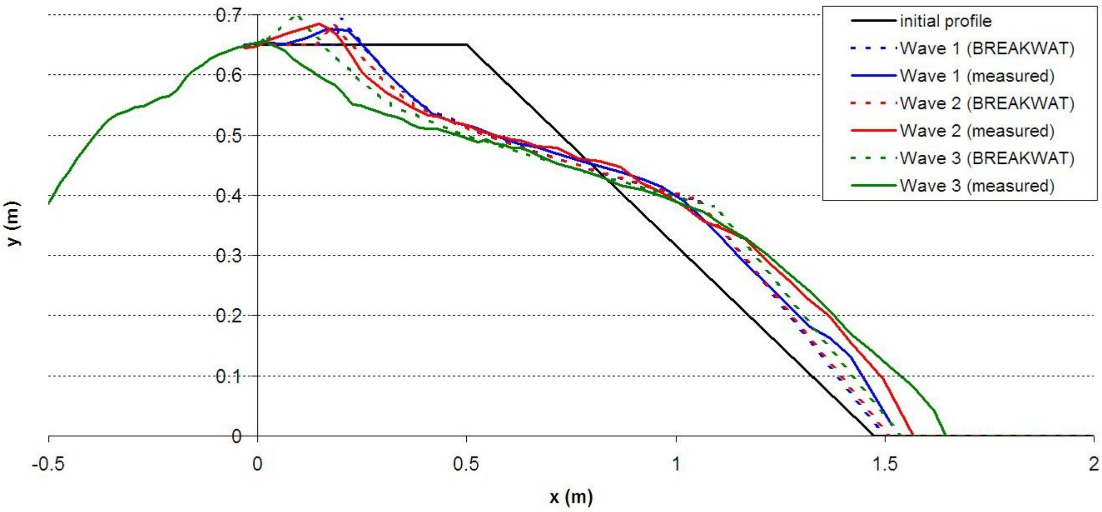

Figure 4.11 – Comparison between measured profiles and BREAKWAT output for Test 1

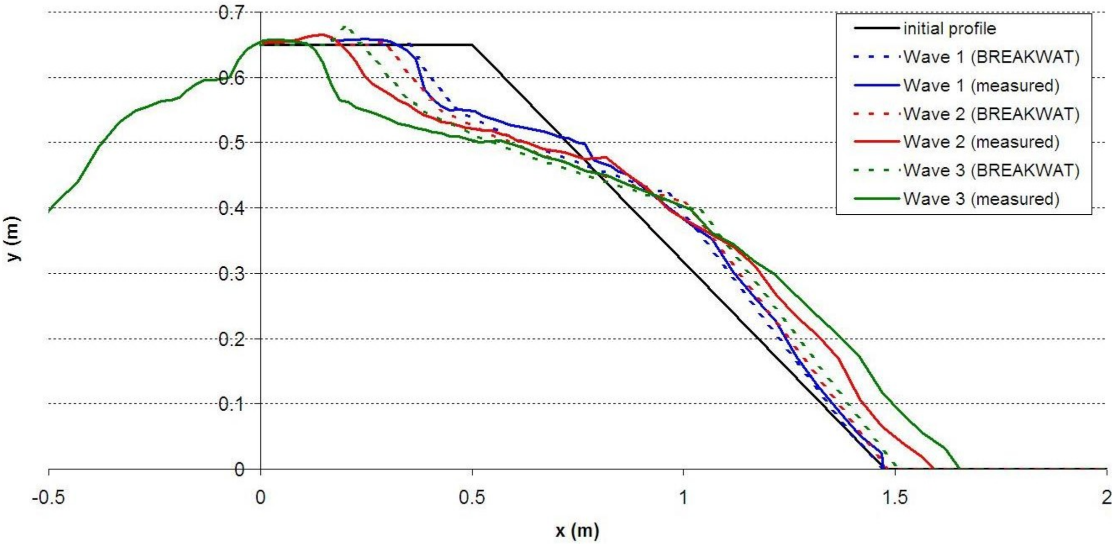

Figure 4.12 - Comparison between measured profiles and BREAKWAT output for Test 2

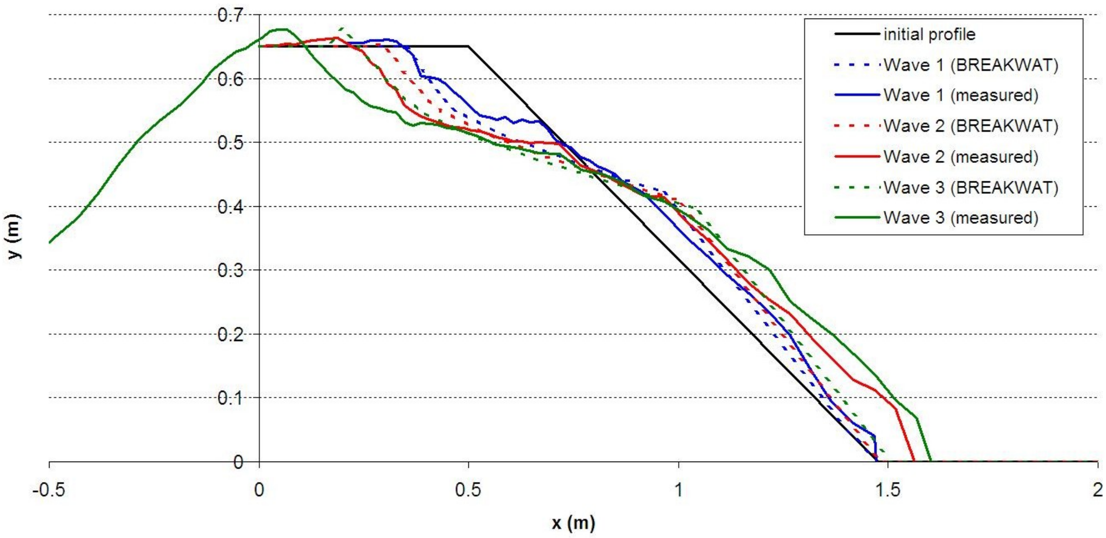

Figure 4.13 - Comparison between measured profiles and BREAKWAT output for Test 3

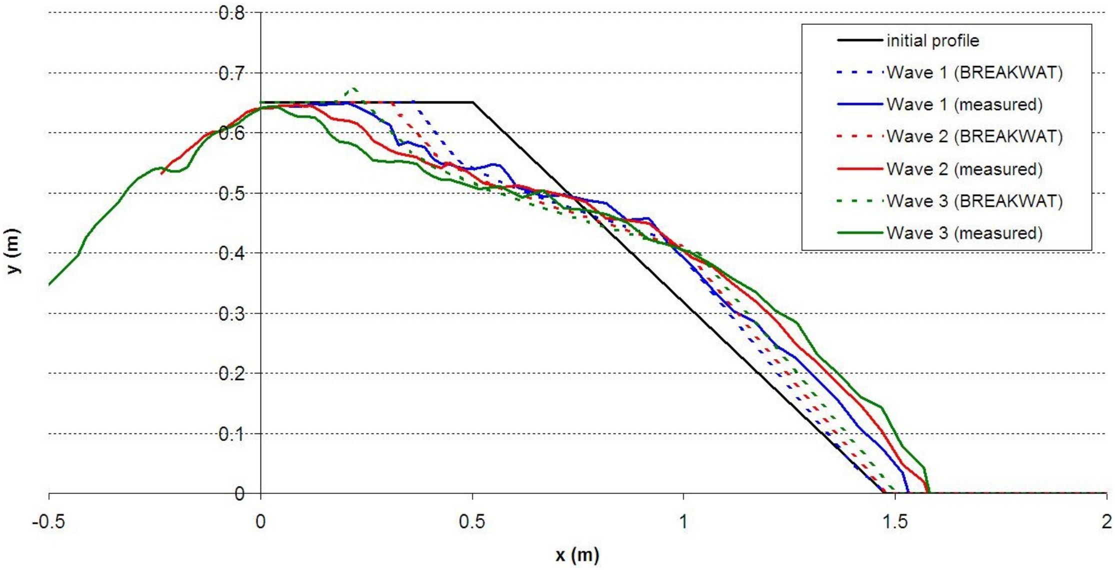

Figure 4.14 - Comparison between measured profiles and BREAKWAT output for Test 6

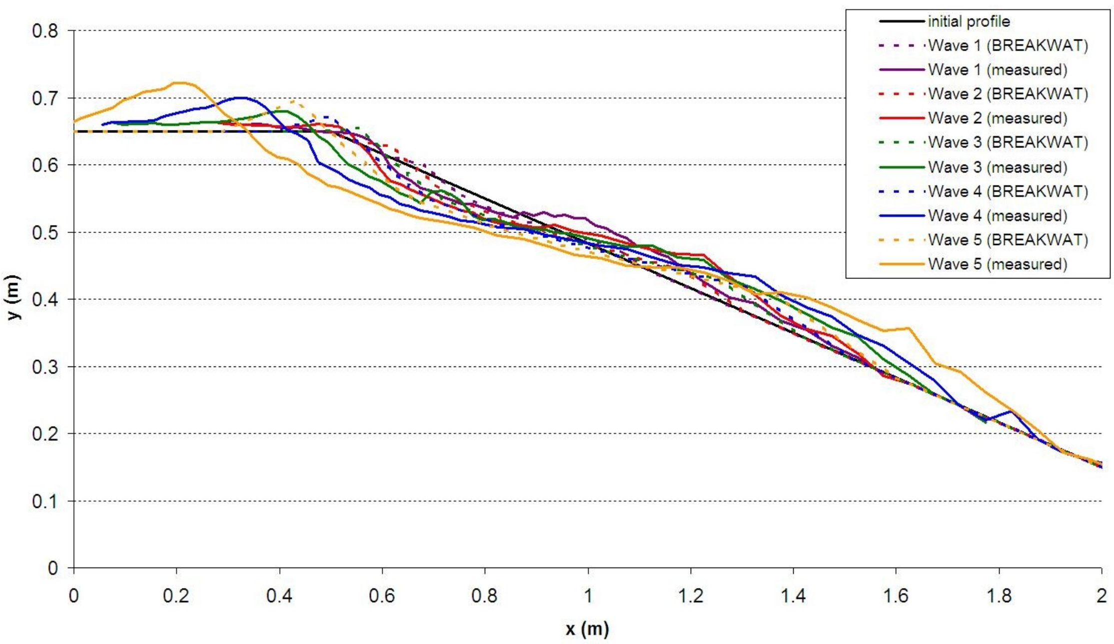

Figure 4.15 - Comparison between measured profiles and BREAKWAT output for Test 5

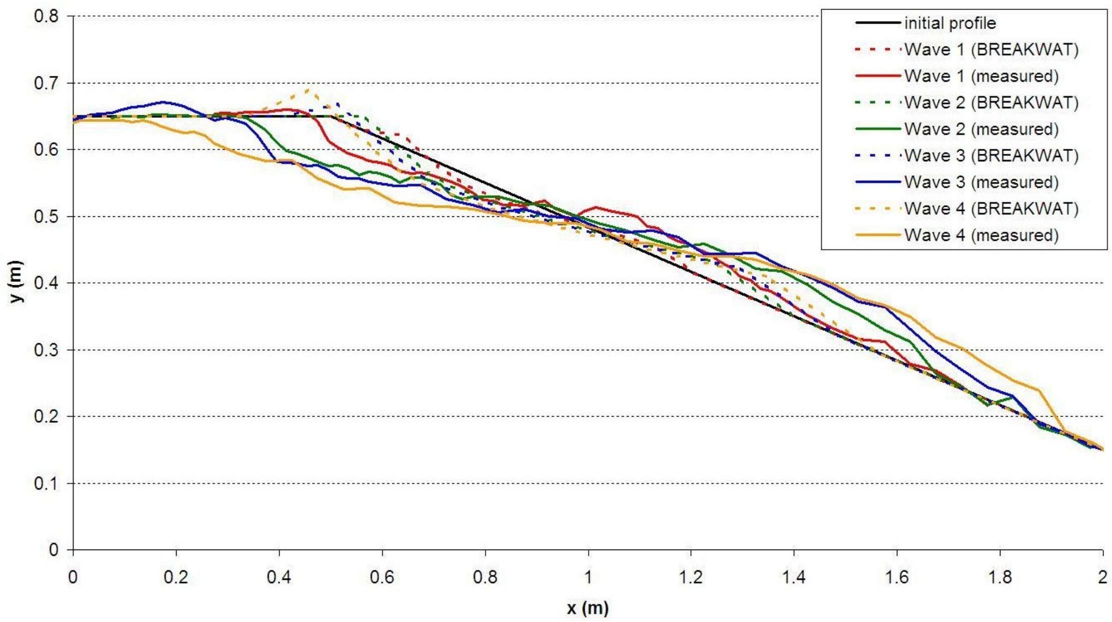

Figure 4.16 - Comparison between measured profiles and BREAKWAT output for Test 8

A first remark has to be made about the grading. Although this parameter is not included in the equations of van der Meer, the software requires it as input with the aim of warning the user if the validity range of this parameter is not respected. This happens in all the present cases, as the maximum value of D_{85} / D_{15} accepted by the model is 2.5.

It is immediately clear that the best agreement between the measured profiles and the prediction of the model is found for the lowest value of grading. For the higher gradings the profiles still show a similar shape, but the horizontal extent of the reshaping is larger in the measurements than in the model predictions.

The same cannot be said for the layout of the profiles in the vertical direction: for example, while for Test 3 a good agreement between in the height of the crest is recognizable, for Test 5 this parameter turns out to be higher in all the measurements.

This consideration confirms the trend already noticed by van der Meer (see par 2.3.2), according to whom the profile below the mean water level should be longer for a very wide grading. The graphs of Fig. 4.11 – 4.16 show that also above the mean water level the effect of the wide grading is felt.

In general, a fair agreement is found in the overall shape of the profile, with a well defined “crest” in all the measurements and a rather evident change of slope below the water level, similar to the “step” defined by van der Meer. The enhanced dynamism if the stones due to the segregation process induced by the wide grading may partly explain why the horizontal displacements in the physical model are larger.

In the next chapter the correspondence between the formulas of van der Meer and the measured profiles will be investigated in a more quantitative way, with respect to the different range of values of the grading studied in the present case.

Chapter 5

Derivation of a new design tool

As concluded in the previous paragraph, also in the case of wide grading the formulas derived by van der Meer are fairly suited to describe at least the general aspect of a modified profile, although they provide a smaller horizontal scale of the reshaping compared to the measurements from the physical model tests. It seems reasonable to assume that this trend is related to the wide grading of the constituting material as a dynamic segregation mechanism is strongly enhanced by the high variability of the stone sizes. In a qualitative way, this behavior was already deduced by van der Meer while commenting the results of his tests, although his analysis was limited to a value of D_{85}/D_{15} equal to 2.25 (see Fig. 2.9): therefore the narrow range of the grading justifies the exclusion of this variable in the parameterization of the profile which results from his data analysis.

In this chapter the influence of the stone-size gradation will be analyzed in a quantitative way, with the aim of introducing the variable D_{85}/D_{15} in the functional relationships proposed by van der Meer. Eventually, with the modification of some of his formulas and the introduction of new formulas fitting the data from the laboratory tests, a simple model for the calculation of a reshaped profile will be derived.

5.1 Parameterization of the profiles

Based on his definitions of “crest” and “step”, van der Meer identifies certain parameters which schematize the whole reshaped profile (see also Fig. 2.7). Then, a quantitative comparison between the measured and computed profiles goes through the definition of the same geometrical parameters for the collected data. This can be done for 21 profiles measured during tests 1, 2, 3, 5, 6 and 8, whenever the crest of the structure was not yet completely washed away by the waves.

In particular, for the data set, 7 parameters directly related to the ones of van der Meer are determined as follows, defining as local origin the intersection between the reshaped profile and the mean water level (see Fig. 5.1):

- θ_1: slope of the line interpolating the last six points measured on the reshaped profile. Such points are just above the bottom of the flume for the tests with slope 1:1.5 and just above the original slope in the other tests;
- θ_2: slope of the line interpolating the measured profile below the local origin, until the slope of the profile does not become permanently steeper than 0.3. The interpolation line passes through the local origin;

- l_s : horizontal offset between the intersection of the two lines defined above and the local origin;
- h_s : vertical offset between the intersection of the two lines defined above and the local origin;
- θ_3 : slope of the line connecting the observed crest and the local origin;
- l_c : horizontal offset between the crest of the reshaped profile and the local origin;
- h_c : vertical offset between the crest of the reshaped profile and the local origin.

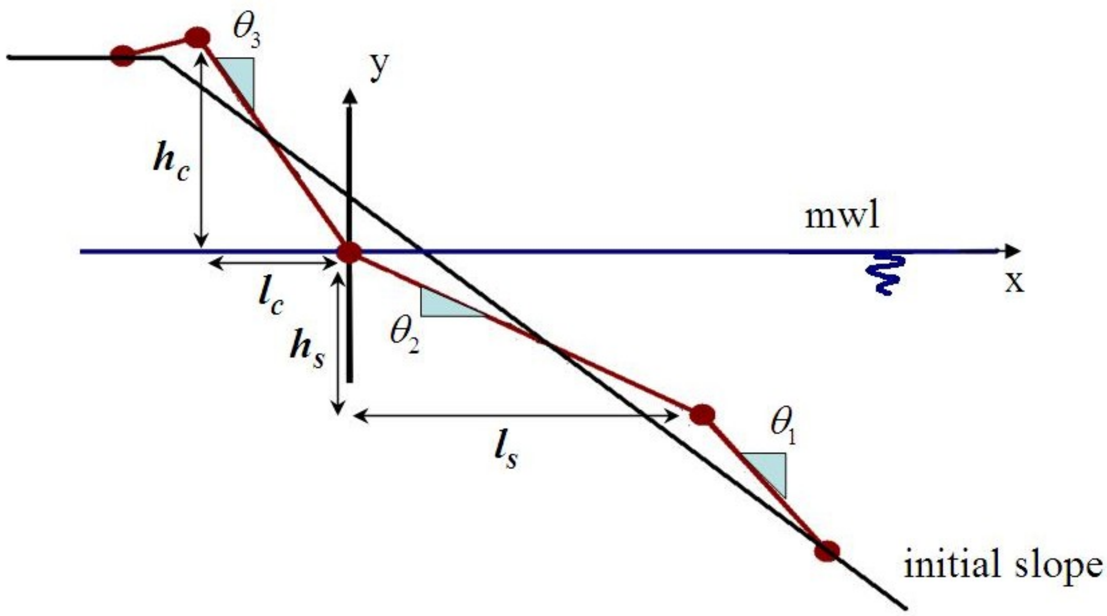

Figure 5.1 – Parameterization of a generic reshaped profile

This parameterization leads to the schematic representation of the measured profiles shown in Fig. 5.2, where the *x*-axis has its 0 at the local origin. It can be deduced from the graph that parameters like θ_2 and in particular θ_3 should be somehow related to the grading. The whole set of parameters is reported in Appendix A.

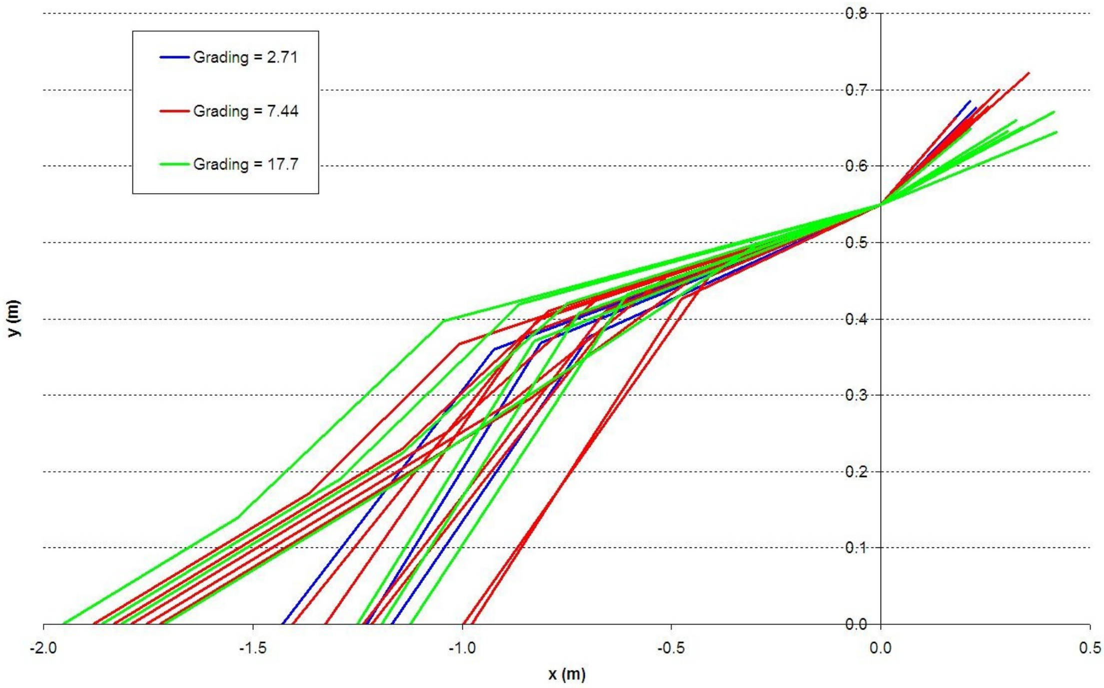

Figure 5.2 – Representation of all the parameterized profiles

At this stage, a direct comparison between the profile parameters measured in the tests and the ones estimated through van der Meer formulas can be done, with the latter given as output by the software BREAKWAT. Even though the step below mean water level was not always clearly evident, the parameters l_c, l_s, h_c and h_s from the data set correspond to the ones defined by van der Meer. Figures 5.3 and 5.4 show this comparison differentiating the two "length" parameters from the "height" parameters.

It appears clear from Fig. 5.3, as anticipated in the previous chapter, how the length parameters calculated by BREAKWAT are smaller than the measured ones: a clear dependence of this trend on the grading is shown in the graph, where the data are further away from the line with slope 1:1 as the value of D_{85}/D_{15} increases. Such trend is not identified in Fig. 5.4, where out of the dispersion of the data it can be only deduced a fair correspondence of the average values for the height parameters.

In the van der Meer formulas one of the governing parameters in determining the intensity of wave attack is the number of waves. Van der Meer states that the influence on the number of waves cannot be neglected and it is reasonable not to ignore this variable in the comparison which is being made in this chapter.

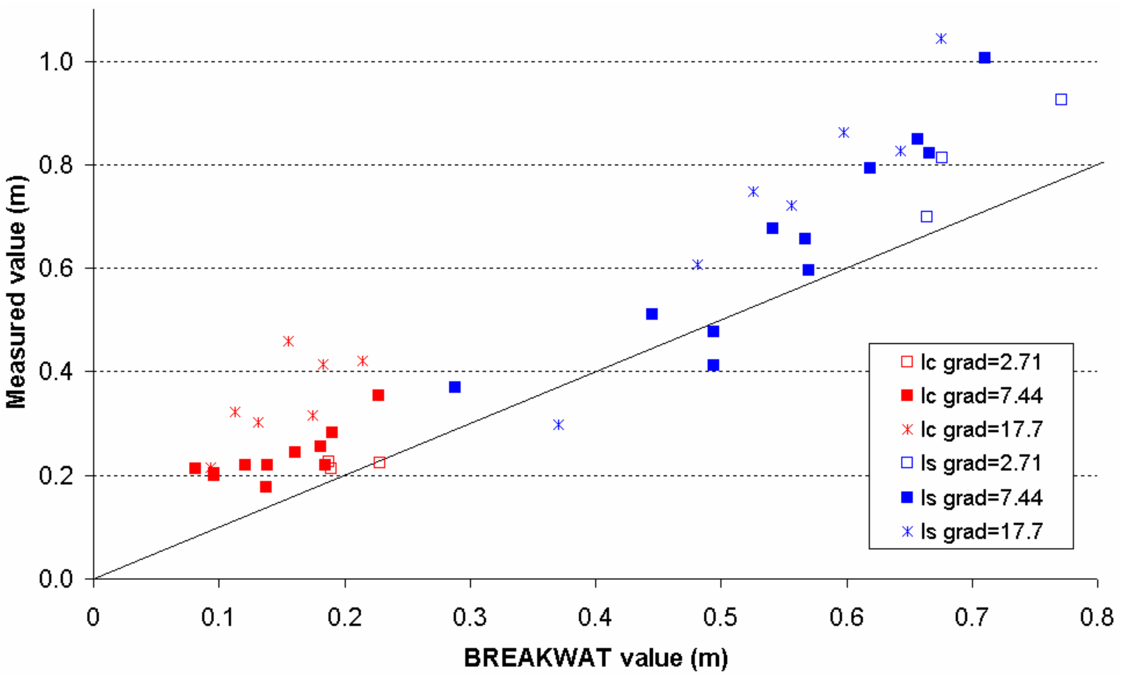

Figure 5.3 – Comparison between measured and computed values of l_c and l_s

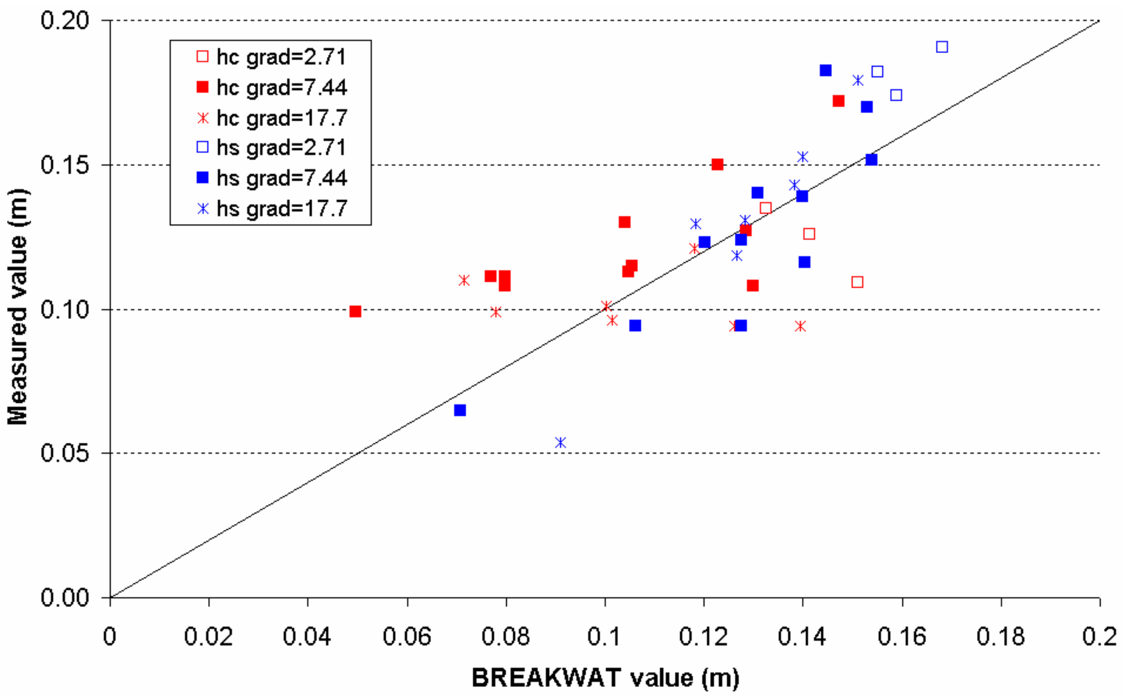

Figure 5.4 – Comparison between measured and computed values of h_c and h_s

In this respect, a limitation of the tests carried out for this research study consists in an inaccurate value of the number of waves N as successive wave trains were sent to the structure without restoring the original profile every time the load was changed. This means that although in every train about 2000 waves were generated, this number neglects the damaged already produced by the previous wave attacks (see also Par. 4.1).

The comparison shown in Fig. 5.3 and 5.4 is limited to the parameters l_c, l_s, h_c and h_s is affected by a non precise definition of the number of waves N in the input for BREAKWAT (see also par. 4.3.3). A further insight into the variability of all the profile parameters will be carried out after a more precise definition of the number of incident waves: this can be done following a statistical procedure explained below.

5.2 Principal Components Analysis of the data and definition of an equivalent number of waves

It is known that every wave train consisted of 2000 waves. However, the damage state shown by the structure at the beginning of every wave train, which is due to the previous load history, should not be neglected if a correct value of the parameter N has to be assigned to every reshaped profile.

A useful step in the definition of N is then to express the damage observed before the attack of a wave train, defined by certain H_s and T_m, as the result of a number of equivalent waves with the same characteristics. This number, added to 2000, will give an estimation of the real number of waves needed to reach the final damage state.

The method adopted to define an equivalent number of waves includes a Principal Component Analysis (PCA) of the data and will be explained below, with all the values of the matrixes involved reported in Appendix C.

The set of data used for this analysis consists of 21 measured profiles, and for each of them the 7 geometrical parameters described in Par. 5.1 are defined. As the slopes θ_2 and θ_3 are direct functions of the length and height parameters, only 5 geometrical entities are strictly needed to characterize each profile. The PCA consists of combining linearly these 5 parameters, in order to define 5 "components" (called f) which explain better the variability of the whole data set.

As an example, if all the profiles showing a long step were also characterized by a steep slope below the step, one of the components would be given by a linear combination o the 5 parameters with high coefficients for l_s and θ_1.

The [5x21] matrix of the standardized parameters, $\tilde{Y}$, and the unknown matrix of the coefficients defining the components, F, should be such that:

$$F = A \cdot \tilde{Y} \qquad (5.1)$$

with A (matrix of *factor scores*) to be obtained.

The covariance of $\tilde{Y}$ can be calculated: it is a [5x5] symmetrical matrix. The eigenvectors of the matrix $\mathrm{cov}(\tilde{Y})$, ordered according to the corresponding eigenvalues and multiplied by the square root of the eigenvalues themselves, form the matrix *B* (matrix of *factor loadings*).

B gives the weighted contribution of the different components in the description of the initial data set. In matrix form:

$$\tilde{Y} = \left(B\right)^T \cdot F \tag{5.2}$$

The matrix *A* can be determined, combining Eq. 5.1 and 5.2, as the transpose matrix of the inverse of *B*:

$$A = \left(B^{-1}\right)^T \tag{5.3}$$

The PCA is commonly used in statistic to reduce the dimension of the variability of a data set. This can be achieved provided that the last columns of *B* contain small numbers, due to small eigenvalues: reducing the number of components by setting the last columns of *B* to 0, the estimation of the observed data given by Eq. 5.3 is still good. This method was used in a similar study by Archetti (1998). Other references can be found in Kramer (1991).

The columns of matrix *F* should better explain the trends of the data set. Following the reasoning of Archetti (1998), considering the values in matrix *A* (see Appendix C) it can be noticed that the component f_1 (first column of the matrix *F*) is strongly related to the overall intensity of the wave attack, being mainly determined by the parameters l_s and h_s which represent the entity of the reshaping.

Choosing the 21-elements vector f_1 as representative of the intensity of wave attack, an empirical equation will be found to define this component as a function of the main governing variables. All the possible non-dimensional governing variables are assumed in this function: grading, H_0, H_0T_0, s_m (wave steepness), α (initial slope) and *N*. The function will look like this:

$$f_1 = k\left(\frac{D_{85}}{D_{15}}\right)^a \left(H_0\right)^b \left(H_0T_0\right)^c \left(s_m\right)^d \left(\alpha\right)^e \left(N\right)^f + m \tag{5.4}$$

Let us assume that a certain damage state, represented by f_1, is described by Eq. 5.4 for two successive wave trains. Then, the equivalent number of waves of the second wave train giving that damage state is given by:

$$N_2 = \left(\frac{g_1}{g_2}\right)^{\frac{a}{f}} \left(\frac{H_{01}}{H_{02}}\right)^{\frac{b}{f}} \left(\frac{H_0T_{01}}{H_0T_{02}}\right)^{\frac{c}{f}} \left(\frac{s_{m1}}{s_{m2}}\right)^{\frac{d}{f}} \left(\frac{\alpha_1}{\alpha_2}\right)^{\frac{e}{f}} \tag{5.5}$$

where $g = \frac{D_{85}}{D_{15}}$ and the subscripts 1 and 2 indicate the first and second wave train.

This procedure was applied to the whole data set, and Fig. 5.5 shows the agreement between the calculated values of f_1 and the ones estimated through Eq. 5.4, with the following values for the exponents: $a = -0.042$, $b = 0.049$, $c = 0.469$, $d = 0.011$, $e = 0.165$, $f = 0.064$.

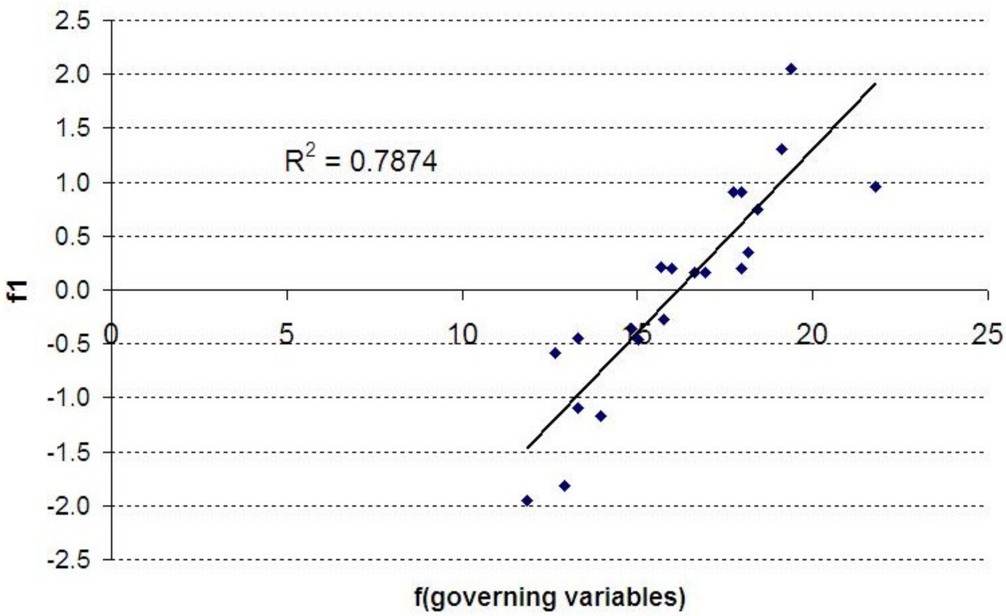

Figure 5.5 – Comparison between calculated and estimated values of f_1

The resulting *N* values assumed from now on in the analysis are given in Tab. 5.1.

Test	Wave	*N*	Test	Wave	*N*	Test	Wave	*N*
1	1	7300	3	2	2172	6	1	2000
1	2	2000	3	3	2286	6	2	2190
1	3	2327	5	1	2000	6	3	2300
2	1	2000	5	2	2182	8	1	2000
2	2	2160	5	3	2287	8	2	2222
2	3	2253	5	4	2502	8	3	2535
3	1	2000	5	5	2663	8	4	2851

Table 5.1 – Modified values for the number of waves

5.3 Introduction of the parameter grading in van der Meer formulas

The values of N determined above allow a more quantitative comparison between the profile parameters measured in the present test series and the corresponding values predicted by the empirical formulas of Van der Meer.

Fig. 5.2 showed clearly how the values of the "length" parameters l_s and l_c measured in the tests are significantly higher than the ones predicted by BREAKWAT. Moreover, this trend seems to be somehow governed by the grading of the material. Therefore in this section new formulas for the estimation of these parameters, taking into account the grading, will be derived through curve-fitting of the measured data.

Van der Meer suggests 2 formulas for the step length:

$$H_0T_0 = 3.8(l_s / D_{n50}N^{0.07})^{1.3} \tag{5.6}$$

$$H_0T_0 = 2.6(l_s / D_{n50}N^{0.07})^{1.3} + 70\cot\alpha_2 - 210 \tag{5.7}$$

with the intersection between the two curves giving the transition H_0T_0 number, above which Eq. 5.6 should be used. α_2 is a fictitious angle, function of the initial seaward slope defined by van der Meer (1992), for which the values given by BREAKWAT are used.

It should be noticed that the transition values H_0T_0 for the data set turns out to be negative for the lowest α_2 (about 1.5) or anyway smaller than 50 for α_2 equal to 3 or higher. This doesn't agree with the graph of Fig. 5.6, presented by van der Meer (1988), which shows that the initial slope should have influence until the H_0T_0 number reaches the value of about 1000. Thus, an effect if the seaward slope is expected on the trend of the data as the values of H_0T_0 observed during the present tests range in the interval 100-300.

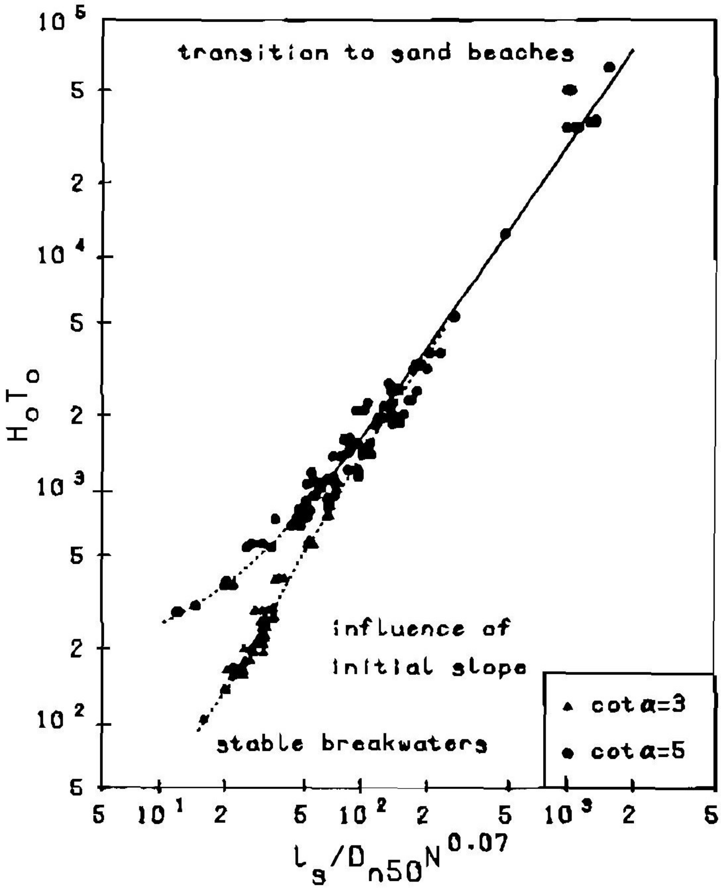

Figure 5.6 – Influence of initial slope on l_s according to van der Meer (1988)

In Fig. 5.7 the measured l_s are plotted against the parameter H_0T_0 according to Eq. 5.6. The graph confirms the effect of the parameter grading on l_s as a curve passing through the origin should have a milder inclination to fit points characterized by wider grading: the same trend was already shown already by Fig. 5.3. In Fig. 5.7 is also evident that the milder slope has a stabilizing effect on the profile: compared to the steep slope for the same value of H_0T_0, it gives a shorter step.

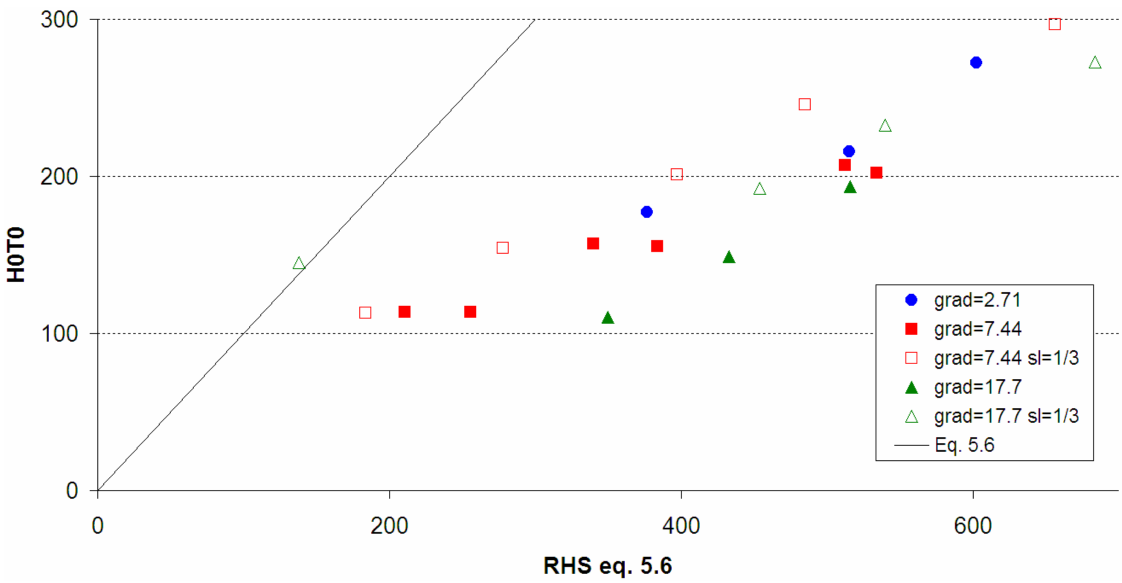

Figure 5.7 – Comparison between measured l_s and estimation by van der Meer (1992)

Then a curve fitting procedure is carried out, in order to define an expression similar to the one of van der Meer which includes the grading. As an effect of the initial slope is also pointed out by the tests, a term including this variable is inserted as intercept as in to Eq. 5.7. The modified equation should look like this:

$$H_0T_0 = c_1(l_s / D_{n50}N^{0.07})^{1.3}\left(\frac{D_{85}}{D_{15}}\right)^{e_1} + c_2\left(\cot\alpha_2\right)^{e_2} + c_3 \qquad (5.8)$$

where *c* and *e* are curve fitting coefficients and exponents, respectively. The exponent e_1 is expected to be negative, as a wider grading is shown to generate a larger reshaping for the same H_0T_0 parameter. Furthermore, the exponent e_2 does not show effect in the goodness of the curve fitting and can be set equal to 1. The curve fitting consists in a variation of the values of the coefficients *c* and *e* until the maximum R^2 is found between the measured data and Eq. 5.8.

A correlation coefficient $R^2 = 0.95$ is found for Eq. 5.9, as shown also in Fig. 5.8:

$$H_0T_0 = 1.66(l_s / D_{n50}N^{0.07})^{1.3}\left(\frac{D_{85}}{D_{15}}\right)^{-0.15} + 29.1\cot\alpha_2 - 9.38 \qquad (5.9)$$

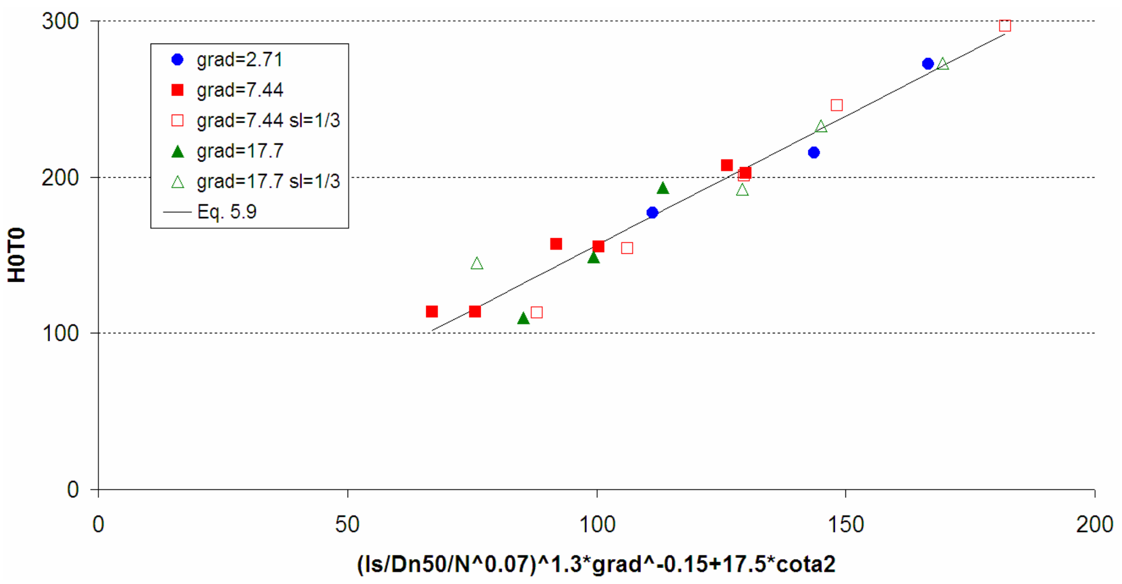

Figure 5.8 – Optimal curve fitting of the data for l_s

Also for the parameter l_c van der Meer (1992) gives 2 formulas:

$$H_0T_0 = 21\left(l_c / D_{n50}N^{0.12}\right)^{1.2} \tag{5.10}$$

$$H_0T_0 = \left(3\cot\alpha_1 + 25\right)l_c / D_{n50}N^{0.12} \tag{5.11}$$

with the intersection between the two curves giving the transition H_0T_0 number, above which Eq. 5.10 should be used. The data from the present tests are plotted below according to Eq. 5.11, although for some of them H_0T_0 is above the transition value. This will also allow an evaluation of how well Eq. 5.11 predicts the effect of the different slope.

Fig. 5.9 confirms that the influence of the grading should be considered in the slope of a line passing through the origin. Moreover, the points obtained for the milder slope are shifted to the right with respect to the ones obtained for steep slope and same grading or H_0T_0. This fact suggests to include the effect of the slope in a formula where an intercept is introduced.

The points are well fitted by a function having the following expression:

$$H_0T_0\left(\cot\alpha_1\right)^{e_1} = c_1\left(l_c / D_{n50}N^{0.12}\right)^{e_2}\left(\frac{D_{85}}{D_{15}}\right)^{e_3} + c_2(\cot\alpha_1)^{e_1} + c_3 \tag{5.12}$$

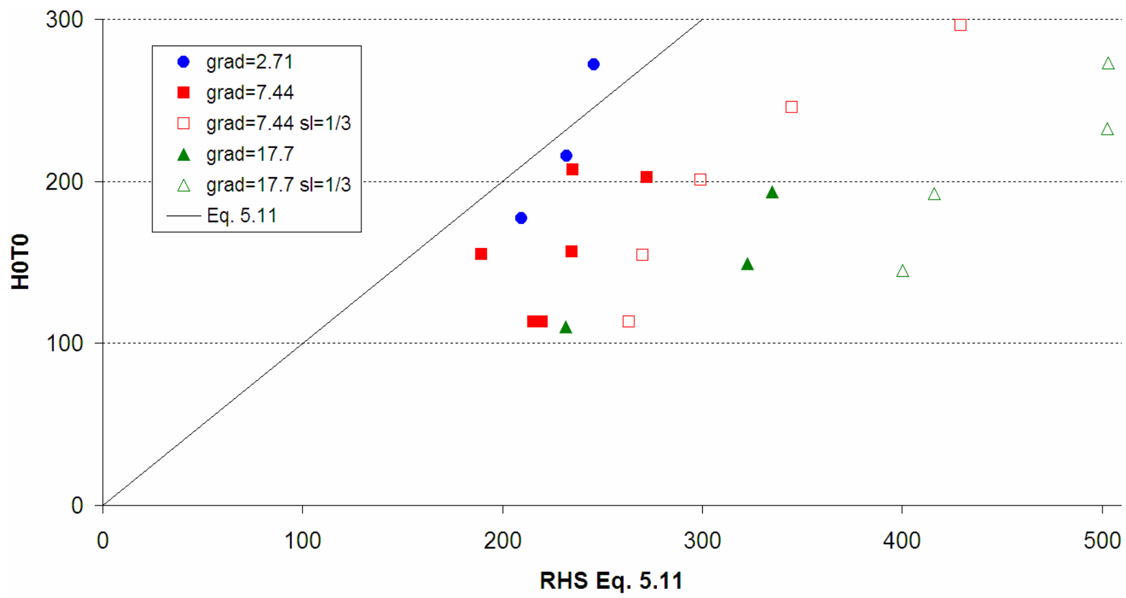

Figure 5.9 - Comparison between measured l_c and estimation by van der Meer (1992)

The exponents e_1 and e_2 can be set to 1 without significant loss in precision of the fitting. A coefficient $R^2 = 0.91$ is obtained for the following equation (see also Fig. 5.10):

$$(H_0T_0 - 183)\cot\alpha_1 = 139\left(l_c / D_{n50}N^{0.12}\right)\left(\frac{D_{85}}{D_{15}}\right)^{-0.29} - 667 \qquad (5.13)$$

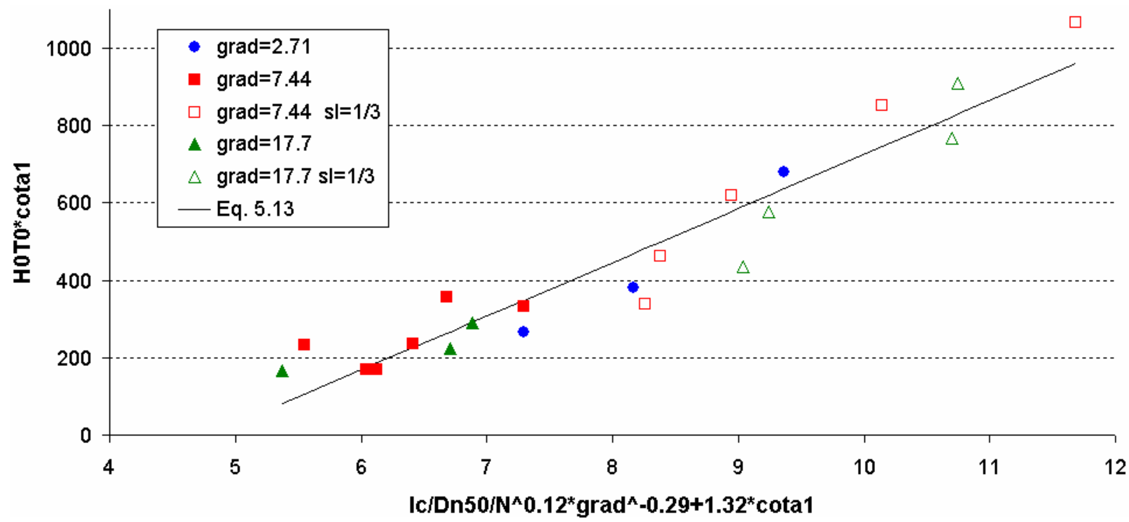

Figure 5.10 – Optimal curve fitting of the data for l_c

5.4 New formulas for the estimation of crest recession

A curve fitting procedure similar to the ones described above will be carried out in order define equation to estimate the value of θ_3 and the recession of the crest. A definition for θ_3 is particularly interesting because this parameter can be considered fairly independent from the height of the model structure above mean water level, and would allow an estimation of the recession of the crest regardless of its initial height. On the other hand, a formula able to predict directly the recession derived from the direct measurements would have the validity limited to a specific model geometry.

Fig. 5.2 shows that the slope of the profiles above mean water level (θ_3) is milder for D_{85}/D_{15} equal to 17.7 than for narrower gradings, with a trend of increasing slope as the grading decreases. Fig. 5.11 confirms this trend, showing also that there is no significant influence of the initial slope.

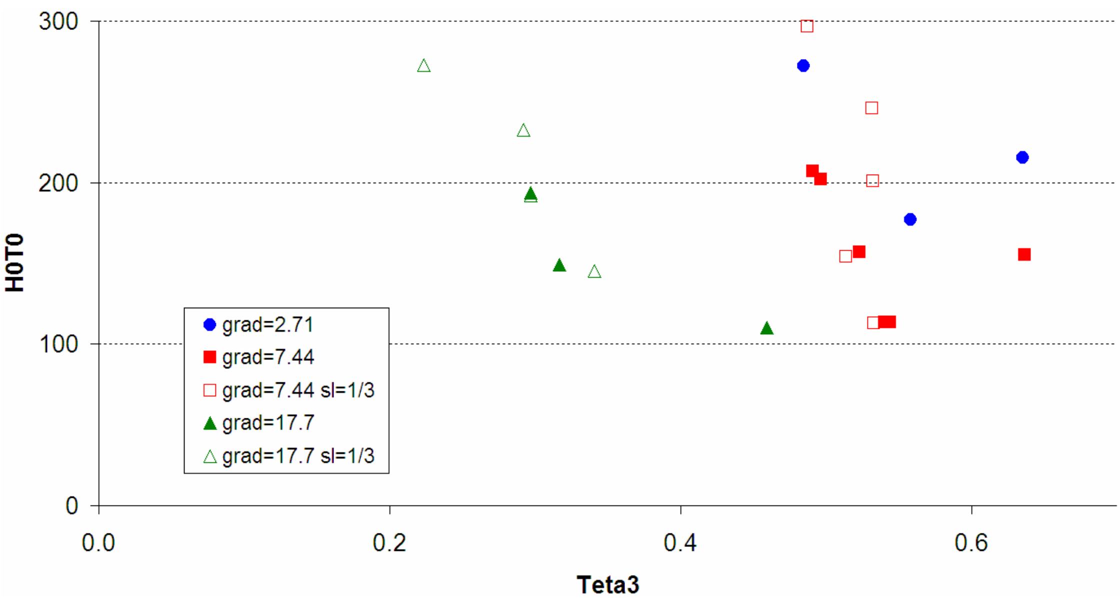

Figure 5.11 – Measured θ_3 *vs* H_0T_0

Then the measured data are interpolated using an equation as below:

$$\theta_3^{-1} = c_1 \left(\frac{D_{85}}{D_{15}} \right)^{e_1} \left(H_0 T_0 \right)^{e_2} + c_2 \qquad (5.14)$$

and a coefficient $R^2 = 0.92$ is found for the following equation (see also Fig. 5.12):

$$\theta_3^{-1} = 0.00023\left(\frac{D_{85}}{D_{15}}\right)^{1.58}\left(H_0T_0\right)^{0.84} + 1.50 \tag{5.15}$$

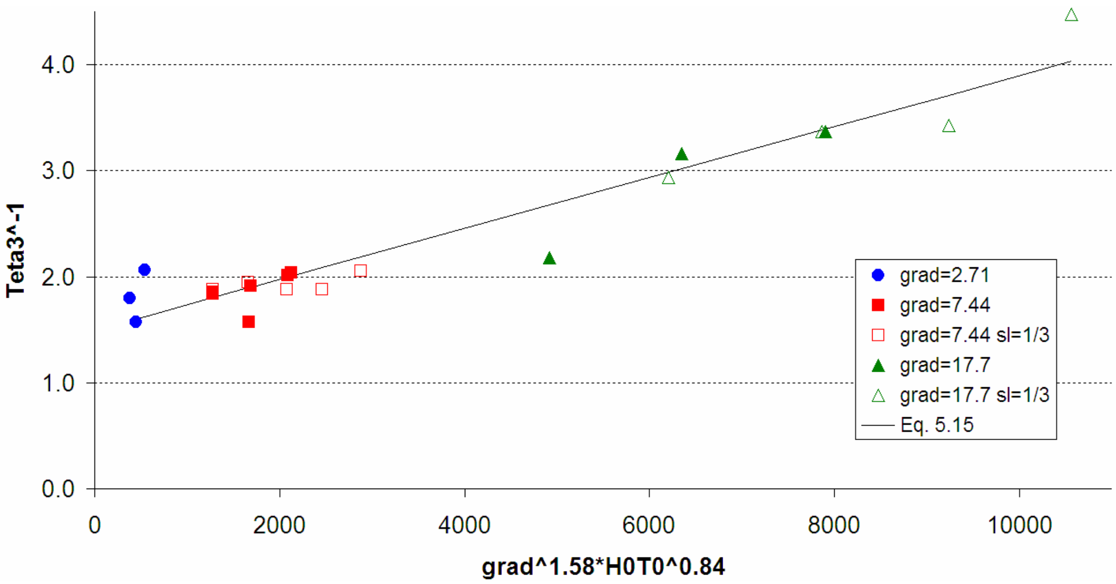

Figure 5.12 – Optimal curve fitting of the data for θ_3

The measured crest recessions are plotted in Fig. 5.13, where the points relative to the first 2 wave trains of Test 5 are omitted as the erosion phenomenon did not reach the crest of the structure. The graph shows clearly a linear dependence on the parameter H_0T_0, as similar slopes for the lines interpolating points relative to the same test can be hypothesized. The trend of the data is also determined by the values of grading and initial slope, with wider gradings as well as steeper slopes resulting in a larger recession.

Because of these considerations, curve fitting of the data is carried out using the following expression:

$$\frac{\text{Rec}}{D_{n50}} = c_1H_0T_0 + c_2\frac{D_{85}}{D_{15}} + c_3\tan\alpha + c_4 \tag{5.16}$$

and a coefficient $R^2 = 0.95$ is given by the following equation (see also Fig. 5.14):

$$\frac{\text{Rec}}{D_{n50}} = 0.218H_0T_0 + 1.62\frac{D_{85}}{D_{15}} + 105\tan\alpha - 91.5 \tag{5.17}$$

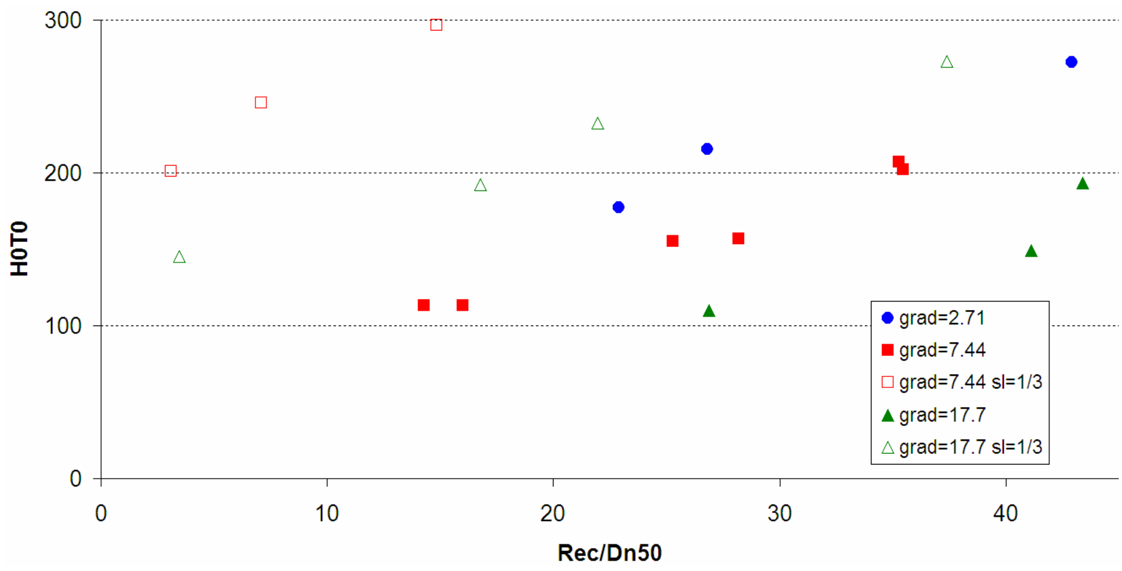

Figure 5.13 - Measured Rec/D_{n50} *vs* H_0T_0

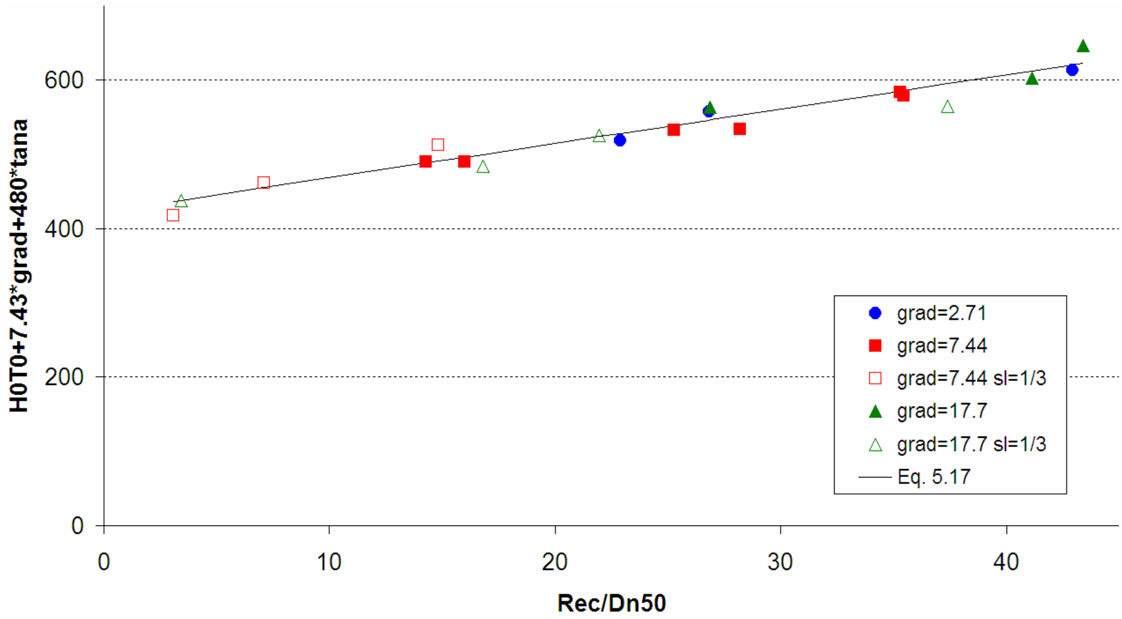

Figure 5.14 – Optimal curve fitting of the data for Rec/D_{n50}

5.5 Validity of the proposed formulas

At this stage it is important to clarify the range of validity of the new formulas presented above (Eq. 5.9, 5.13, 5.15, 5.17). With respect to the variables directly included in the formulas, the set of values investigated during laboratory tests defines the following ranges:

$$\frac{D_{85}}{D_{15}} < 20 \tag{5.18}$$

$$100 < H_0 T_0 < 300 \tag{5.19}$$

$$1.5 < \cot\alpha < 3 \tag{5.20}$$

Moreover, it should be reminded that the wave steepness was varied within a very short range:

$$0.43 < s_m < 0.49 \tag{5.21}$$

with only a few "outliers" out of this interval.

The absolute values of the crest freeboard R_c and the water level d were constant, with the latter always sufficiently high to consider that the test were carried out in deep water. The ranges of these parameters, if made non-dimensional over the significant wave height, are given below:

$$0.75 < \frac{R_c}{H_s} < 1.43 \tag{5.22}$$

$$4.1 < \frac{d}{H_s} < 7.9 \tag{5.23}$$

The parameter D_{n50} was not varied at all, with the stones having all an angular shape: the percentage of rounded stones P_R defined by Kao and Hall (1990) was always set to 0 when their formula was applied. As a general recommendation, the predictions given by the new formulas if used outside the above boundaries should be assumed with care.

A direct comparison between the estimations given by Eq. 5.9, 5.13 and 5.15 and the estimations given by van der Meer formulas for the same profile parameters is presented in the following paragraphs, within the ranges defined above.

The available design formulas for l_s are listed below.

Van der Meer (1992), high H_0T_0:

$$H_0T_0 = 3.8(l_s / D_{n50} N^{0.07})^{1.3} \tag{5.6}$$

Van der Meer (1992), low H_0T_0:

$$H_0T_0 = 2.6(l_s / D_{n50} N^{0.07})^{1.3} + 70\cot\alpha_2 - 210 \tag{5.7}$$

Present study:

$$H_0T_0 = 1.66(l_s / D_{n50} N^{0.07})^{1.3} \left(\frac{D_{85}}{D_{15}}\right)^{-0.15} + 29.1\cot\alpha_2 - 9.38 \tag{5.9}$$

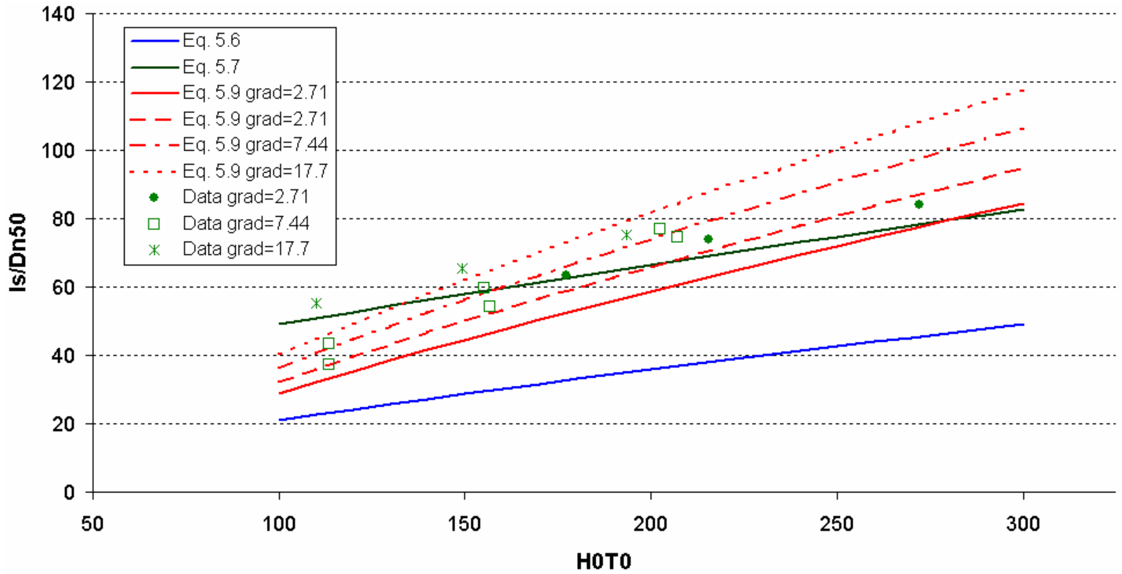

Figure 5.15 – Comparison between the estimations of l_s by different formulas

In this case a consideration should be repeated about the two formulas by van der Meer. Although the transition value of H_0T_0 calculated analytically imposes the use of Eq. 5.6, Fig. 5.6 (given by van der Meer, 1988) would suggest that the initial slope has to be taken into account. Fig. 5.15 confirms the last hypothesis, with Eq. 5.7 (where the initial slope is included) being more suited to interpolate the measured points. In particular it can be noticed that, for rather uniform material, Eq. 5.7 and Eq. 5.9 predict similar l_s if H_0T_0 is above 200.

In the graphs of Fig. 5.15 it is assumed: $D_{n50} = 0.011$ m, $\cot\alpha_2 = 1.5$ and $N = 2000$. For $\cot\alpha_2 = 3$, the curves would show a similar trend.

The formulas for the estimation of l_c are the following.

Van der Meer (1992), high H_0T_0:

$$H_0T_0 = 21\left(l_c / D_{n50}N^{0.12}\right)^{1.2} \tag{5.10}$$

Vand der Meer (1992), low H_0T_0:

$$H_0T_0 = \left(3\cot\alpha_1 + 25\right)l_c / D_{n50}N^{0.12} \tag{5.11}$$

Present study:

$$(H_0T_0 - 183)\cot\alpha_1 = 139\left(l_c / D_{n50}N^{0.12}\right)\left(\frac{D_{85}}{D_{15}}\right)^{-0.29} - 667 \tag{5.13}$$

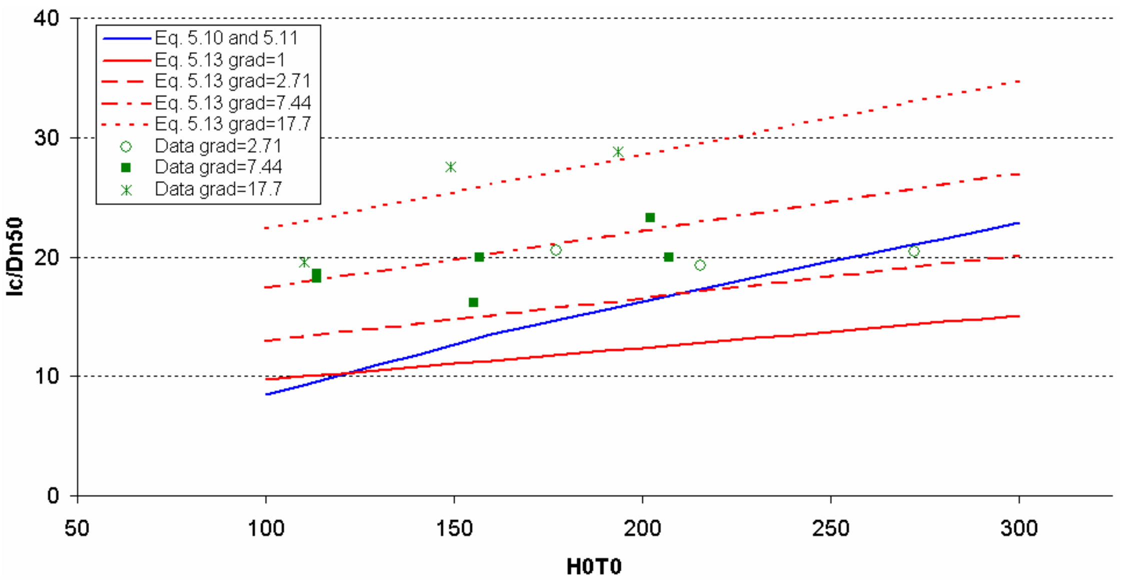

Figure 5.16 - Comparison between the estimations of l_c by different formulas

In Fig. 5.16, where $D_{n50} = 0.011$ m, $\cot\alpha_2 = 1.5$ and $N = 2000$ are assumed, depending on H_0T_0 both Eq. 5.10 and 5.11 are used (the transition value is 161). The graph shows how the agreement between the formulas is good for rather uniform material (D_{85}/D_{15} equal to 1-3), and Eq. 5.13 may constitute a reliable extrapolation in case of wider grading. Again, assuming $\cot\alpha_2 = 3$, the curves would show a similar trend.

Finally a comparison on the estimation of θ_3 is carried out. Using the formulas of van der Meer, θ_3 can be determined as the ratio between h_c and l_c. Instead, Eq. 5.15 gives:

$$\theta_3^{-1} = 0.00023\left(\frac{D_{85}}{D_{15}}\right)^{1.58}\left(H_0T_0\right)^{0.84} + 1.50 \tag{5.15}$$

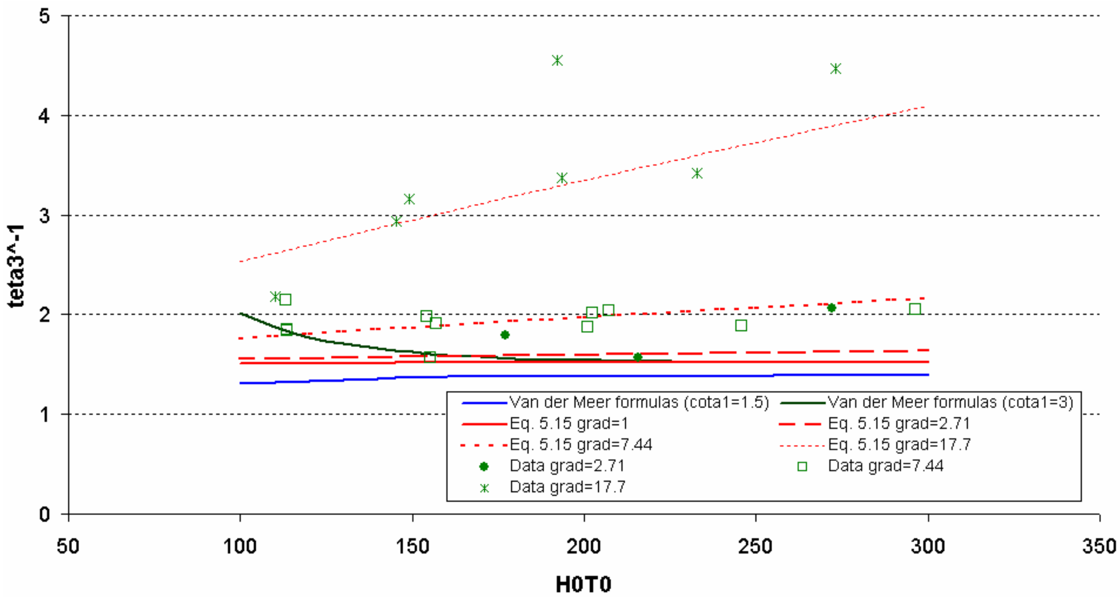

Figure 5.17 - Comparison between the estimations of θ_3 by different formulas

A small influence of the initial slope in the value of θ_3 is given by the formulas of van de Meer, while Eq. 5.15 doesn't take it into account. Also for this parameter the comparison shows that there is good agreement between the formulas for rather uniform material, and Eq. 5.15 provides, at least with respect to the measured data, a good extrapolation for wider gradings.

5.6 Derivation of a numerical model

A direct application of the results shown in the previous chapter lies in the possibility to represent, although in a very simplified way, the reshaped profile of a slope after a certain wave attack.

With reference to the same parameterization described in Par. 5.1, the following list summarizes the variables actually needed to define a complete reshaped profile (for initial slope steeper than 1:3). It is assumed as local origin the intersection between the mean water level and the reshaped profile.

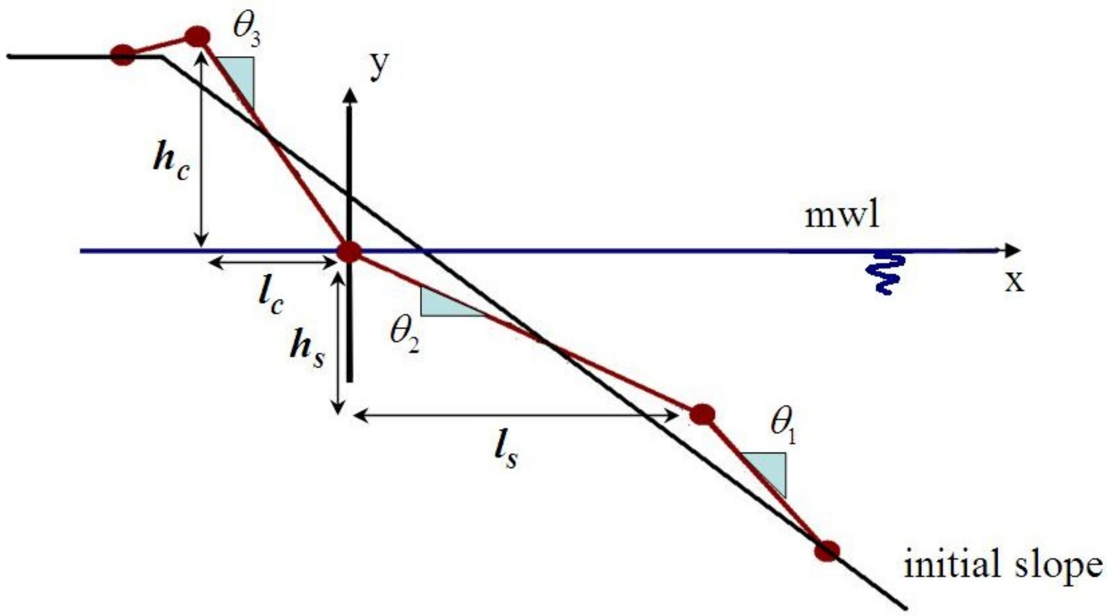

Figure 5.18 – Parameterization of a generic reshaped profile

- l_s: horizontal offset between the step (below mean water level) and the local origin;
- h_s: vertical offset between the step and the local origin;
- θ_1: slope connecting the step to the original profile;
- l_c: horizontal offset between the crest (above mean water level) and the local origin;
- θ_3: slope of the line connecting the observed crest and the local origin;
- l_r or *run-up length*: horizontal offset between the point where the initial and the reshaped profile come together behind the crest and the local origin.

Three of these parameters can be determined through the formulas derived in the previous chapter:

$$H_0T_0 = 1.66(l_s / D_{n50}N^{0.07})^{1.3}\left(\frac{D_{85}}{D_{15}}\right)^{-0.15} + 29.1\cot\alpha_2 - 9.38 \tag{5.9}$$

$$(H_0T_0 - 183)\cot\alpha_1 = 139\left(l_c / D_{n50}N^{0.12}\right)\left(\frac{D_{85}}{D_{15}}\right)^{-0.29} - 667 \tag{5.13}$$

$$\theta_3^{-1} = 0.00023\left(\frac{D_{85}}{D_{15}}\right)^{1.58}\left(H_0T_0\right)^{0.84} + 1.50 \tag{5.15}$$

while θ_1 and h_s can be determined according to van der Meer (1992). The angles α_1 and α_2 found in the formulas are also defined by van der Meer (1992) as a function of the initial slope of the structure.

The run-up length l_r was not considered in the analysis of chapters 4 and 5 as the limited width of the crest of the model structure did not always allow a clear definition of this parameter. The value of l_r should not even be determined through the equations of van der Meer because, for wide gradings, its value may become lower than the estimated value of l_c for the same input profile. A simplified solution to this problem can be found determining the run-up length with the hypothesis that, behind the crest, the material assumes its natural slope.

Once a profile similar to the one of Fig. 5.18 is derived through the empirical formulas, shifting it horizontally until the equilibrium of mass is respected will give the final reshaped profile. A simple MATLAB application which can do this operation is presented in Appendix D. Some simplifications are done in the script: the values of α_1, α_2 and α_3 are all set to the initial slope of the structure, and the slope behind the crest is assumed equal to 1:1.5.

An improvement of the model may be achieved in the estimation of the profile just above and below mean water level, which should not be simplified with straight lines but can be represented more realistically through parabolic functions. However, the “numerical model” in its actual development can already be considered as a design tool of quick and practical use for engineers and contractors.

The model can be used also to assess the recession of the berm, mainly governed by the parameter θ_3 which is supposed to be independent form the specific height of the structure. This will allow a reliable output of the model even for values of the crest freeboard different from the one tested in the laboratory. The reliability of the results of the model is shown by Fig. 5.19, where both the measured and the computed values of berm recession are shown, together with the prediction of Eq. 5.17.

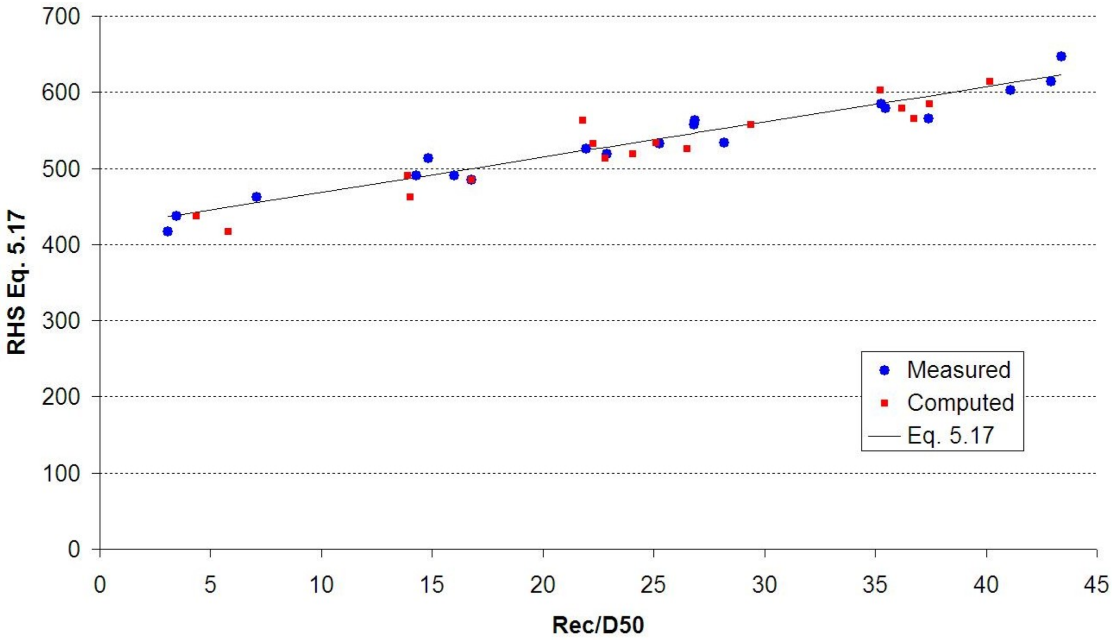

Figure 5.19 – Comparison between values of the berm recession obtained in different ways

The good agreement shown by Fig. 5.19 may not be surprising, as the model was actually calibrated on the measured data (although not directly on the recession). Further developments of the model may be achieved through a validation over data from other physical model tests, possibly focused on the effects of a wide grading.

Chapter 6

Calibration of a numerical model

Some of the measured data will be chosen for a brief comparison with the results given by the numerical model XBeach: in particular the measurements of the pressure sensors collected during the test may provide validation for the modelling of the wave propagation inside the porous structure. The results show how some of the parameters in the model (e.g. the permeability of the material) can be better assessed through this kind of calibration.

6.1 Features of the model XBeach

XBeach is an open source two-dimensional numerical model able to simulate, together with the hydrodynamic of waves, related phenomena like the wave propagation through porous media and the sediment transport. It is therefore a suited tool in the investigation of the behaviour of dunes, beaches and barriers under the attack of sea storms. It is mainly developed by UNESCO-IHE, in consortium with Delft Hydraulics (now Deltares), Delft University of Technology and the University of Miami.

The main feature of the model is a first order upwind numerical implementation which, combined with an automatic time step based on Courant criterion, makes the model stable and robust. The short wave propagation, non-stationary shallow water equations and sediment transport are combined in a way to provide a proper modelling of phenomena governed by strong gradients in space and time, i.e. extreme conditions such as the attack of hurricanes (Roelvink et al, 2008).

The representation of groundwater flow in XBeach is based on Darcy law, being therefore limited to laminar flow conditions. In the case turbulence becomes dominant in the flow regime, full momentum equations, e.g. the ones developed by van Gent (1995), should be implemented. The sediment transport, based on a depth averaged advection-diffusion equation, is calculated through the Soulsby-van Rijn formulation. Further details on the implementation of XBeach can be found in the XBeach Model Description and Manual (Roelvink et al. 2008), available online.

6.2 Comparison of groundwater flow

Simulations with XBeach have been carried out to compare the calculated pressures inside the structure, directly resulting from the groundwater flow implementation, with some of the measurements provided by the test series. The total head above the mean water level is assumed as the pressure predicted by the model. Input for XBeach is the time series of the water level, directly obtained from the measurements of the wave gauges resulting from the tests. In these simulations the morphological changes are not taken into account, which means that the calculated values of pressure neglect the erosion of the physical model which reduces the actual length of the porous flow.

The graphs presented below refer to a wave load characterized by H_s equal to 0.07 m and T_m equal to 0.96 s (first wave train of Test 6) on a structure with seaward slope 1:1.5 and D_{85}/D_{15} equal to 17.7. The location where the pressures are calculated (and measured) is below the rear edge of the crest, which means at about 10 cm from the free water surface at the lee side of the structure.

The result shown in Fig. 6.1 is obtained for a permeability in all the directions equal to 0.04 m/s. The permeability is the only parameter to vary in order to represent the wide grading, as the grain-size characteristics are only considered when the sediment transport is computed: for lower values of the permeability the pressure oscillations increase in amplitude, being far from the measured signal (Fig. 6.2), until for the value 0.001 the whole crest gets saturated and large overtopping occurs. If the permeability is set to 0.05 on the other hand, the results show instability.

Despite the different frequency of the oscillations, the same main peaks of pressure corresponding to the highest waves can be recognised in the graphs above. However, the two sets of pressure values are rather different in two senses:

- there is ratio of about 3 in the magnitudes of the values (higher in the numerical model);
- the peaks of the pressure signal predicted by XBeach are more pronounced than the troughs, while they are more or less balanced in the physical model.

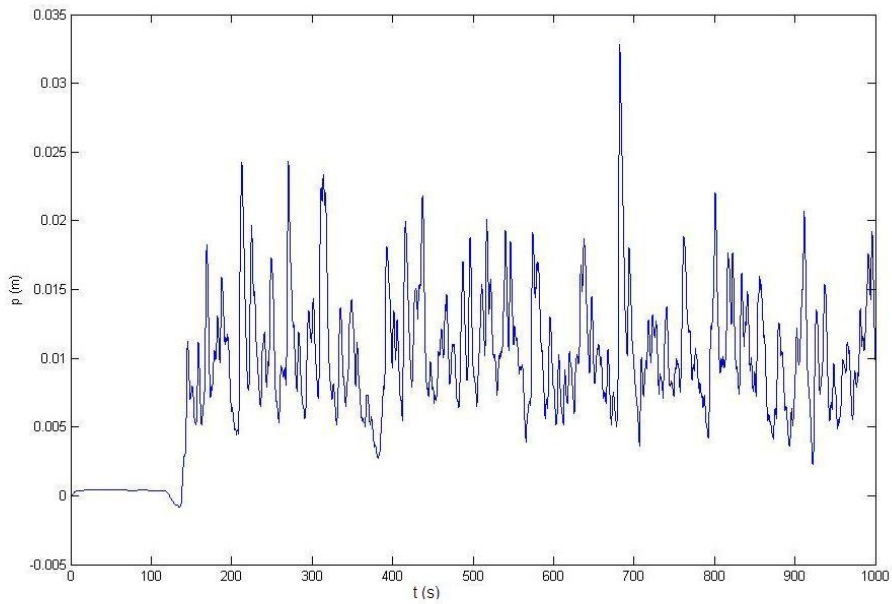

Figure 6.1 – Pressure signal simulated by XBeach

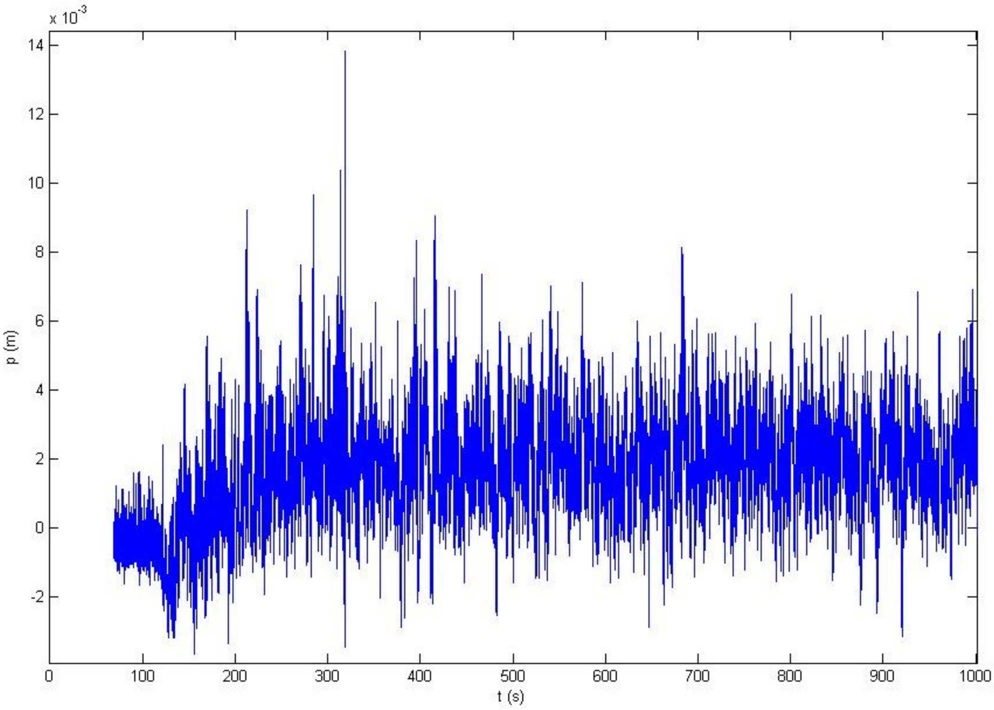

Figure 6.2 – Pressure signal measured during the laboratory tests

The first difference, more relevant, can be explained with the fact that the numerical model assumes only hydrostatic pressures. An indication of how wrong is this assumption may be given by measurements of pressure at different heights inside the structure. In the determination of the magnitude of the pressure, also the permeability on the vertical direction may play a role. Further attempts of calibration can be carried out with differentiation of the parameter permeability in the *x* and *z* directions.

The second difference may result from the boundary condition of water level imposed at a short distance behind the structure.

6.3 Comparison of morphological changes

Including the sediment transport calculations in the numerical model, a comparison between the computed and observed reshaping of the structure can be carried out.

Considering the same wave load of the previous paragraph, the model overestimates the morphological changes if the input grain-size distribution parameters are the same of the physical model. Increasing the median diameter of the material in the model slows down the reshaping of the structure: assuming D_{50} equal to 0.025 m (and D_{90} equal to 0.04 m), the numerical model calculates after 500 s a profile similar to the one measured at the end of the real wave attack (1750 s) at least in term of crest erosion and toe accretion, as shown in the graphs below.

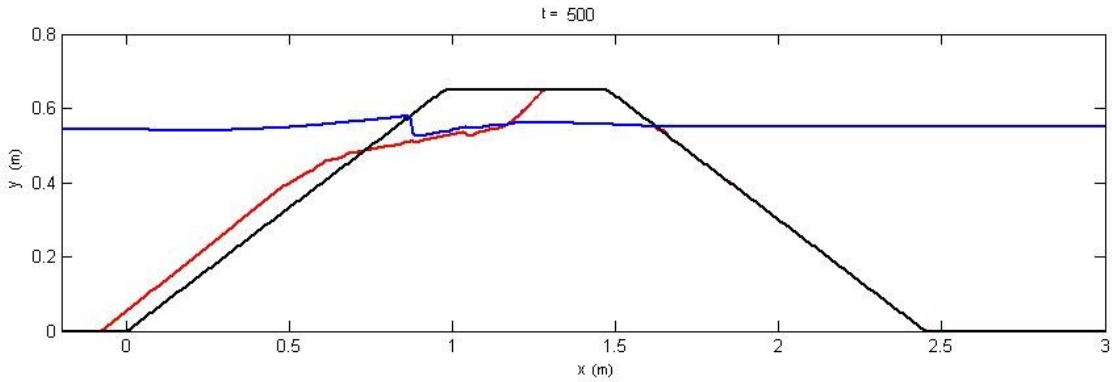

Figure 6.3 – Reshaping calculated by XBeach after a wave attack of 500 s (with "fictitious" D_{50})

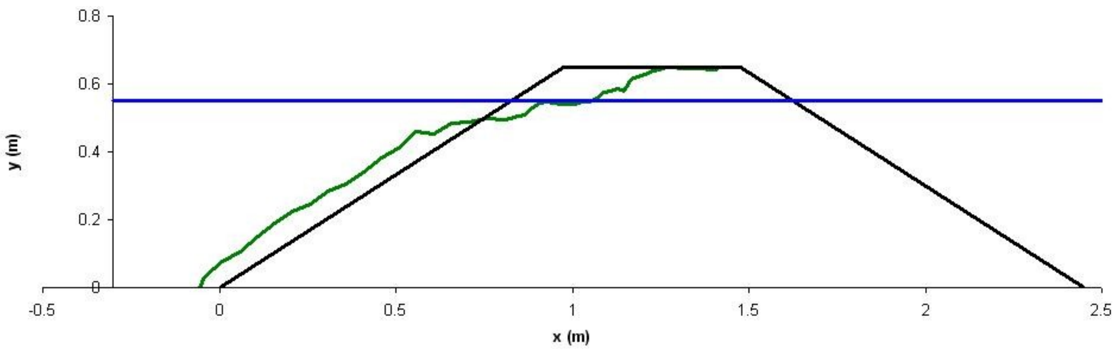

Figure 6.4 – Reshaping measured in the physical model after a wave attack of 1750 s

However the effect of increasing the median diameter is small, and higher values of this parameter were not included in further simulations. The inaccuracy of the model may consist in the formulation assumed for the sediment transport computation (Soulsby-van Rijn), which may not be suited for the particular flow regime and is certainly not meant for sediments with the size of centimetres.

In the representation of the wide grading of the material, other parameters like the permeability and the D_{90} may play a role. While in the simulation of Fig. 6.3 the permeability was equal to 0.01 in all the directions, a value of 0.03 results in more damage, with the difference increasing as the wave attack becomes longer. An increase of the value of D_{90} (0.05 m or more) results in an avalanching phenomenon on the initial slopes both at the front and at the rear side of the structure, with a resulting decrease of stability and increase of damage.

6.4 Conclusions

The few examples presented above show how the predictions of a model meant for the simulation of the reshaping of highly dynamic bodies are not too far from the reality observed during the physical model tests carried out in this study.

In the implementation of the model some restrictive choices are done. Some are listed below:

- the representation of the groundwater flow is done through the Darcy law, valid only for laminar flow conditions;
- the sediment transport is computed according to the Soulsby-van Rijn formulation, not suited in the case the material is coarser than sand;
- the pressures are assumed hydrostatic.

By virtue of this specific implementation, comparable results between the physical and the numerical model can not be obtained if the D_{50} is not varied in the latter. Nevertheless, a rough calibration can still be carried out with respect to relevant parameters like the permeability in the horizontal and vertical direction, the Courant number and the D_{90}.

Given these preliminary results, the measurements from physical model tests like the ones carried out in the present study may provide a useful term of comparison in the development of a numerical model like XBeach.

Chapter 7

Conclusions and directions for further research

7.1 Wide grading and stability

The main objective of this study, and at the same time its significance, is the approach of a well-known issue, the stability of coastal structures, from a rather new point of view, which is the focus on the grading of constituting material, following the need of designers and contractors for guidance during the planning and execution of maritime works.

The literature review of Chapter 2 pointed out how previous researchers did not investigate a range in the parameter grading typical of the material commonly used in practice. The outcome of both physical and numerical models, however, provided a better insight in the physical phenomena directly related to the widening of the grading. In particular it was observed that:

- A more graded wide material is more impermeable, thus reducing the dissipation of wave energy and enhancing the instability;
- The presence of different grain sizes leads to a segregation mechanism and the accumulation of big stones in certain areas of the reshaping profiles may result in better stability.

Due to these apparently contrasting effects of the grading on the stability, the conclusion drawn by other researchers are not always in accordance. In particular, available design tools for the estimation of geometrical parameters like the erosion of the berm give inverse trend in the influence of the grading. The formula by Hall and Kao (1991) finds a minimum in the stability for D_{85}/D_{15} equal to about 3. On the other hand, the formula by Tørum et al. (2003) predicts a maximum in the stability for D_{85}/D_{15} equal to 1.2.

Laboratory tests were carried out to provide direct insight in the issues of above (see Chapter 3). It was clearly visible that the segregation mechanism moves the bigger stones at the toe of the profile, thus they do not provide any stability to the more dynamic part of the profile. The general trend deduced from the tests is that, for high values of grading, the stability decreases and the erosion of the structure is enhanced.

The results of the tests seem to agree with the interpretation of Tørum et al., at least in qualitative terms. A quantitative comparison between the estimations by Hall and Kao and Tørum et al. and the results of the tests is not completely reliable due to the different investigated ranges of the parameter grading, and to the different set-up of the tests. This is shown in Chapter 4.

Significant results come out, instead, comparing the measured profiles and the parameterization of a dynamic profile given by van der Meer (1988, 1992). In general it was observed that, although the appearance of the reshaped profiles is similar, the effect of the wide grading shown by the tests is a greater horizontal spreading of the stone displacements.

The features of the measured profiles show also that the slope of the structure is a governing parameter for the stability, with a steeper initial slope enhancing the reshaping mechanism. This is in accordance with the findings of van der Meer when the parameter H_0T_0 assumes relatively low values, which is the case of the present tests, meant to simulate wave attacks with low return period.

7.2 A new design tool

As the parameter grading is not included in the formulas by van der Meer (1992), a curve fitting procedure allowed to derived new formulas to describe the features of the reshaped profiles taking into account the grading, some of them consisting of an adaptation of the formulas by van der Meer. The H_0T_0 number proved to be a suitable synthetic representation of the wave load intensity in the interpolation of the measured data.

The new set of formulas derived in Chapter 5 lead to the implementation of a numerical model for the calculation of a reshaped profile. With the necessary refinements, it may provide engineers and contractors with a simple and practical design tool.

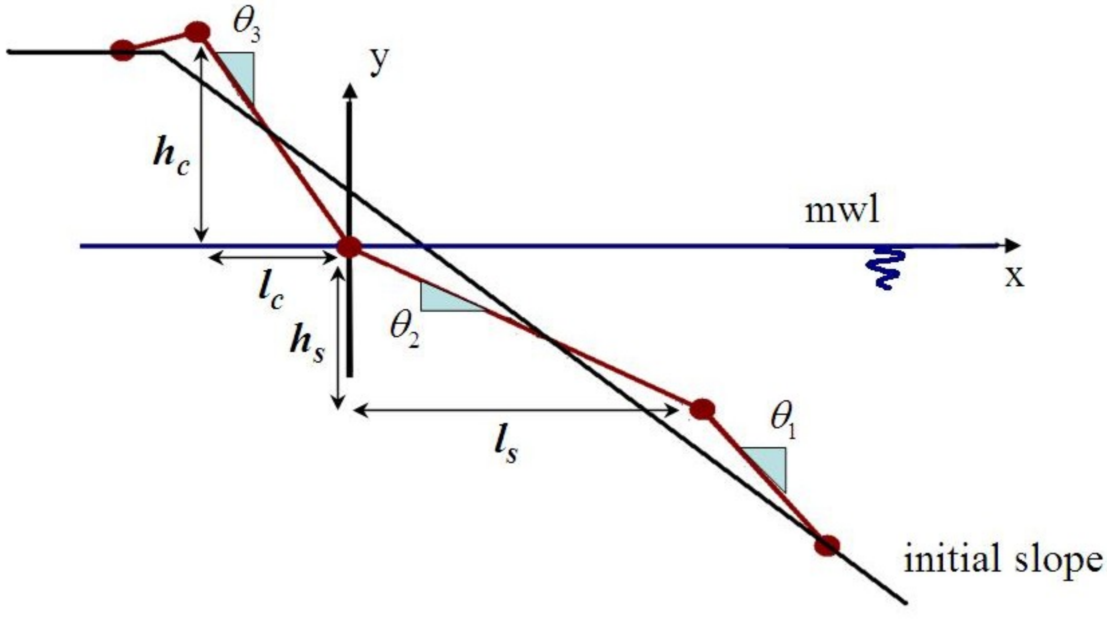

Figure 7.1 – Parameterization of a generic reshaped profile

With reference to Fig. 7.1, the following list summarizes the equations which constitute the numerical model in its actual development stage (presented in Appendix D).

- Slope θ_1 (van der Meer, 1992):

$$\theta_1 = 1.1 \tan \alpha_3{}^A \tag{7.1}$$

- Length of the step, l_s (present study):

$$H_0T_0 = 1.66(l_s / D_{n50} N^{0.07})^{1.3} \left(\frac{D_{85}}{D_{15}} \right)^{-0.15} + 29.1 \cot \alpha_2 - 9.38 \tag{7.2}$$

- Height of the step, h_s (van der Meer, 1992):

$$h_s / H_s N^{0.07} = 0.22 s_m{}^{-0.3} \quad (H_0T_0 > 300 \cot\alpha_2) \tag{7.3}$$

$$H_0T_0 = 27\left(H_s / D_{n50} N^{0.07}\right)^{1.3} + 125 \cot \alpha_2 - 475 \quad (H_0T_0 < 300 \cot\alpha_2) \tag{7.4}$$

- Length of the crest, l_c (present study):

$$(H_0T_0 - 183) \cot \alpha_1 = 139\left(l_c / D_{n50} N^{0.12}\right)\left(\frac{D_{85}}{D_{15}} \right)^{-0.29} - 667 \tag{7.5}$$

- Slope θ_3 (present study):

$$\theta_3^{-1} = 0.00023 \left(\frac{D_{85}}{D_{15}} \right)^{1.58} \left(H_0T_0\right)^{0.84} + 1.50 \tag{7.6}$$

- Run-up length, l_r: given by the intersection between the original profile and a slope equal to 1:1.5 behind the crest.

In all the above equations, given that θ_1 corresponds to β (see Fig. 2.7), the meaning of the symbols is in accordance with van der Meer (1992).

7.3 Further developments of this research

Not all the data collected during the tests were used in the analysis described above. In particular, video recordings of the reshaping process and digital pictures of the modified grain size along the slope may provide further insight in the trend of displacements and segregation induced by the wave attacks.

A direct measurement of porosity or permeability was missing in the present study, although they are supposed to be related to the parameter D_{85}/D_{15}. Indirectly, the measured values of pressure at different locations inside the model structure may be used to fill this gap. A deeper analysis of how the grading affects the mechanical properties of a porous material like a rubble mound will constitute a useful theoretical basis for a similar research. In this respect, physical models are still to be considered the most suitable way to investigate phenomena like porous flow or segregation of stones which are not prone to an analytical approach.

All the possible sources of inaccuracy of the measurements described in Chapter 3 should be considered both in the use of the data coming from this research and in the set-up and execution of new laboratory tests. For the present tests, although the flow regime inside the model structure is probably modified by the geometrical scaling with respect to an ideal prototype, scale effects in the representation of the stability phenomenon are supposed to be small.

Moreover, the results presented in Chapter 6 show how the pressures measured during the laboratory tests may also constitute a reliable term of comparison with the output of numerical models like XBeach, with the measured water levels providing a detailed set of boundary conditions. In this way a significant contribution in the development of such models can be given.

In conclusion, further investigations based on the findings of this research are strongly recommended, either through additional laboratory tests or maybe coupling numerical and physical modelling. Using a suitable similarity, this research will hopefully constitute a proper “bund” waiting for un upcoming “reclamation”.

References

Archetti R (1998), *Rimodellamento di frangiflutti dinamicamente stabili*. Doctoral Thesis, Politecnico di Milano, Politecnico di Torino, Università di Bologna, Università di Pavia

Burcharth HF, Andersen OH (1995), *On the one-dimensional steady and unsteady porous flow equations*. Coastal Engineering 24: 233-257, Elsevier

Burcharth HF, Liu Z, Troch P (1999), *Scaling of core material in rubble mound breakwater model tests*. Proceedings of COPEDEC V: 1518-1528, Cape Town, South Africa

CIRIA/CUR/CETMEF (2007), *The Rock Manual - The use of rock in hydraulic engineering (2nd edition)*. CIRIA C683, London

Hall KR, Kao JS (1991), *The influence of armour stone gradation on dynamically stable breakwaters*. Coastal Engineering 15: 333-346, Elsevier

Hudson RY (1959), *Laboratory investigations of rubble mound breakwaters*. WES Report, Vicksburg, USA

Hughes SA (1993), *Physical models and laboratory techniques in coastal engineering*. Advanced Series on Ocean Engineering – Volume 7, World Scientific

Hydronamic (2006), *Technical Evaluation Design and Engineering*. Ras Laffan Port Expansion Project

Jensen OJ, Klinting P (1983), *Evaluation of scale effects in hydraulic models by analysis of laminar and turbulent flows*. Coastal Engineering 7: 319-329, Elsevier

Juhl J, Sloth P (1998), *Berm Breakwaters - Influence of Stone Gradation, Permeability and Armouring*. 26th International Conference on Coastal Engineering: 1394-1406, ASCE, Copenaghen, Denmark

Kao JS, Hall KR (1990), *Trends in Stability of Dynamically Stable Breakwaters*. 22nd International Conference on Coastal Engineering: 1730-1741, ASCE, Delft, The Netherlands

Kramer MA (1991), *Nonlinear Principal Component Analysis Using Autoassociative Neural Networks*. AIChE Journal, vol. 37 n. 2: 233-243

Lamberti A, Tomasicchio GR (1997), *Stone mobility and longshore transport at reshaping breakwaters*. Coastal Engineering 29: 263-289, Elsevier

Mansard EPD, Davies MH, Caron O (1996), *Model Study of Reservoir Riprap Stability*. 25th International Conference on Coastal Engineering: 1748-1761, ASCE, Orlando, Florida

PIANC (2003), *State-of-art of designing and constructing berm breakwaters*. MarCom Report of Working Group 40, PIANC, Brussels

Roelvink JA, Reniers A, van Dongeren A, van Thiel de Vries J, Lescinski J, McCall R (2008), *Xbeach Model Description and Manual*. Unesco-IHE Institute for Water Education, Deltares and Delft University of Technology

Rouault P, Marth R, Nehrig M (2005), *Resulting composition of breakwater core due to rock size separation caused by the construction method*. Paper presented at International Coastal Symposium, June 5-8, Höfn, Iceland

Rubin DM (2004), *A simple autocorrelation algorithm for determining grain size distribution from digital images of sediment*. Journal of Sedimentary Research, January 2004: 160-165, SEPM

Sigurdarson S, Viggosson G, Smarason OB (2005), *Recent berm breakwater projects*. Paper presented at International Coastal Symposium, June 5-8, Höfn, Iceland

Tørum A (1998), *On the stability of berm breakwaters in shallow and deep water*. 26th International Conference on Coastal Engineering: 1435-1448, ASCE, Copenaghen, Denmark

Tørum A, Kuhnen F, Menze A (2003), *On berm breakwaters. Stability, scour, overtopping*. Coastal Engineering 49: 209-238, Elsevier

Tørum A, Sveinung L, Myhra H (2005), *Sirevåg berm breakwater – comparison between model and prototype reshaping*. Paper presented at International Coastal Symposium, June 5-8, Höfn, Iceland

Van der Meer JW (1988), *Rock Slopes and Gravel Beaches under Wave Attack*. Doctoral Thesis, Technical University Delft

Van der Meer JW, Pilarczyk KW (1987), *Dynamic stability of rock slopes and gravel beaches*. Delft Hydraulics Communication No. 379, Delft

Van der Meer JW (1992), *Stability of the seaward slope of berm breakwaters*. Coastal Engineering 16: 205-234, Elsevier

Van der Meer JW, Tutuarima WH, Burger G (1996), *Influence of rock shape and grading on stability of low-crested structures*. 25th International Conference on Coastal Engineering: 1957-1970, ASCE, Orlando, Florida

Van Gent MRA (1994), *The modeling of wave action on and in coastal structures*. Coastal Engineering 22: 311-339, Elsevier

Van Gent MRA (1995), *Wave interaction with permeable coastal structures*. Doctoral Thesis, Technical University Delft

Van Gent MRA (1996), *Numerical modelling of wave interaction with dynamically stable structures*. 25th International Conference on Coastal Engineering: 1930-1943, ASCE, Orlando, Florida

Verhage L, van Dongeren A (2003), *DELFT/AUKE – GENERATE Wave board computation software manual,* version 3.00. WL|Delft Hydraulics

APPENDIX A

Input and output parameters of the tests

INPUT:

Test n.	Wave train n.	α	ρ	Δ	D_n50	D_{85}/D_{15}	H_s	T_m	s_m	N_s=H_0	H_0T_0	N
			[kg/m^3]		[m]		[m]	[s]				
1	1	0.667	2652	1.652	0.01093	2.71	0.0720	1.483	0.0210	3.99	177	7300
1	2	0.667	2652	1.652	0.01093	2.71	0.1071	1.212	0.0467	5.94	216	2000
1	3	0.667	2652	1.652	0.01093	2.71	0.1236	1.327	0.0450	6.85	272	2000
1	4	0.667	2652	1.652	0.01093	2.71	0.1213	1.466	0.0361	6.72	295	2000
2	1	0.667	2650	1.650	0.01100	7.44	0.0710	0.971	0.0483	3.91	113	2000
2	2	0.667	2650	1.650	0.01100	7.44	0.0873	1.091	0.0470	4.81	157	2000
2	3	0.667	2650	1.650	0.01100	7.44	0.1057	1.192	0.0477	5.82	207	2000
2	4	0.667	2650	1.650	0.01100	7.44	0.1176	1.295	0.0449	6.48	251	2000
2	5	0.667	2650	1.650	0.01100	7.44	0.1142	1.451	0.0347	6.29	273	2000
3	1	0.667	2650	1.650	0.01100	7.44	0.0710	0.971	0.0483	3.91	113	2000
3	2	0.667	2650	1.650	0.01100	7.44	0.0872	1.082	0.0477	4.80	155	2000
3	3	0.667	2650	1.650	0.01100	7.44	0.1039	1.183	0.0475	5.72	202	2000
3	4	0.667	2650	1.650	0.01100	7.44	0.1160	1.295	0.0443	6.39	247	2000
3	5	0.667	2650	1.650	0.01100	7.44	0.1112	1.442	0.0343	6.13	264	2000
4	1	0.667	2650	1.650	0.01100	7.44	0.1126	1.437	0.0349	6.20	266	3000
5	1	0.333	2650	1.650	0.01100	7.44	0.0714	0.964	0.0492	3.93	113	2000
5	2	0.333	2650	1.650	0.01100	7.44	0.0861	1.089	0.0466	4.75	154	2000
5	3	0.333	2650	1.650	0.01100	7.44	0.1027	1.191	0.0464	5.66	201	2000

5	4	0.333	2650	1.650	0.01100	7.44	0.1156	1.293	0.0443	6.37	246	2000
5	5	0.333	2650	1.650	0.01100	7.44	0.1198	1.504	0.0339	6.60	297	2000
5	6	0.333	2650	1.650	0.01100	7.44	0.1338	1.680	0.0304	7.37	370	2000
6	1	0.667	2659	1.659	0.01102	17.7	0.0701	0.963	0.0484	3.83	110	2000
6	2	0.667	2659	1.659	0.01102	17.7	0.0845	1.082	0.0463	4.62	149	2000
6	3	0.667	2659	1.659	0.01102	17.7	0.1003	1.182	0.0460	5.49	193	2000
6	4	0.667	2659	1.659	0.01102	17.7	0.1090	1.278	0.0427	5.97	228	2000
6	5	0.667	2659	1.659	0.01102	17.7	0.1050	1.434	0.0327	5.75	246	2000
7	1	0.667	2659	1.659	0.01102	17.7	0.1060	1.436	0.0330	5.80	249	3000
8	1	0.333	2659	1.659	0.01102	17.7	0.0828	1.075	0.0459	4.53	145	2000
8	2	0.333	2659	1.659	0.01102	17.7	0.0995	1.184	0.0455	5.44	192	2000
8	3	0.333	2659	1.659	0.01102	17.7	0.1111	1.283	0.0432	6.08	233	2000
8	4	0.333	2659	1.659	0.01102	17.7	0.1118	1.496	0.0320	6.12	273	2000
8	5	0.333	2659	1.659	0.01102	17.7	0.1244	1.693	0.0278	6.81	344	2000
9	1	0.667	2657	1.657	0.01099	17.7	0.0698	0.968	0.0477	3.83	111	2000
9	2	0.667	2657	1.657	0.01099	17.7	0.0835	1.072	0.0465	4.59	147	2000
9	3	0.667	2657	1.657	0.01099	17.7	0.0975	1.167	0.0458	5.35	187	2000
9	4	0.667	2657	1.657	0.01099	17.7	0.1045	1.267	0.0417	5.74	217	2000

OUTPUT:

Test n.	Wave train n.	θ_1	h_s	l_s	θ_2	h_c	l_c	θ_3	Rec
			[m]	[m]		[m]	[m]		[m]
1	1	0.801	0.174	0.699	0.249	0.126	0.226	0.558	0.250
1	2	0.883	0.182	0.812	0.224	0.135	0.213	0.635	0.293
1	3	0.712	0.191	0.926	0.206	0.109	0.225	0.484	0.469
2	1	0.779	0.094	0.411	0.229	0.108	0.200	0.454	0.176
2	2	0.701	0.116	0.597	0.195	0.115	0.220	0.523	0.310
2	3	0.682	0.152	0.821	0.185	0.108	0.220	0.491	0.388
3	1	0.849	0.124	0.476	0.260	0.111	0.204	0.544	0.157
3	2	0.707	0.139	0.656	0.212	0.113	0.178	0.637	0.278
3	3	0.793	0.170	0.848	0.200	0.127	0.256	0.496	0.390
5	1	0.407	0.065	0.370	0.175	0.099	0.212	0.250	0.025
5	2	0.445	0.094	0.511	0.184	0.111	0.220	0.269	-0.033
5	3	0.489	0.123	0.676	0.182	0.130	0.244	0.532	0.034
5	4	0.513	0.140	0.792	0.177	0.150	0.282	0.531	0.078
5	5	0.541	0.182	1.005	0.182	0.172	0.353	0.487	0.163
6	1	0.835	0.119	0.608	0.195	0.099	0.216	0.459	0.296
6	2	0.866	0.143	0.721	0.198	0.096	0.303	0.316	0.453
6	3	0.877	0.179	0.828	0.216	0.094	0.317	0.297	0.478
8	1	0.362	0.054	0.297	0.182	0.110	0.323	0.341	0.038
8	2	0.498	0.129	0.748	0.173	0.101	0.460	0.222	0.185
8	3	0.535	0.131	0.863	0.152	0.121	0.414	0.292	0.242
8	4	0.523	0.153	1.044	0.147	0.094	0.421	0.223	0.412

APPENDIX B

Profile measurements

The toe of the structure is the origin of the measurements (x = y = 0)

Test	**1**	**Test**	**1**	**Test**	**1**	**Test**	**1**	**Test**	**2**
Wave	**1**	**Wave**	**2**	**Wave**	**3**	**Wave**	**4**	**Wave**	**1**
x (cm)	**y (cm)**	**x (cm)**	**y (cm)**	**x (cm)**	**y (cm)**	**x (cm)**	**y (cm)**	**x (cm)**	**y (cm)**
-9.2	0	-9.4	0	-17	0	-22.8	0	0.3	0
-4.2	1.8	-2.2	9.4	-14.2	4.2	-19.2	4.5	0.8	2.4
0.8	7.6	0.8	11.7	-9.2	8.3	-14.2	8.6	5.8	5.2
5.8	13.3	5.8	15.6	-4.2	11.2	-9.2	12.1	10.8	8.9
10.8	16.3	10.8	19.9	0.8	14.3	-4.2	13.6	15.8	12.8
15.8	18.2	15.8	22.7	5.8	17	0.8	18	20.8	17.1
20.8	21.8	20.8	26	10.8	20.9	5.8	18.9	25.8	22.7
25.8	25.3	25.8	29	15.8	24.2	10.8	22	30.8	26.3
30.8	28.5	30.8	32.7	20.8	27.1	15.8	22.9	35.8	30.3
35.8	32.4	35.8	34.3	25.8	30.1	20.8	24.7	40.8	35.3
40.8	36	40.8	35.7	30.8	32.8	25.8	27.7	45.8	37.4
45.8	39.1	45.8	38.3	35.8	34.9	30.8	28.9	50.8	39.9
50.8	41.3	50.8	40.4	40.8	37.2	35.8	31.3	55.8	42.5
55.8	42.7	55.8	42.1	45.8	38.4	40.8	32.6	60.8	45.2
60.8	43.9	60.8	44.7	50.8	39.8	45.8	33.4	62.8	45.6
65.8	44.8	65.8	45.7	55.8	40.9	50.8	35	64.8	46.4
70.8	45.8	70.8	46.1	60.8	41.6	55.8	36.2	66.8	46.8
75.8	46.9	75.8	47.8	65.8	43.1	60.8	37.3	68.8	47.4
80.8	48	80.8	48.1	70.8	44.2	65.8	38.6	70.8	49.8
85.8	48.7	82.8	48.7	75.8	45.2	70.8	39.7	72.8	50.1
90.8	49.9	84.8	49.1	80.8	46.8	75.8	40.4	74.8	50.7
95.8	51.3	86.8	49.2	82.8	47.4	80.8	41.3	76.8	50.8
100.8	52.2	88.8	49.7	84.8	47.9	85.8	42.1	78.8	51.4
105.8	53.6	90.8	49.9	86.8	47.9	90.8	44.2	80.8	51.7
110.8	56.5	92.8	50.3	88.8	48.4	95.8	44.8	82.8	52
115.8	59.8	94.8	50.8	90.8	48.5	100.8	45.2	84.8	52.3
120.8	63.8	96.8	51.5	92.8	49.2	105.8	45.7	86.8	52.5
125.8	67.4	98.8	51.9	94.8	48.9	110.8	46.2	88.8	52.8
130.8	67.6	100.8	52.1	96.8	49.2	115.8	47.2	90.8	53.3
135.8	66.1	102.8	52.7	98.8	49.8	120.8	47.3	92.8	53.6
140.8	65.2	104.8	53.1	100.8	50.2	125.8	49.1	94.8	54.1

145.8	65.3	106.8	53.3	102.8	50.7	130.8	48.9	96.8	54.8
150.8	65	108.8	54	104.8	51	135.8	50.1	98.8	55
		110.8	54.7	106.8	51.1	140.8	50.5	100.8	55.1
		112.8	55.5	108.8	51.2	145.8	51.8	102.8	54.9
		114.8	56.3	110.8	51.7	150.8	53	104.8	55.6
		116.8	57.1	112.8	52.6	155.8	53.5	106.8	56.6
		118.8	58.3	114.8	53.1	160.8	53.5	108.8	58.1
		120.8	59.4	116.8	53.4	165.8	54.3	110.8	62.7
		122.8	60.8	118.8	53.9	170.8	54.8	112.8	64.1
		124.8	63	120.8	54.3	175.8	54.3	114.8	64.9
		126.8	65	122.8	54.9	180.8	54.6	116.8	65.5
		128.8	66.8	124.8	55.1	185.8	54.1	118.8	65.8
		130.8	67.8	126.8	56.7	190.8	54	120.8	65.8
		132.8	68.5	128.8	58.2	195.8	52.2	122.8	65.9
		134.8	68.1	130.8	58.9	200.8	50.6	124.8	65.7
		136.8	67.7	132.8	59.8			126.8	65.7
		138.8	67.2	134.8	60.7			128.8	65.6
		140.8	66.8	136.8	61.6			130.8	65.7
		142.8	66.2	138.8	62.5				
		144.8	65.8	140.8	63.9				
		146.8	65	142.8	64.6				
		148.8	64.6	144.8	65.1				
		150.8	64.5	146.3	65.9				
				146.8	65.4				
				148.8	65.2				
				150.8	64.8				
				152.8	64.4				
				154.8	63.9				
				156.8	63.4				
				158.8	62.6				
				160.8	61.6				
				162.8	60.8				
				164.8	59.4				
				166.8	57.4				
				168.8	56.4				
				170.8	56.1				
				172.8	55.5				
				174.8	54.8				
				176.8	54.7				
				178.8	53.9				
				180.8	53.6				
				182.8	52.7				
				184.8	51.3				
				186.8	49.7				

188.8	47.9
190.8	46.1
192.8	43.8
194.8	42
196.8	39.5
198.8	37.4
200.8	35.4

Test	**2**	**Test**	**2**	**Test**	**2**	**Test**	**2**	**Test**	**3**
Wave	**2**	**Wave**	**3**	**Wave**	**4**	**Wave**	**5**	**Wave**	**1**
x (cm)	**y (cm)**	**x (cm)**	**y (cm)**	**x (cm)**	**y (cm)**	**x (cm)**	**y (cm)**	**x (cm)**	**y (cm)**
-11.8	0	-17.8	0	-19.9	0	-25	0	0.3	0
-9.2	1.7	-14.2	3.2	-19.2	3.5	-24.2	3.9	0.8	4.1
-4.2	4	-9.2	5.4	-14.2	6.2	-19.2	4.9	5.8	6
0.8	6.6	-4.2	8.4	-9.2	7.5	-14.2	8	10.8	9.3
5.8	10.7	0.8	11.9	-4.2	13.1	-9.2	11.7	15.8	14.2
10.8	16.8	5.8	17.1	0.8	15.9	-4.2	13.7	20.8	19.7
15.8	20.5	10.8	20.5	5.8	19.1	0.8	16.2	25.8	23.4
20.8	23.3	15.8	23.4	10.8	22.1	5.8	18.4	30.8	26.4
25.8	26.8	20.8	26.5	15.8	23	10.8	21.2	35.8	29.1
30.8	31.1	25.8	29.7	20.8	26.3	15.8	22.7	40.8	32.3
35.8	34.1	30.8	31.8	25.8	29.3	20.8	25.9	45.8	35.2
40.8	35.9	35.8	34.5	30.8	32.5	25.8	28.2	50.8	38.8
45.8	37.7	40.8	36.1	35.8	34.7	30.8	29.8	55.8	42.1
50.8	39.6	45.8	39.7	40.8	35.7	35.8	32.8	60.8	43.9
55.8	42.9	50.8	41.1	45.8	37.5	40.8	34.1	62.8	45
60.8	45.2	55.8	42.3	50.8	37.9	45.8	35.7	64.8	45.7
65.8	47.7	60.8	43.6	55.8	38.9	50.8	37	66.8	46.2
70.8	47.5	65.8	45	60.8	40.5	55.8	38.1	68.8	47.1
75.8	48.5	70.8	45.7	65.8	41.8	60.8	40.2	70.8	47.7
80.8	49	75.8	47.1	70.8	42.5	65.8	40.7	72.8	49.1
82.8	49.5	80.8	47.9	75.8	44.2	70.8	40	74.8	49.6
84.8	50	85.8	49.3	80.8	45.1	75.8	41.8	76.8	50.4
86.8	50.3	90.8	50.3	85.8	47.4	80.8	43.2	78.8	52.3
88.8	51.1	95.8	50	90.8	47.2	85.8	43.5	80.8	53.3
90.8	51.4	100.8	50.9	95.8	47.3	90.8	44.9	82.8	53.2
92.8	51.8	102.8	51	100.8	48	95.8	44.9	84.8	53.6
94.8	51.9	104.8	51.5	105.8	49.9	100.8	46.7	86.8	53
96.8	52.1	106.8	51.6	110.8	50	105.8	46.3	88.8	54
98.8	52.2	108.8	52	115.8	50.5	110.8	49.7	90.8	53.6

100.8	52.6	110.8	52.3	120.8	52.3	115.8	50.4	92.8	54
102.8	53	112.8	52.6	125.8	51.5	120.8	48.4	94.8	54.2
104.8	53.2	114.8	52.9	130.8	52.3	125.8	49.1	96.8	55.2
106.8	53.8	116.8	53.5	135.8	54.5	130.8	48.7	98.8	56.7
108.8	54.2	118.8	54	140.8	56.4	135.8	51.3	100.8	57.7
110.8	55	120.8	54.5	145.8	57.2	140.8	52.1	102.8	59
112.8	55.8	122.8	55	150.8	57	145.8	52.8	104.8	60
114.8	56.5	124.8	55.3	152.8	57.2	150.8	53	106.8	60.2
116.8	57.4	126.8	56.2	155.8	57.3	155.8	55.1	108.8	60.4
118.8	58.1	128.8	56.5	160.8	56.5	160.8	56.8	110.8	63.7
120.8	58.9	130.8	58.9	165.8	55.9	165.8	56.4	112.8	64.8
122.8	60.1	132.8	62.3	170.8	54.1	170.8	55.4	114.8	65.8
124.8	62.3	134.8	64.4	175.8	53.8	175.8	53.4	116.8	66.1
126.8	63.9	136.8	65.2	180.8	53.5	180.8	54	118.8	66
128.8	65.2	138.8	65.4	185.8	52.7	185.8	52.5	120.8	66
130.8	66.1	140.8	65.6	190.8	51.3	190.8	51.4	122.8	65.5
132.8	66.5	142.8	65.7	195.8	49.5	195.8	50.9	124.8	65.6
134.8	66.4	143.8	65.8	200.8	46.6	200.8	48.8	126.8	65.5
136.8	66.1	144.8	65.8	205.8	43.4	205.8	45.8		
138.8	65.8	146.8	65.6			210.8	41.8		
140.8	65.5	148.8	65			215.8	38.3		
142.8	65.4	150.8	64.2			220.8	35.2		
144.8	65.4	152.8	62.6			225.8	30.3		
146.8	65.3	154.8	59.9			230.8	25.6		
		156.8	59.7						
		158.8	59.6						
		160.8	59.6						
		162.8	58.9						
		164.8	58						
		166.8	56.9						
		168.8	56.5						
		170.8	56.3						
		172.8	55.9						
		174.8	55.3						
		176.8	54.9						
		178.8	54.1						
		180.8	53.1						
		185.8	49.3						
		190.8	43.9						
		195.8	40.9						
		200.8	36.9						

Test	3	Test	3	Test	3	Test	3	Test	4
Wave	**2**	**Wave**	**3**	**Wave**	**4**	**Wave**	**5**		
x (cm)	**y (cm)**	**x (cm)**	**y (cm)**	**x (cm)**	**y (cm)**	**x (cm)**	**y (cm)**	**x (cm)**	**y (cm)**
-8.7	0	-12.7	0	-16.2	0	-24.2	0	-22.9	0
-4.2	8.4	-9.2	6.9	-14.2	3.5	-19.2	5.7	-19.2	3.7
0.8	11.2	-4.2	9.6	-9.2	10	-14.2	10.3	-14.2	10
5.8	12.8	0.8	13.7	-4.2	13.2	-9.2	12.5	-9.2	12
10.8	16.2	5.8	16.9	0.8	14.8	-4.2	14.1	-4.2	13.6
15.8	19.5	10.8	20	5.8	17.3	0.8	17.7	0.8	15.6
20.8	23.1	15.8	22.4	10.8	20.8	5.8	19.6	5.8	19.7
25.8	25.4	20.8	25.1	15.8	24.2	10.8	22.1	10.8	20.2
30.8	28	25.8	30.1	20.8	27.1	15.8	23.4	15.8	23.4
35.8	31.5	30.8	32.1	25.8	29.7	20.8	27	20.8	26.7
40.8	34.9	35.8	33.3	30.8	31.4	25.8	28.1	25.8	29.1
45.8	37.8	40.8	36.5	35.8	34.1	30.8	31	30.8	30.1
50.8	41.4	45.8	38.8	40.8	36.6	35.8	33.1	35.8	31.6
55.8	41.6	50.8	40.8	45.8	38.2	40.8	33.1	40.8	33.4
60.8	43.4	55.8	41.7	50.8	39.6	45.8	34.3	45.8	36.1
65.8	45	60.8	43.8	55.8	39.7	50.8	36.3	50.8	37.6
70.8	46.3	65.8	45	60.8	40.8	55.8	38.2	55.8	38.2
75.8	49.8	70.8	45.7	65.8	44.1	60.8	40.2	60.8	39.5
80.8	50	75.8	48.2	70.8	45	65.8	40.6	65.8	41.9
82.8	49.9	80.8	48.3	75.8	46	70.8	43.2	70.8	43.1
84.8	50.1	85.8	49.1	80.8	45.4	75.8	44	75.8	43.9
86.8	50.2	90.8	49.6	85.8	47.1	80.8	43.7	80.8	45.5
88.8	50.5	95.8	51.1	90.8	47.8	85.8	44.4	85.8	43.6
90.8	50.8	100.8	52.1	95.8	48.2	90.8	47.1	90.8	44.7
92.8	51.3	102.8	52.3	100.8	48.9	95.8	47.7	95.8	46.4
94.8	51.7	104.8	52.8	105.8	51.5	100.8	48.5	100.8	45.9
96.8	51.9	106.8	52.9	110.8	51.8	105.8	48.1	105.8	47
98.8	52.3	108.8	53	115.8	51.1	110.8	49.8	110.8	48
100.8	52.4	110.8	52.6	120.8	54.2	115.8	49.7	115.8	49.4
102.8	52.6	112.8	53.2	125.8	54.4	120.8	52	120.8	50.1
104.8	53.2	114.8	54.7	130.8	54.6	125.8	51	125.8	51
106.8	53.5	116.8	54.9	135.8	54.5	130.8	51.9	130.8	51.4
108.8	54.1	118.8	55.4	140.8	55.2	135.8	54.2	135.8	52
110.8	54.9	120.8	55.6	145.8	56.6	140.8	52.9	140.8	53.2
112.8	55.7	122.8	56.4	150.8	56.7	145.8	54.2	145.8	53.7
114.8	58.2	124.8	57.7	155.8	54.9	150.8	56.2	150.8	53.8
116.8	59.2	126.8	58.3	160.8	54.5	155.8	56.8	155.8	55.3
118.8	61.6	128.8	59.5	165.8	54.9	160.8	55.4	160.8	53
120.8	62.4	130.8	60.6	170.8	55.1	165.8	54.6	165.8	54.2
122.8	64.2	132.8	62.1	175.8	53.6	170.8	53.4	170.8	55

124.8	64.8	134.8	63.5	180.8	53.5	175.8	51.9	175.8	54.4
126.8	65.6	136.8	65.3	185.8	51.2	180.8	51.4	180.8	54
128.8	66.3	138.8	66.7	190.8	49.7	185.8	52.1	185.8	53.5
130.8	66.2	140.8	67.6	195.8	45.1	190.8	50.5	190.8	51.2
132.8	66.1	141.8	67.7	200.8	42.6	195.8	48.6	195.8	50.5
134.8	65.9	142.8	67.7	205.8	38.7	200.8	45.4	200.8	47.2
136.8	65.7	144.8	67.4	210.8	35.5	205.8	43.4	205.8	43.9
138.8	65.3	146.8	66.3	215.8	31.1	210.8	37.6	210.8	40
140.8	65.4	148.8	65.5	220.8	27.2	215.8	33.7	215.8	37.5
142.8	65.2	150.8	64.7	225.8	23.6	220.8	30.2	220.8	32.9
144.8	65.2	152.8	64.2	230.8	16.6	225.8	26.3	225.8	28.9
146.8	65	154.8	63.3			230.8	23.1	230.8	24.9
		156.8	62.3						
		158.8	61.3						
		160.8	59.5						
		165.8	56.1						
		170.8	53.6						
		175.8	50.7						
		180.8	46.6						
		185.8	42.1						
		190.8	38.1						
		195.8	35.4						
		200.8	32.4						

Test	**5**	**Test**	**5**	**Test**	**5**	**Test**	**5**	**Test**	**5**
Wave	**1**	**Wave**	**2**	**Wave**	**3**	**Wave**	**4**	**Wave**	**5**
x (cm)	**y (cm)**	**x (cm)**	**y (cm)**	**x (cm)**	**y (cm)**	**x (cm)**	**y (cm)**	**x (cm)**	**y (cm)**
87.5	28.9	67.5	21.6	67.5	21.6	2.0	0.0	1	0
92.5	31.3	72.5	24.1	72.5	24.2	2.5	1.6	2.5	1.7
97.5	33.1	77.5	25.8	77.5	25.7	7.5	3.4	7.5	3.5
102.5	35.4	82.5	27.4	82.5	28.6	12.5	4.2	12.5	5
107.5	36.8	87.5	28.6	87.5	31	17.5	6.8	17.5	6.5
112.5	39.4	92.5	31.9	92.5	34.4	22.5	7.6	22.5	7.8
117.5	40.3	97.5	34.5	97.5	35.8	27.5	9.2	27.5	9.6
122.5	42.6	102.5	35.5	102.5	37.8	32.5	10.8	32.5	10.6
127.5	45.2	107.5	37.5	107.5	39.7	37.5	12.1	37.5	12.3
129.5	46.3	112.5	40.6	112.5	41.5	42.5	15.2	42.5	14.6
131.5	46.8	117.5	43.3	117.5	43	47.5	16.0	47.5	16.2
133.5	47.7	122.5	46.6	122.5	45.9	52.5	17.2	52.5	17.2
135.5	47.9	127.5	46.7	127.5	46.2	57.5	19.1	57.5	20.5

137.5	49.1	132.5	47.3	132.5	47.9	62.5	23.3	62.5	23.5
139.5	49.7	137.5	48.3	137.5	47.8	67.5	22.0	67.5	26.1
141.5	50.6	142.5	49.4	142.5	48.6	72.5	24.1	72.5	29.2
143.5	50.9	147.5	50.1	147.5	49.6	77.5	27.8	77.5	30.4
145.5	52	149.5	50.5	149.5	49.8	82.5	30.4	82.5	35.6
147.5	52.1	151.5	51.1	151.5	49.9	87.5	33.0	87.5	35.3
149.5	52.5	153.5	50.7	153.5	50.4	92.5	34.7	92.5	36.9
151.5	52.3	155.5	50.7	155.5	50.4	97.5	37.4	97.5	38.7
153.5	52.9	157.5	50.9	157.5	50.5	102.5	38.8	102.5	40.2
155.5	52.4	159.5	51.3	159.5	50.9	107.5	40.6	107.5	41
157.5	52.9	161.5	51.2	161.5	51.5	112.5	43.3	112.5	40.8
159.5	52.2	163.5	51.6	163.5	51.9	117.5	43.9	117.5	42.7
161.5	52.6	165.5	52.1	165.5	51.8	122.5	44.7	122.5	44
163.5	53.1	167.5	52.9	167.5	52.4	127.5	45.1	127.5	44.7
165.5	53.7	169.5	53.2	169.5	54.5	132.5	46.2	132.5	44.7
167.5	54.1	171.5	53.8	171.5	55.5	137.5	47.4	137.5	45
169.5	54.2	173.5	54.3	173.5	56.1	142.5	47.9	142.5	46.1
171.5	54.8	175.5	55	175.5	55.9	147.5	48.7	147.5	46.6
173.5	55.3	177.5	55.7	177.5	54.3	152.5	49.4	152.5	47.8
175.5	56.2	179.5	56.3	179.5	55.2	157.5	50.4	157.5	49
177.5	56.5	181.5	57.2	181.5	55.8	162.5	50.7	162.5	49.5
179.5	57.7	183.5	57.6	183.5	56.8	167.5	51.5	167.5	50.7
181.5	58.5	185.5	59.4	185.5	57.6	169.5	51.7	172.5	51.4
183.5	59.9	187.5	61.7	187.5	58.3	171.5	52.2	177.5	52
185.5	62.4	189.5	63.1	189.5	59.2	173.5	52.5	179.5	52.4
187.5	63.7	191.5	64.9	191.5	60	175.5	52.9	181.5	53
189.5	64.4	193.5	65.7	193.5	61.6	177.5	53.2	183.5	53.4
191.5	64.7	195.5	65.9	195.5	63.3	179.5	53.8	185.5	54.2
193.5	64.9	197.5	66.1	197.5	64.2	181.5	54.2	187.5	54.8
195.5	64.9	199.5	65.9	199.5	66	183.5	55.1	189.5	55.4
197.5	65	201.5	65.7	201.5	67.2	185.5	55.5	191.5	56
199.5	65.2	203.5	65.6	203.5	68	187.5	56.7	193.5	56.6
201.5	65.6	205.5	65.7	205.5	68	189.5	57.1	195.5	56.9
203.5	65.5	207.5	65.8	207.5	67.7	191.5	57.8	197.5	57.9
205.5	65.6	209.5	65.9	209.5	67.2	193.5	58.9	199.5	58.6
207.5	66	211.5	66	211.5	67	195.5	59.6	201.5	60.1
209.5	66.1	213.5	66	213.5	66.7	197.5	60.4	203.5	60.9
211.5	66	215.5	66.1	215.5	66.4	199.5	63.6	205.5	61.1
213.5	66.1	217.5	66.3	217.5	66.3	201.5	64.6	207.5	62.1
215.5	66.2			219.5	66.3	203.5	65.2	209.5	63.5
217.5	66.3			221.5	66.2	205.5	66.6	211.5	65.2
				223.5	66.1	207.5	68.4	213.5	66.5
				225.5	66	209.5	69.4	215.5	67.4
				227.5	66	211.5	70.0	217.5	68.9

				229.5	66.2	213.5	70.0	219.5	70.7
				231.5	66.1	215.5	69.6	221.5	71.8
				233.5	66.1	217.5	69.0	223.5	72.2
				235.5	66	219.5	68.5	225.5	72.2
				237.5	66.3	221.5	68.3	227.5	71.3
						223.5	67.9	229.5	71
						225.5	67.6	231.5	70.8
						227.5	67.2	233.5	70.1
						229.5	66.6	235.5	69.6
						231.5	66.5	237.5	68.5
						233.5	66.4	239.5	68
						235.5	66.3	241.5	67.4
						237.5	66.3	243.5	66.9
						239.5	66.0	245.5	66.2
								247.5	65.7
								249.5	64.8
								251.5	64.1
								253.5	63.3
								255.5	62.5
								257.5	61.4
								259.5	60.2
								261.5	59.4
								263.5	57.9
								265.5	55.4
								267.5	54.9

Test	**5**	**Test**	**6**	**Test**	**6**	**Test**	**6**	**Test**	**6**
Wave	**6**	**Wave**	**1**	**Wave**	**2**	**Wave**	**3**	**Wave**	**4**
x (cm)	**y (cm)**	**x (cm)**	**y (cm)**	**x (cm)**	**y (cm)**	**x (cm)**	**y (cm)**	**x (cm)**	**y (cm)**
-1.5	0	-5.7	0	-10.2	0	-10.7	0	-19.2	0
-2.5	1.5	-4.2	3.3	-9.2	1.9	-9.2	4.3	-19.2	2.2
2.5	2.8	0.8	7.6	-4.2	4.8	-4.2	7.7	-14.2	5.1
7.5	4.2	5.8	10.7	0.8	10.4	0.8	14.2	-9.2	9
12.5	5.8	10.8	15.2	5.8	14.8	5.8	16.1	-4.2	14.1
17.5	7.3	15.8	18.9	10.8	18.1	10.8	19.8	0.8	16.6
22.5	9	20.8	22.4	15.8	21.7	15.8	22.9	5.8	19.6
27.5	10.2	25.8	24.6	20.8	24.6	20.8	28.4	10.8	21.5
32.5	11.2	30.8	28.5	25.8	28.8	25.8	30.4	15.8	24.8
37.5	14.9	35.8	30.4	30.8	32	30.8	33.6	20.8	26.8
42.5	19.6	40.8	34	35.8	34.8	35.8	35.6	25.8	29.9
47.5	20.9	45.8	38.1	40.8	37.7	40.8	38	30.8	32.4

52.5	23.4	50.8	41.2	45.8	39.3	45.8	40	35.8	34.5
57.5	25.1	55.8	45.8	50.8	42.1	50.8	41.2	40.8	37.1
62.5	26.4	60.8	45.4	55.8	44.9	55.8	42.3	45.8	39.1
67.5	28.6	65.8	48.3	60.8	45.4	60.8	45	50.8	40.2
72.5	30.4	70.8	48.8	65.8	45.7	65.8	46.5	55.8	42.9
77.5	31.8	75.8	49.7	70.8	48.6	70.8	47.2	60.8	43.5
82.5	33	80.8	49.4	75.8	49.5	75.8	47.4	65.8	43.4
87.5	34.4	82.8	49.9	80.8	50.3	80.8	50.3	70.8	44.8
92.5	35.9	84.8	50.5	82.8	50.3	85.8	49.3	75.8	45.2
97.5	36.4	86.8	50.9	84.8	50.9	90.8	51.1	80.8	46.7
102.5	37	88.8	52.9	86.8	51.2	95.8	50.6	85.8	47.2
107.5	38.5	90.8	54.5	88.8	51	100.8	51.8	90.8	47.4
112.5	39.7	92.8	54.7	90.8	50.8	102.8	52.2	95.8	49.7
117.5	41.2	94.8	54.3	92.8	51.3	104.8	52.1	100.8	50.1
122.5	41.2	96.8	54	94.8	51.6	106.8	52.7	105.8	52.1
127.5	42	98.8	54	96.8	52.6	108.8	53.6	110.8	52.1
132.5	42	100.8	54.2	98.8	53.5	110.8	54.8	115.8	53.3
137.5	43.1	102.8	54.7	100.8	54.1	112.8	55.1	120.8	53.9
142.5	43.4	104.8	54.8	102.8	54.9	114.8	55.2	125.8	55
147.5	43.8	106.8	55.7	104.8	54.1	116.8	55.1	130.8	57.9
152.5	45.1	108.8	57.6	106.8	54.5	118.8	55.3	135.8	58.7
157.5	44.2	110.8	57.9	108.8	55.1	120.8	55.4	140.8	57.4
162.5	45.6	112.8	58.5	110.8	56	122.8	56.7	145.8	55.8
167.5	46.9	114.8	57.9	112.8	56.2	124.8	57.7	150.8	58.6
172.5	48.3	116.8	61.3	114.8	56.5	126.8	58.3	155.8	59.6
177.5	48.6	118.8	62	116.8	57.1	128.8	58.5	160.8	57.4
182.5	49.2	120.8	62.9	118.8	57.9	130.8	59.4	165.8	54.9
187.5	49.6	122.8	63.7	120.8	58.6	132.8	61.4	170.8	54.8
192.5	50.4	124.8	64.3	122.8	60.4	134.8	62.5	175.8	53.7
197.5	50.1	126.8	64.9	124.8	61.5	136.8	62.6	180.8	50.4
202.5	52.5	128.8	64.8	126.8	61.9	138.8	62.7	185.8	48.1
207.5	52.2	130.8	64.7	128.8	62.1	140.8	63.2	190.8	43.9
212.5	53.7	132.8	64.6	130.8	62.4	142.8	64	195.8	40.4
217.5	54.4	134.8	64.7	132.8	63.4	143.8	64.4	200.8	36.5
222.5	54.3	136.8	64.5	134.8	64.2	144.8	64.3	205.8	33.1
227.5	53.9	138.8	64.3	135.8	64.5	146.8	64.2	210.8	30.1
232.5	54.3	140.8	64.3	136.8	64.4	148.8	63.5	215.8	24.8
237.5	54.5			138.8	64.6	150.8	62.7	220.8	20.8
242.5	55			140.8	64.5	152.8	61.6	225.8	18.1
247.5	55.6			142.8	64.5	154.8	60.8	230.8	15.9
252.5	57			144.8	64.1	156.8	60.4		
257.5	57.8			146.8	64.1	158.8	59.7		
262.5	56.8			148.8	63.9	160.8	58.6		
267.5	56.4			150.8	63.4	162.8	56.8		

272.5	55.8
277.5	55
282.5	54.7
287.5	54.3
292.5	53.8
297.5	51.5
302.5	46.7
307.5	43.8
312.5	39.6
317.5	35.9
322.5	31.2
327.5	26.8
332.5	22.5
337.5	16.9

152.8	62.2
154.8	61.2
156.8	60.2
158.8	60.2
160.8	59.4
162.8	58.2
164.8	57.1
166.8	55.8
168.8	55
170.8	53.2

164.8	54.3
166.8	53.6
168.8	53.6
170.8	54.1
172.8	53.8
174.8	53
176.8	52.2
178.8	50.6
180.8	48.7
182.8	47.1
184.8	45.8
186.8	44.4
188.8	42.5
190.8	39.5
192.8	38.2
194.8	36.6
196.8	35.4
198.8	33.6
200.8	32

Test	**6**	**Test**	**7**	**Test**	**8**	**Test**	**8**	**Test**	**8**
Wave	**5**			**Wave**	**1**	**Wave**	**2**	**Wave**	**3**
x (cm)	**y (cm)**	**x (cm)**	**y (cm)**	**x (cm)**	**y (cm)**	**x (cm)**	**y (cm)**	**x (cm)**	**y (cm)**
-23.2	0	-19.7	0	67.5	21.6	47.5	15.3	4.0	0.0
-19.2	4.7	-19.2	5.5	72.5	24.5	52.5	17.3	2.5	1.6
-14.2	9.6	-14.2	8.5	77.5	26.8	57.5	18.4	7.5	3.1
-9.2	12.1	-9.2	9.1	82.5	27.8	62.5	22.8	12.5	5.7
-4.2	14.3	-4.2	14	87.5	31.2	67.5	21.8	17.5	6.8
0.8	18.2	0.8	16.2	92.5	31.6	72.5	24.4	22.5	8.7
5.8	19.2	5.8	19	97.5	33.2	77.5	26.3	27.5	10.1
10.8	22.6	10.8	21.8	102.5	35.1	82.5	31.2	32.5	11.9
15.8	25.9	15.8	22.7	107.5	37.8	87.5	32.9	37.5	13.4
20.8	26.3	20.8	25.3	109.5	38.8	92.5	35.3	42.5	14.6
25.8	29.8	25.8	27.9	111.5	39.1	97.5	37.1	47.5	15.5
30.8	32.4	30.8	30	113.5	40.4	102.5	39.7	52.5	17.5
35.8	35.1	35.8	32.1	115.5	41	107.5	41.7	57.5	18.9
40.8	36.3	40.8	35.4	117.5	42.3	112.5	42.1	62.5	23.0
45.8	37.6	45.8	36.5	119.5	43.2	117.5	44.2	67.5	24.4
50.8	39.8	50.8	36.7	121.5	44.4	122.5	45.8	72.5	26.9
55.8	41.6	55.8	39.1	123.5	45	127.5	45.3	77.5	29.7
60.8	42.1	60.8	40.9	125.5	45.9	132.5	46.5	82.5	33.1

65.8	43.1	65.8	42.5	127.5	46.2	137.5	47.8	87.5	36.4
70.8	43.9	70.8	44	129.5	46.9	142.5	48.8	92.5	37.2
75.8	45.2	75.8	44.7	131.5	48.2	147.5	50.1	97.5	39.2
80.8	46	80.8	44.4	133.5	48.4	152.5	51.6	102.5	41.0
85.8	45.5	85.8	46.3	135.5	49.9	157.5	51.9	107.5	42.5
90.8	46	90.8	46.9	137.5	50.3	162.5	52.9	112.5	44.5
95.8	46.9	95.8	47	139.5	50.5	167.5	52.9	117.5	44.3
100.8	47.9	100.8	47.3	141.5	50.9	169.5	52.5	122.5	44.4
105.8	48.9	105.8	48.7	143.5	51.3	171.5	53.2	127.5	46.8
110.8	49.7	110.8	49.4	145.5	50.8	173.5	54.6	132.5	47.8
115.8	50.6	115.8	50.8	147.5	50	175.5	55.3	137.5	47.6
120.8	52.5	120.8	52	149.5	50.5	177.5	55.8	142.5	48.1
125.8	54.3	125.8	52.2	151.5	51.2	179.5	55.8	147.5	49.7
130.8	54.4	130.8	54	153.5	52.3	181.5	55	152.5	50.0
135.8	56	135.8	54.8	155.5	51.9	183.5	55.9	157.5	51.0
140.8	56.2	140.8	56.6	157.5	51.6	185.5	56.4	162.5	50.6
145.8	56	145.8	58	159.5	51.7	187.5	56.6	167.5	51.7
150.8	56.1	150.8	58.1	161.5	51.7	189.5	56.1	172.5	52.5
155.8	56.3	155.8	57.4	163.5	52.3	191.5	57.2	177.5	54.7
160.8	55.4	160.8	57	165.5	52.4	193.5	57.6	182.5	54.5
165.8	55.8	165.8	55.4	167.5	53.6	195.5	57.5	187.5	55.2
170.8	55.4	170.8	54.3	169.5	54.4	197.5	58.1	189.5	55.6
175.8	53.7	175.8	53.8	171.5	55.1	199.5	58.8	191.5	55.6
180.8	50.3	180.8	51.7	173.5	55.6	201.5	59.4	193.5	55.9
185.8	47.8	185.8	50.5	175.5	56.2	203.5	59.8	195.5	56.9
190.8	45	190.8	47.9	177.5	56.5	205.5	61	197.5	57.6
195.8	41.9	195.8	44.1	179.5	56.4	207.5	62.9	199.5	57.5
200.8	38.7	200.8	40.9	181.5	56.8	209.5	63.9	201.5	57.9
205.8	35.9	205.8	37.1	183.5	57.6	211.5	64.7	203.5	58.0
210.8	34.5	210.8	33.5	185.5	58	213.5	65	205.5	58.1
215.8	31	215.8	29	187.5	58.2	215.5	65.1	207.5	60.2
220.8	24.7	220.8	25.9	189.5	58.9	217.5	65.1	209.5	62.4
225.8	20.8	225.8	20.6	191.5	59.4	219.5	65.1	211.5	63.8
230.8	16.6	230.8	13.9	193.5	60.2	221.5	65	213.5	64.4
				195.5	61.3	223.5	65.1	215.5	64.7
				197.5	64.2	225.5	65.1	217.5	64.4
				199.5	65.4	227.5	65.2	219.5	65.1
				201.5	65.9	229.5	65.2	221.5	65.7
				203.5	66	231.5	64.9	223.5	66.4
				205.5	65.9	233.5	65	225.5	66.8
				207.5	65.6	235.5	65	227.5	67.1
				209.5	65.6	237.5	64.7	229.5	66.8
				211.5	65.6			231.5	66.5
				213.5	65.4			233.5	66.3

				215.5	65.5			235.5	66.0
				217.5	65.4			237.5	65.5
								239.5	65.3
								241.5	65.2
								243.5	64.7
								245.5	64.3
								247.5	64.2
								249.5	63.9
								251.5	63.4
								253.5	62.7
								255.5	61.8
								257.5	60.9

Test	**8**	**Test**	**8**	**Test**	**9**	**Test**	**9**	**Test**	**9**
Wave	**4**	**Wave**	**5**	**Wave**	**1**	**Wave**	**2**	**Wave**	**3**
x (cm)	**y (cm)**	**x (cm)**	**y (cm)**	**x (cm)**	**y (cm)**	**x (cm)**	**y (cm)**	**x (cm)**	**y (cm)**
3	0	1.5	0	-10.2	0	-10.7	0	-17.7	0
2.5	2.7	2.5	2.7	-9.2	2.1	-9.2	4.5	-14.2	6.4
7.5	4	7.5	4.9	-4.2	3	-4.2	7.5	-9.2	8.9
12.5	5.7	12.5	6.3	0.8	8.9	0.8	13.3	-4.2	12.6
17.5	7.4	17.5	8.1	5.8	12.1	5.8	17.1	0.8	16
22.5	8.8	22.5	9.1	10.8	16.9	10.8	20.1	5.8	18
27.5	10.8	27.5	10.4	15.8	21	15.8	23.1	10.8	19.8
32.5	11.9	32.5	11.3	20.8	24.3	20.8	26.1	15.8	22.5
37.5	13.6	37.5	13.1	25.8	27.1	25.8	29.1	20.8	25
42.5	14.2	42.5	17.3	30.8	29.7	30.8	30.2	25.8	29.8
47.5	16.2	47.5	21.3	35.8	31.1	35.8	33.1	30.8	32
52.5	17.8	52.5	23.9	40.8	34.1	40.8	36.6	35.8	35.6
57.5	23.8	57.5	26.5	42.8	34.6	45.8	37.6	40.8	37.8
62.5	25.3	62.5	28.1	44.8	36.3	50.8	40.9	45.8	39.6
67.5	27.6	67.5	30.1	46.8	37	55.8	42.6	50.8	40.1
72.5	30.2	72.5	32.1	48.8	38.8	60.8	44.2	55.8	42.8
77.5	31.8	77.5	33.4	50.8	39.4	65.8	45.7	60.8	43.6
82.5	34.9	82.5	34.4	52.8	40.8	70.8	46.5	65.8	44.4
87.5	36.7	87.5	36	54.8	42.6	75.8	48.1	70.8	45.5
92.5	37.7	92.5	37.1	56.8	44	80.8	51.2	75.8	46.9
97.5	39.7	97.5	36.4	58.8	44.8	85.8	51.5	80.8	47.1
102.5	41.3	102.5	36.8	60.8	45.3	90.8	52.4	85.8	48.5
107.5	42.1	107.5	39.4	62.8	46.2	95.8	52.5	90.8	49.3
112.5	43.5	112.5	40.3	64.8	47.8	100.8	53.6	95.8	49.6
117.5	44	117.5	41.5	66.8	48.4	102.8	53.2	100.8	49.9

122.5	44	122.5	41.4	68.8	48.6	104.8	52.4	105.8	50.8
127.5	44.9	127.5	43	70.8	47.4	106.8	53	110.8	51.9
132.5	45.9	132.5	41.4	72.8	47.9	108.8	53.5	115.8	52.3
137.5	46.2	137.5	42.2	74.8	48.3	110.8	54.4	120.8	54.3
142.5	47.9	142.5	44.3	76.8	48.7	112.8	54.7	125.8	54.4
147.5	49	147.5	44.4	78.8	49.4	114.8	55	130.8	54.9
152.5	48.9	152.5	46.4	80.8	50.4	116.8	55.3	135.8	56.9
157.5	49.3	157.5	46.2	82.8	50.9	118.8	55.8	140.8	58.1
162.5	50.3	162.5	45.3	84.8	51.3	120.8	56.2	145.8	56.3
167.5	51	167.5	48	86.8	51.2	122.8	56.8	150.8	57.1
172.5	51.4	172.5	48	88.8	51.6	124.8	57.1	155.8	57.4
177.5	51.6	177.5	48.5	90.8	51.8	126.8	57.7	160.8	56.2
182.5	52.1	182.5	49.8	92.8	51.8	128.8	59	165.8	54.1
187.5	54.2	187.5	50.2	94.8	52.5	130.8	59.4	170.8	54.1
192.5	54	192.5	51.6	96.8	52.7	132.8	60	175.8	53.5
197.5	55.7	197.5	51.7	98.8	53.1	134.8	59.9	180.8	51.7
202.5	58.4	202.5	51.8	100.8	54.3	136.8	61.5	185.8	49.5
207.5	58.3	207.5	52.6	102.8	54.6	138.8	62.6	190.8	46
212.5	59.2	212.5	52.2	104.8	55.2	140.8	63.4	195.8	42.4
217.5	60.9	217.5	53.2	106.8	55.8	142.8	63.9	200.8	39.1
219.5	62.1	222.5	54.1	108.8	56.6	144.8	63.9	205.8	35.9
221.5	62.6	227.5	56.6	110.8	57.1	146.8	63.8	210.8	32.1
223.5	62.5	232.5	57.1	112.8	58.1	148.8	63.5	215.8	28.6
225.5	62.8	237.5	57.8	114.8	58.4	150.8	63.5	220.8	24
227.5	63.4	242.5	58.7	116.8	58.2	152.8	63.2	225.8	20
229.5	64	247.5	56.8	118.8	58.8	154.8	62.5	230.8	15.3
231.5	64.3	252.5	56.9	120.8	60.5	156.8	60.1		
233.5	64.1	257.5	56.6	122.8	61.3	158.8	59.6		
235.5	64.3	262.5	54.8	124.8	61.9	160.8	58.4		
237.5	64.4	267.5	54.9	126.8	62.7	162.8	57.7		
239.5	64.4	272.5	53.7	128.8	64	164.8	56.7		
241.5	64.3	277.5	53.7	130.8	64.3	166.8	55.6		
243.5	64.3	282.5	52.7	131.8	64.3	168.8	54.7		
245.5	63.9	287.5	50.1	132.8	64.4	170.8	54.2		
247.5	63.8	292.5	48.2	134.8	64.4	172.8	53		
249.5	63.1	297.5	45.1	136.8	64.4	174.8	52.2		
251.5	62.1	302.5	41.9	138.8	64.3	176.8	50.3		
253.5	59.7	307.5	38.9	140.8	63.9	178.8	48.6		
255.5	58.6	312.5	36.1	145.8	63.7	180.8	47.2		
257.5	58.7	317.5	33.1			182.8	46.1		
259.5	58.5	322.5	28.7			184.8	44.3		
261.5	58	327.5	24.1			186.8	42.8		
263.5	57.6	332.5	20.9			188.8	41.2		
265.5	56.5	337.5	16.2			190.8	40.1		

267.5	54.1	342.5	13.2			192.8	39
272.5	51.5	347.5	9			194.8	36.8
277.5	48.5	352.5	3			196.8	35.9
282.5	44.8	357.5	0.5			198.8	33.8
287.5	41.4	360.5	0			200.8	32.2
292.5	38.8						
297.5	34.7						
302.5	31.2						
307.5	27.1						
312.5	24.1						
317.5	20.3						
322.5	16.3						
327.5	12.1						
332.5	9.2						

Test 9

Wave 4

x (cm)	y (cm)	x (cm)	y (cm)	x (cm)	y (cm)
-22.2	0	90.8	48.1	205.8	38.6
-19.2	5.3	95.8	49.3	210.8	35.2
-14.2	8.9	100.8	48.9	215.8	30.6
-9.2	11.3	105.8	49.5	220.8	26.1
-4.2	12.6	110.8	50	225.8	20.4
0.8	15.8	115.8	50.1	230.8	15.4
5.8	18.4	120.8	51.1		
10.8	21.3	125.8	51.4		
15.8	24	130.8	53.3		
20.8	26.2	135.8	55.2		
25.8	28.9	140.8	55.3		
30.8	32.2	145.8	55.2		
35.8	33.7	150.8	55		
40.8	35.7	155.8	56.1		
45.8	37.5	160.8	56		
50.8	39.4	165.8	55.9		
55.8	41.1	170.8	55.1		
60.8	41.9	175.8	53.6		
65.8	42.6	180.8	53.7		
70.8	45.5	185.8	51		
75.8	45.4	190.8	48.2		
80.8	46.3	195.8	44.9		
85.8	46.7	200.8	41.6		

APPENDIX C

Principal Component Analysis

Standardized measured parameters:

$$
\begin{array}{ll}
 & \begin{array}{ccccc} h_s & l_s & h_c & l_c & \theta_3 \end{array} \\
\tilde{Y} = & \begin{bmatrix}
1.002 & -0.009 & 0.532 & -0.564 & 0.947 \\
1.217 & 0.551 & 0.996 & -0.728 & 1.524 \\
1.450 & 1.108 & -0.343 & -0.574 & 0.401 \\
-1.106 & -1.423 & -0.395 & -0.881 & 0.176 \\
-0.519 & -0.509 & -0.034 & -0.636 & 0.686 \\
0.415 & 0.593 & -0.395 & -0.636 & 0.449 \\
-0.313 & -1.102 & -0.240 & -0.832 & 0.845 \\
0.082 & -0.220 & -0.137 & -1.158 & 1.533 \\
0.900 & 0.726 & 0.584 & -0.193 & 0.488 \\
-1.878 & -1.625 & -0.859 & -0.734 & -1.344 \\
-1.103 & -0.930 & -0.240 & -0.636 & -1.202 \\
-0.341 & -0.121 & 0.738 & -0.335 & 0.754 \\
0.108 & 0.452 & 1.769 & 0.129 & 0.751 \\
1.228 & 1.497 & 2.902 & 1.003 & 0.418 \\
-0.452 & -0.453 & -0.859 & -0.690 & 0.214 \\
0.188 & 0.101 & -1.013 & 0.388 & -0.849 \\
1.139 & 0.626 & -1.116 & 0.552 & -0.995 \\
-2.161 & -1.983 & -0.292 & 0.628 & -0.669 \\
-0.170 & 0.234 & -0.756 & 2.313 & -1.554 \\
-0.135 & 0.799 & 0.275 & 1.752 & -1.031 \\
0.450 & 1.688 & -1.116 & 1.829 & -1.541
\end{bmatrix}
\end{array}
$$

Covariance of $\tilde{Y}$:

$$
\operatorname{cov}\left(\tilde{Y}\right) = \begin{bmatrix}
1.00 & 0.86 & 0.26 & -0.30 & 0.36 \\
0.86 & 1.00 & 0.25 & 0.06 & 0.05 \\
0.26 & 0.25 & 1.00 & -0.09 & 0.48 \\
-0.30 & 0.06 & -0.09 & 1.00 & -0.89 \\
0.36 & 0.05 & 0.48 & -0.89 & 1.00
\end{bmatrix}
$$

Eigenvectors of $\operatorname{cov}\left(\tilde{Y}\right)$:

$$E = \begin{bmatrix} 0.604 & -0.101 & 0.423 & 0.070 & 0.664 \\ 0.559 & -0.356 & 0.194 & 0.168 & -0.704 \\ 0.444 & 0.217 & -0.797 & 0.331 & 0.102 \\ 0.068 & -0.675 & -0.382 & -0.611 & 0.144 \\ 0.348 & 0.600 & 0.045 & -0.696 & -0.181 \end{bmatrix}$$

Eigenvalues of $\operatorname{cov}\left(\tilde{Y}\right)$:

$$D = \begin{bmatrix} 2.259 & 1.834 & 0.713 & 0.1301 & 0.0643 \end{bmatrix}$$

Factor loadings:

$$B = \begin{bmatrix} 0.91 & -0.14 & 0.36 & 0.03 & 0.17 \\ 0.84 & -0.48 & 0.16 & 0.06 & -0.18 \\ 0.67 & 0.29 & -0.67 & 0.12 & 0.03 \\ 0.10 & -0.91 & -0.32 & -0.22 & 0.04 \\ 0.52 & 0.81 & 0.04 & -0.25 & -0.05 \end{bmatrix}$$

Factor scores:

$$A = \begin{bmatrix} 0.40 & -0.07 & 0.50 & 0.19 & 2.62 \\ 0.37 & -0.26 & 0.23 & 0.47 & -2.78 \\ 0.30 & 0.16 & -0.94 & 0.92 & 0.40 \\ 0.04 & -0.50 & -0.45 & -1.69 & 0.57 \\ 0.23 & 0.44 & 0.05 & -1.93 & -0.71 \end{bmatrix}$$

Components:

$$F = \begin{bmatrix} 0.750 & 0.714 & 0.303 & -0.194 & 1.867 \\ 1.308 & 0.963 & 0.206 & -0.300 & 0.560 \\ 0.960 & 0.010 & 1.586 & 0.682 & -0.030 \\ -1.089 & 0.910 & -0.100 & -0.086 & 0.268 \\ -0.278 & 0.788 & -0.021 & -0.616 & -0.812 \\ 0.346 & 0.266 & 1.028 & 0.205 & -1.402 \\ -0.448 & 1.064 & 0.239 & -1.016 & 1.067 \\ 0.213 & 1.287 & 0.725 & -1.210 & -0.984 \\ 0.908 & 0.149 & 0.179 & 0.435 & 0.119 \\ -1.957 & 0.199 & -0.243 & 1.926 & -0.212 \\ -1.167 & 0.072 & -0.316 & 2.528 & 0.092 \\ 0.195 & 0.677 & -0.704 & -0.331 & -0.987 \\ 0.914 & 0.426 & -1.530 & 0.187 & -0.722 \\ 2.049 & -0.333 & -2.212 & 1.093 & 0.502 \\ -0.585 & 0.454 & 0.803 & -0.330 & -0.816 \\ -0.365 & -0.773 & 0.853 & 0.134 & 0.629 \\ 0.156 & -1.145 & 1.466 & 0.474 & 1.821 \\ -1.819 & 0.025 & -1.582 & -1.386 & 0.564 \\ -0.460 & -2.013 & -0.446 & -1.537 & 1.025 \\ 0.164 & -1.486 & -0.991 & -0.381 & -0.729 \\ 0.204 & -2.251 & 0.758 & -0.275 & -1.818 \end{bmatrix}$$

APPENDIX D

MATLAB script for the calculation of a reshaped profile

```
clear all
clc
data=load('input.txt')
xz=load('profile.txt')
Hs=data(1);
Tm=data(2);
N=data(3);
alfa=data(4);
h=data(5);
mwl=data(6);
Dn50=data(7);
gr=data(8);
D=data(9);
xm=[-2;xz(:,1);4];
zm=[0;xz(:,2);h];
x1=-2:0.001:4;
z1=interp1(xm,zm,x1);
H0T0=Hs/D/Dn50*sqrt(9.81/Dn50)*Tm
sm=2*3.14*Hs/9.81/Tm^2;
plot(x1,z1)
hold on
xorig=0;
for i=1:length(x1)
    if (round(z1(i)*100)/100)==mwl
        xorig=x1(i);
    end
end

ls=((H0T0+9.38-29.1*alfa)*(gr)^0.15/1.66)^(1/1.3)*Dn50*N^0.07
hs=((H0T0+475-125*alfa)/27)^(1/1.3)*Dn50*N^0.07
t3=0.00023*(gr)^1.58*H0T0^0.84+1.50
lc=((H0T0-183)*alfa+667)/139*gr^0.29*Dn50*N^0.12
beta=1.1/alfa^(1-0.45*exp(-500/N))
xP3=xorig
xP2=xP3+lc
xP1=xP2+abs(lc/t3+mwl-h)*1.5
xP4=xP3-ls
zP1=h
zP2=mwl+lc/t3
zP3=mwl
zP4=mwl-hs
if zP1>=zP2
    xP1=xP3+(h-mwl)*t3
end

cont=0;
```

```
diff=100;
shift=0;
num=0;

for j=-0.001:-0.001:-1
    cont=cont+1;
    xP5r=xP4+j-0.001;

    c=round((xP4+j+1)*1000)+1;
    for i=1:(c-1)
        xtry=xP4+j-i/1000;
        ztry=zP4-i*beta/1000;
        if abs(ztry-z1(c-i))<0.01
            zP5=ztry;
            xP5=xP4+j-i/1000;
            xP5r=xP5;
        end
    end
    for k=1:(1000*(xP5r+2)+1)
        xl(k)=x1(k);
        zl(k)=z1(k);
    end
    xl=xl(1:k);
    zl=zl(1:k);
    xr=[xl';xP4+j;xP3+j;xP2+j;xP1+j;4];
    zr=[zl';zP4;zP3;zP2;zP1;h];
    x2=-2:0.001:4;
    z2=interp1(xr,zr,x2);

    area=sum(z1-z2);
    if abs(area)<diff
        diff=abs(area)
        shift=j;
        xfin=x2;
        zfin=z2;
        num=num+1
        plot(x2,z2,'r')
        hold on
    end
end

for j=0:0.001:1
    cont=cont+1;
    xP5r=xP4+j-0.001;

    c=round((xP4+j+1)*1000)+1;
    for i=1:(c-1)
        xtry=xP4+j-i/1000;
        ztry=zP4-i*beta/1000;
        if abs(ztry-z1(c-i))<0.01
            zP5=ztry;
            xP5=xP4+j-i/1000;
            xP5r=xP5;
        end
    end
    for k=1:(1000*(xP5r+2)+1)
```

```
        xp(k)=x1(k);
        zp(k)=z1(k);
    end
    xp=xp(1:k);
    zp=zp(1:k);
    xr=[xp';xP4+j;xP3+j;xP2+j;xP1+j;4];
    zr=[zp';zP4;zP3;zP2;zP1;h];
    x2=-2:0.001:4;
    z2=interp1(xr,zr,x2);

    area=sum(z1-z2);
    if abs(area)<diff
        diff=abs(area)
        shift=j;
        xfin=x2;
        zfin=z2;
        num=num+1
        plot(x2,z2,'g')
        hold on
    end

end

shift
figure(2)
plot(x1,z1,'b',xfin,zfin,'m')

rec=0;
for i=1:6001
    if abs((zfin(6002-i)-h))<0.01
       rec=xfin(6002-i)
    end
end
recOK=rec-xm(3)
```

Example of file "*input.txt*":

```
0.10
1.2
2000
1.5
0.65
0.55
0.011
2.71
1.65
```

Example of file "*profile.txt*":

```
0     0
0.975 0.65
```